Necroptosis microenvironment directs lineage commitment in liver cancer

Dissertation

der Mathematisch-Naturwissenschaftlichen Fakultät

der Eberhard Karls Universität Tübingen

zur Erlangung des Grades eines

Doktors der Naturwissenschaften

(Dr. rer. nat.)

vorgelegt von

M.Sc. Marco Seehawer

aus Berlin

Tübingen

2018

Gedruckt mit Genehmigung der Mathematisch-Naturwissenschaftlichen Fakultät der Eberhard Karls Universität Tübingen.

Tag der mündlichen Qualifikation:
Dekan: Prof. Dr. Wolfgang Rosenstiel
1. Berichterstatter: Prof. Dr. Lars Zender
2. Berichterstatter: Prof. Dr. Klaus Schulze-Osthoff

Vorveröffentlichung der Dissertation

Ergebnisse aus dieser Arbeit wurden mit Genehmigung der Mathematisch-Naturwissenschaftlichen Fakultät der Universität Tübingen, vertreten durch die Mentoren der Arbeit, im folgenden Beitrag vorab veröffentlicht:

M. Seehawer, F. Heinzmann, L. D'Artista, J. Harbig, P.-F. Roux, L. Hoenicke, H. Dang, S. Klotz, L. Robinson, G. Doré, N. Rozenblum, T.-W. Kang, R. Chawla, T. Buch, M. Vucur, M. Roth, J. Zuber, T. Luedde, B. Sipos, T. Longerich, M. Heikenwälder, X. W. Wang, O. Bischof and L. Zender (2018). "Necroptosis microenvironment directs lineage commitment in liver cancer." Nature **562**(7725): 69-75.

Declaration of contribution:

Author	Author Position	Scientific ideas %	Data generation %	Analysis and interpretation %	Paper writing %
Marco Seehawer	1	33	32	28	28
Florian Heinzmann	1	15	26	19	18
Luana D'Artista	2		5	4	
Jule Harbig	3		5	4	
Pierre-Francois Roux	4		5	4	
Lisa Hönicke	5		2		
Hien Dang	6		2		
Sabrina Klotz	7		2		
Lucas Robinson	8		2		
Grégory Dore	9		2		
Nir Rozenblum	10		2		
Tae-Won Kang	11		2		
Rishabh Chawla	12		2		
Thorsten Buch	13		2		
Mihael Vucur	14		2		
Mareike Roth	15		2		
Johannes Zuber	16			2	
Tom Lüdde	17		1		
Bence Sipos	18			2	
Thomas Longerich	19			2	
Mathias Heikenwälder	20		2		
Xin Wei Wang	21		2	2	
Oliver Bischof	22	1		5	3
Lars Zender	23	51		28	51
title of paper:	**Necroptosis microenvironment directs lineage commitment in liver cancer**				
status in publication process:	**published**				

Table of contents

Abbreviations

AFP	alpha-fetoprotein
AFP-L3	L3 fraction of alpha-fetoprotein
APAP	acetaminophen
ASH	alcoholic steatohepatitis
aSMA	alpha smooth muscle actin
ATAC	Assay for Transposase-Accessible Chromatin
ATP	adenosintriphosphate
BCL2	B-cell lymphoma 2
BDL	bile duct ligation
bp	base pair
BSA	bovine serum albumin
C	Celsius
CA 19-9	carbohydrate antigen 19-9
Casp	caspase
CCA	Cholangiocarcinoma
CCsgp19	CRISPR/Cas9-sg_p19
cDNA	complementary DNA
ChIP	Chromatinimmunoprecipitation
CIP	calf intestinal alkaline phosphatase
CRISPR	Clustered Regularly Interspaced Short Palindromic Repeats
DAI	DNA-dependent activator of IFN-regulatory factors
DAMP	damage associated molecular patterns
DAPI	4',6-diamidino-2-phenylindole
dCCA	distal cholangiocarcinoma
DCP	des-γ carboxyprothrombin
DMSO	dimethylsulfoxide
DNA	deoxyribonucleic acid
dNTP	2'-desoxynukleoside-5'-triphosphate
e.g.	exempli gratia
EDTA	ethylenediaminetetraacetic acid
Epo	in vivo electroporation
ER	endosplamic-reticulum
EtOH	ethanol
FC	flow cytometry
FCS	fetal calf serum
Fig	Figure
gDNA	genomic DNA
GFP	green fluorescent protein
IRI	ischemia-reperfusion injury
IR	inverted repeats
K	cytokeratin
KO	knockout
LB	lysogeny broth
LCM	laser-capture microdissection
LPC	Liver progenitor cell
LPS	lipopolysaccharide
M	molar
MetOh	methanol
min	minute
MLKL	mixed-lineage kinase domain like pseudokinase
MOMP	mitochondrial outer membrane permeabilization
mRNA	messenger RNA
n	number
NaCl	sodium chloride
NAFLD	non-alcoholic fatty liver disease
NASH	nonalcoholic steatohepatitis
NGS	next generation sequencing
NGS	normal goat serum
o/n	over night
OE	overexpression
p	p-value
PBS	phosphate buffered saline
PBST	phosphate buffered saline with tween
pCAA	perihilar cholangiocarcinoma
PCR	polymerase chain reaction
PDAC	pancreatic ductal adenocarcinoma
PFA	paraformaldehyde
PKG	phosphoglycerinkinase
PLC	primary liver cancer
PSC	primary sclerosing cholangitis
PVDF	polyvinylidene difluoride
qRT-PCR	Quantitative Real-time-PCR
RA	retinoic acid
ref	reference
RIPK	receptor interacting serin/threonine protein kinase
RNA	ribonucleic acid

GFP	green fluorescent protein
GP3	glypican 3
GS	Gluthamine-synthetase
H&E	haematoxylin and eosin
HAT	histone acetyltransferases
HBS	HEPES buffered saline
HBV	hepatitis B virus
HCC	hepatocellular carcinoma
HCV	hepatitis C virus
HDAC	histone deacetylases
HDTV	hydrodynamic tail vein injection
HMGB	high mobility group box protein
HNF	hepatocyte nuclear factor
HRP	horseradish peroxydase
HSC	hepatic stellate cell
ICC/iCCA	intrahepatic cholangiocarcinoma
ICH	Immunohistochemistry
IF	immunofluorescence
IRES	internal ribosomal entry site
RNAi	RNA interference
ROS	reactive oxygen species
rpm	rounds per minute
rSAP	recombinant shrimp alkaline phosphatase
RT	room temperature
SB	sleeping beauty
SDS-PAGE	Sodium dodecyl sulphate polyacrylamide gel electrophoresis
SWI/SNF	switch/sucrose non-fermentable
TAA	thioacetamide
TGFβ	transforming growth factor beta
TLR	toll-like-receptor
TLR5x KO	TLR 2, 3, 5, 7 and 9 knockout
TNFRSF	tumor necrosis factor receptor superfamily
TUNEL	Terminal deoxynucleotidyl transferase dUTP nick end labeling
V	volt
WB	western blot
WES	whole exomes sequencing
wt	wildtype

Summary

Primary liver cancer is a major health problem with markedly increasing incidence rates. It is mainly represented by hepatocellular carcinoma (HCC) and intrahepatic cholangiocarcinoma (ICC) which are quite different regarding their morphology and treatment options. Although both share many risk factors as chronic liver damage or inflammation and cirrhosis, the molecular determinants resulting in either HCC or ICC lineage are largely unknown.

Here, using two different transposon-based liver cancer mouse models we show that both HCC and ICC can be induced by overexpressing the same oncogenes.

Taking advantage of a lineage tracing mouse model we prove that both tumors are derived from adult hepatocytes. Lineage commitment is independent of somatic mutations but depends on the hepatic microenvironment in the pre-tumorigenic phase. While in an apoptotic milieu there is an outgrowth of HCC a necroptotic milieu determines ICC development. This is independent of the composition of infiltrating immune cells, however, it is associated with a specific cytokine signature. The specific cytokine signature can be reversed when inhibiting necroptosis chemically or genetically and is followed by a switch from ICC to HCC development.

Epigenetic and transcriptomic analyses of cell lines isolated from hepatocyte-derived HCC or ICC driven by the same oncogene showed specific signatures for each tumor type. Integrative analyses of epigenetic and transcriptomic data revealed Tbx3 and Prdm5 as differentially regulated transcription factors which could also be found in a large cohort of human patients. Functional validation further showed that the interplay of Tbx3 and Prdm5 is sufficient to switch tumor lineage commitment from HCC to ICC. Finally, we identified downstream targets for both transcription factors which revealed quite converse downstream pathways highlighting the importance for their simultaneous interaction in determining lineage commitment in primary liver cancer.

Zusammenfassung

Leberkrebs ist ein globales Gesundheitsproblem mit deutlich ansteigender Inzidenz. Das Hepatozelluläre Karzinom (HCC) und das Cholangiozelluläre Karzinom (ICC) sind die zwei am häufigsten vorkommenden primären Leberkrebstypen, welche sich sowohl in ihrer Morphologie als auch hinsichtlich ihrer Therapien sehr unterscheiden. Obwohl bekannt ist, dass beide gemeinsame Risikofaktoren, wie chronische Leberentzündung oder Zirrhose, haben, sind die genauen molekularen Ursachen zur HCC oder ICC Entstehung nicht bekannt.

In dieser Studie konnte ich mithilfe von Transposon-basierten mosaiken Mausmodellen zeigen, dass sowohl HCCs als auch ICCs durch Überexpression derselben Onkogene induziert werden können. In einem „Lineage-Tracing"-Modell habe ich bewiesen, dass sich beide Tumorentitäten aus adulten Hepatozyten entwickeln können. Die Entwicklung des spezifischen Tumortyps ist unabhängig von somatischen Mutationen, jedoch ist sie abhängig von der Mikroumgebung in der pro-tumorigenen Phase. Während ein apoptotisches Milieu die Entstehung von HCC fördert, fördert ein nekroptotisches Milieu die Entstehung von ICC. Dies ist unabhängig von der Komposition der infiltrierenden Immunzellen, jedoch mit einer spezifischen Zytokinsignatur assoziiert. Diese kann durch Inhibition von Nekrose auf chemischem oder genetischem Wege revertiert werden, was einen Wechsel von ICC zu HCC zur Folge hat.

Epigenetik- und Transkriptomanalysen von Zelllinien, welche aus murinen HCC- und ICC-Tumoren isoliert wurden konnten zeigen, dass es Tumortyp-spezifische Signaturen gibt, obwohl beide Tumorarten initial durch Transfektionen von Hepatozyten mit denselben Onkogenen induziert wurden. Integrative Analysen von Epigenom- und Transkriptomdatensätzen zeigten, dass die Transkriptionsfaktoren Tbx3 und Prdm5 zwischen HCC und ICC epigenetisch differentiell reguliert sind, was auch in einer großen Kohorte humaner Proben validiert werden konnte. Funktionelle Experimente zeigten, dass das Zusammenspiel von Tbx3 und Prdm5 die Tumorentwicklung vom HCC zum ICC ändern kann. Analysen von Downstream-Targets zeigten, dass beide Transkriptionsfaktoren unterschiedliche Signalwege kontrollieren, was die Wichtigkeit der Wechselwirkung beider Faktoren für die Bestimmung der Entwicklung von primären Lebertumoren zeigt.

1. Introduction

1.1. Primary liver cancer

1.1.1. Etiology and risk factors

With more than 1 million newly diagnosed patients per year primary liver cancer (PLC) represents a major health problem[1]. The incidence rates were increasing by 21% from 2006 to 2016 especially in western countries. It is the fourth leading cause of neoplasia-related death with more than 800,000 people dying each year which is mainly based on the lack of reliable biomarkers, efficient therapies and late diagnosis[2-4].

The two most prominent subtypes of PLC are hepatocellular carcinoma (HCC) accounting for 80% of all PLC and the cholangiocarcinoma (CCA) counting for 10-20%. While the ratio between male and female is 3-5:1 for HCC it is less gender dependent for CCA with a ratio of 1.2-1.5:1[5]. HCC account for more than 700,000 deaths per year worldwide with still increasing incidence rates from 1.4/100,000 cases per year between 1976 and 1980 to 6.2/100,000 cases per year in 2011[6, 7].

HCC preferably develops in patients with chronic liver diseases like cirrhosis, non-alcoholic fatty liver disease (NAFLD), non-alcoholic steatohepatitis (NASH) or alcoholic steatohepatitis (ASH)[8, 9]. Chronic liver damage and inflammation due to obesity, metabolic disorders, alcohol abuse or infection with hepatitis B virus (HBV) or hepatitis C virus (HCV) are predispositions for these diseases. However, recent anti-HCV therapies lead to high success rates in eradicating HCV[10].

Classification of CCA is based on the localization within biliary tree. Extrahepatic tumors arising at the distal end are classified as distal CCA (dCCA) and extrahepatic tumors at the bifurcation of the common bile duct as perihilar CAA (pCCA) while intrahepatic tumors are classified as iCCA or ICC. However, these classifications are sometimes difficult to diagnose in patients which lead to misclassification within these tumor entities. As a consequence mortality rates are quite different between most reported studies. Some studies reported decreasing rates within the last years while other reported an increase up to 15-fold[11]. While in Eastern countries infections with liver flukes like *Opisthorchis viverrini* or *Clonorchis sinensis* are predominantly favoring ICC development in Western countries risk factors are more variable. It has

been shown that infection with HBV or HCV, or cirrhosis also increases the risk for ICC development as well as alcohol abuse and fatty liver diseases[12-15]. Interestingly, as described earlier these are also risk factors for HCC. Collectively, ICC as well as HCC both develop in a milieu of chronic liver damage and inflammation[16].

1.1.2. Diagnosis and treatment options

A major issue of liver cancer therapy is the diagnosis due to the lack of early symptoms. Most patients are diagnosed when they already have advanced HCC or ICC limiting their treatment options[2]. The use of biomarkers is generally a good tool for early detection of diseases. However, until now alpha-fetoprotein (AFP) is the only widely used biomarker for HCC. The problem is the lack of sensitivity and that this marker usually correlates with advanced stages reducing their predictive use. So, additional methods as imaging or biopsy are still necessary[17]. The only curative therapy for HCC is surgical removal of the tumors or total liver transplantation. However, due to late diagnosis and limited availability of donor organs only a small number of patients are eligible for surgical treatment[18, 19].

The only approved drug for first line HCC treatment is the multi-kinase inhibitor sorafenib which, however, can only give a survival benefit of 2.8 months[20]. Recently, regorafenib and cabozantinib were approved as a second line therapy for patients who formerly received sorafenib treatment which could further increase the survival for 2.8 and 2.2 months, respectively[21, 22]. Furthermore, due to good results from a phaseI/II study the checkpoint-blocking antibody nivolumab was also approved as second-line therapy after sorafenib treatment[23].

Similar to HCC diagnosis of ICC often occurs at late stages. The mostly used biomarker are carbohydrate antigen 19-9 (CA 19-9) and carcinoembryonic antigen (CEA), however, they are not sufficient for a clear diagnosis and histopathological analysis of a biopsy is still necessary in clinical routine[24]. Surgical resection is still the only curative option although the 5-year survival rate after resection is low (32%) due to high recurrence rates of the tumors[25-27]. A systemic therapy treatment with gemcitabine and cisplatin is the standard drug treatment, however, on average it can only prolong the survival by 3.6 months compared to gemcitabine alone[28]. By now, there is no targeted therapy which is approved for ICC.

1.1.3. Molecular and cellular pathogenesis

Both HCC and ICC develop in an environment of chronic damage and inflammation. Liver-resident immune cells as stellate or Kupffer cells mainly contribute to these circumstances via releasing pro-inflammatory cytokines or directly interacting with liver cells[29-32]. Although the liver has a remarkable regenerative capacity it can be exhausted under long-term damage. In the context of chronically damaged, cirrhotic livers dysplastic nodules develop, which show genetic aberrations[8, 33]. Similar to their risk factors HCC and ICC also share many of these genetic aberrations. Comparative analyses of different TCGA datasets showed that mutations in Tumor protein p53 (*TP53,* 25% in HCC, 21% in ICC), AT-rich interactive domain-containing protein 1A *(ARID1A,* 12% in HCC, 14% in ICC), myeloid/lymphoid or mixed-lineage leukemia (*MLL,* 5% in HCC, 5% in ICC) and synaptic nuclear envelope protein 1 (*SYNE1,* 5% in HCC, 3% in ICC) occur frequently in both tumor entities[34-37]. Summarizing the shared mutations into signaling pathways showed that cell cycle control and epigenetic regulation are key factors of HCC as well as ICC development[5].

However, each of the tumor types also harbors unique alterations. HCC for example often has mutations in Telomerase reverse transcriptase (*TERT,* 59-68%), catenin beta-1 (*CTNNB1,* 16-62.5%) or Janus kinase 1 (*JAK1,* 45.5%). Mutations enhancing telomerase activity were shown to be an early event to enhance regenerative capacity, while *CTNNB1* mutations lead to activation of pro-survival and proliferative Wnt/β-catenin pathway[38].

On the other hand ICC show mutations in Kirsten rat sarcoma viral oncogene homolog (*KRAS,* 54%), Isocitrate dehydrogenase (*IDH1/2,* 8-16%), BRCA1 associated protein-1 (*BAP1,* 20%) or fibroblast growth factor receptor 2 (*FGFR2*-fusion, 14-45%) (Fig. 1)[5, 39]. Especially *KRAS* mutations and *FGFR2*-fusion affect uncontrolled proliferation of these tumors. Importantly, mutational landscape of ICC strongly depends on liver-fluke infection status[40].

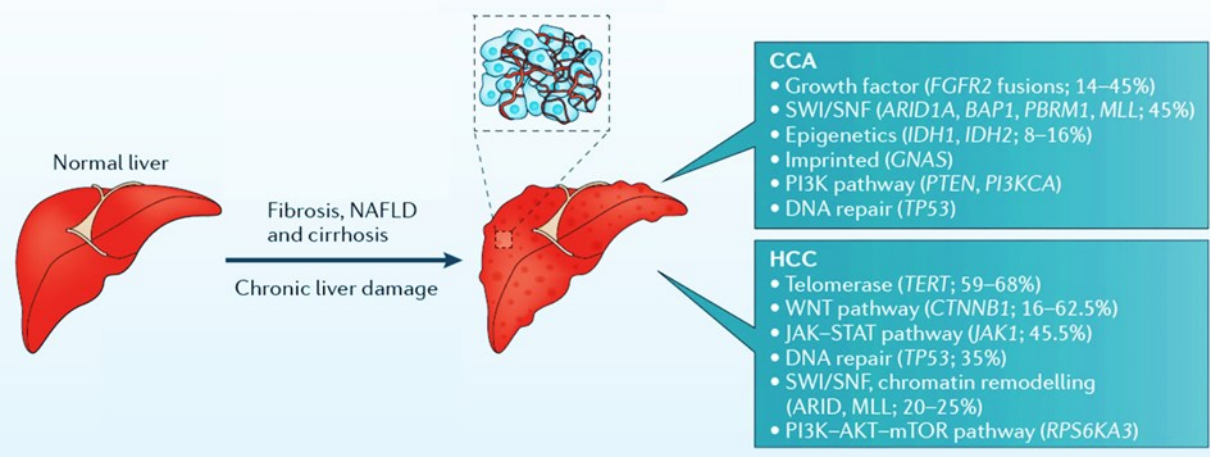

Figure 1 Genetic alterations in HCC and ICC Shown are the most prominent alterations and pathways in HCC and ICC development (adapted from[5]).

Studies to identify the cell of origin for HCC, ICC or mixed HCC/ICC tumors are conducted since many years, however, the results are still diverse. Historically it has been suggested that HCC derives from hepatocytes and ICC derive from cholangiocytes. However, there is increasing evidence that lineage commitment in PLC development is much more complex and plastic than that[41, 42].

Cholangiocytes were thought to be the cells of origin for ICC due to their similarities in morphology and histopathology. Evidences for this theory came from a lineage tracing mouse model where cholangiocyte specific deletion of *Trp53* together with thioacetamide (TAA) induced liver damage induced ICC development. However, this study also showed that hepatocytes express cholangiocarcinoma-specific Notch after liver injury suggesting that cholangiocytes are not the only cells of origin[43].

Liver progenitor cells (LPC) are able to differentiate into hepatocytes or cholangiocytes upon liver damage to maintain the regenerative capacity of the liver. It has been suggested by several studies that LPC can also develop into both HCC and ICC[44, 45]. Further, it has been demonstrated that suppression of p53 in LPC restricts stem cell capacity and can lead to HCC as well to ICC development[46]. Another study showed that IDH mutations in LPC lead to suppression of hepatocyte nuclear factor 4 alpha (HNF4alpha) favoring ICC initiation[33].

Interestingly, several recent studies further proved that hepatocytes can also develop into both HCC and ICC. These studies demonstrated that activation of the Hippo-YAP pathway or PI3kinase and MEK-ERK pathway in hepatocytes lead to HCC development[47, 48]. In contrast hepatocyte-specific forced activation of Notch or Notch and PI3kinase pathway induces ICC development[49-51]. This was accompanied with a

reprogramming of the hepatocytes into a biliary-type cell (Fig.2). Interestingly, it has further been shown that such a reprogramming event also occurs upon liver injury[52].

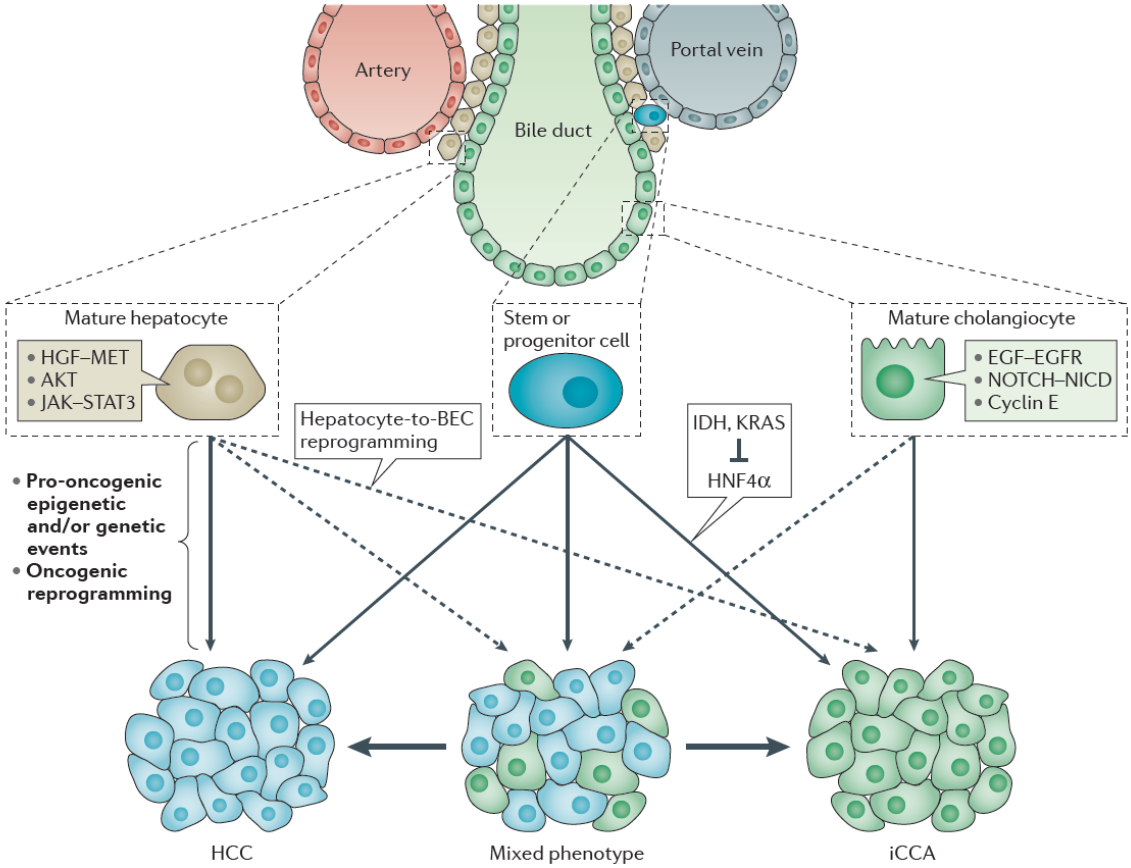

Figure 2 Cells of origin in PLC Overview of different putative cells of origin for HCC, mixed HCC/ICC and ICC and the main oncogenic drivers. (adapted from[5]).

Independent of the cell of origin the morphology of HCC and ICC are quite different. HCC usually growth in a dense or trabecular pattern without stromal parts. Immunohistopathological markers used for classification and diagnosis are gluthamine-synthetase (GS) or glypican 3 (GP3)[53]. In contrast, ICC growth occurs in glandular, bile-duct-like, structures with up to 60% of stroma tissue showing high similarities to pancreatic ductal adenocarcinoma (PDAC). Typically used markers for PDAC as well as ICC are cytokeratins 7 and 19 (K7/K19)[3, 54].

1.2. Cell death in chronic liver disease

Hepatocyte cell death frequently occurs in chronically damaged livers. There are two major forms of cell death the unregulated and the regulated one. Unregulated cell death, also described as necrosis, occurs under extreme conditions like physical, chemical or heat induced stress which directly disrupts cell integrity. Regulated cell

death on the other hand has a huge variety of different forms which have specific trigger events and downstream pathways[55].

The most prominent one is apoptosis which itself can be separated into the intrinsic and extrinsic from. Intrinsic apoptosis occurs under harmful conditions for the cell, for example starvation, high levels of reactive oxygen species (ROS), DNA damage or replicative stress[56, 57]. These conditions can alter the balance of pro- and anti-apoptotic members of the B-cell lymphoma 2 (BCL2) family like BAX, BAK or BOK and BCL-2 or BCL-XL, respectively[58-61]. The pro-apoptotic members can then induce permeabilization of the outer mitochondrial membrane (MOMP) resulting in a release of cytochrome-c and similar factors finally activating caspases as CASP9, CASP3 or CASP7[62-66]. These caspases then execute the final steps of the apoptotic cascade like DNA degradation and disruption of the membrane into apoptotic bodies[67, 68].

Extrinsic apoptosis can be triggered via cell death receptors as CD95 (also known as Fas) or members of the tumor necrosis factor receptor superfamily (TNFRSF). Activation of these receptors leads to induction of extensive downstream signaling cascade finally again activating same caspases as in the intrinsic pathway[69].

Another form of controlled cell death is necroptosis, also called controlled necrosis. Necroptosis can be triggered via activation of several receptors like TNFR1/2, Fas, toll-like-receptor (TLR) 3 or 4 or cell intrinsically via DNA sensors like DAI[70-72]. These receptors can then activate receptor interacting serin/threonine protein kinase (RIPK) 3 in a RIPK1 dependent or independent manner. However, this can only happen if caspase-8 is inactive as it is able to inhibit this mechanism[55, 69]. Activated RIPK3 then phosphorylates mixed-lineage kinase domain like pseudokinase (MLKL), subsequently forming multimeric pores integrating into the plasma membranes[73, 74]. This disruption of membrane integrity leads to release of high amount of damage-associated molecular patterns (DAMPs) as adenosintriphosphate (ATP), high mobility group box protein (HMGB) 1, interleukin 33 (Il-33) or cellular DNA and RNA. Due to this extensive release necroptosis is usually followed by inflammatory events (Fig. 3)[69, 75, 76].

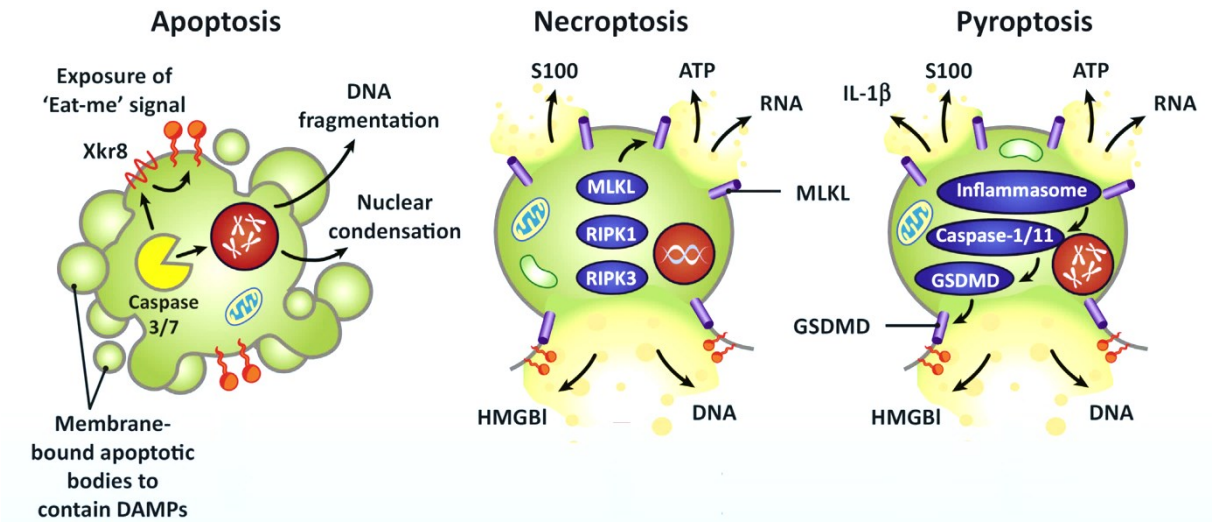

Figure 3 Cell death mechanisms Overview of the three most important cell death mechanisms and their intracellular pathways and DAMP release (adapted from [77]).

Apart from these two forms of controlled cell death there are many other forms of cell death. Especially in the last years more and more were identified or newly defined, e.g. pyroptosis which is induced by pathogen infection, anoikis which occurs when cells loose integrin-dependent anchorage or autophagy-related cell death[55, 78, 79]. Most of these cell death mechanisms share the core machinery, however, induction and execution differ between them.

Hepatocyte cell death is one of the most important markers for chronic liver damage or disease as NASH, NAFLD or cirrhosis (Fig.4)[69]. Necrosis induction in the liver is well studied in mouse models, nonetheless data on necrosis in livers of human patients are limited as necrosis is difficult to identify. It has been shown that acute intake of alcohol or drugs (e.g. acetaminophen (APAP)) or ischemia-reperfusion injury (IRI) can induce high amounts of necrosis in the liver[80].

Apoptosis is much more studied in the induction of liver diseases. Extrinsic apoptosis can be induced via HBV or HCV infection, activation of cell death receptors by pro-inflammatory immune cells or Fas activation by bile-acids in cholestatic livers. These conditions can lead to decreased cellular functions which then might induce further intrinsic apoptosis activation due to nutrient starvation or accumulation of endosplamic-reticulum (ER) or genotoxic stress[69, 81-83]. Importantly, hepatocytes are the most prominent but not the only cells undergoing cell death in the liver. It has been shown that also cholangiocytes or liver-resident immune cells undergo cell death in chronically damaged livers[84, 85].

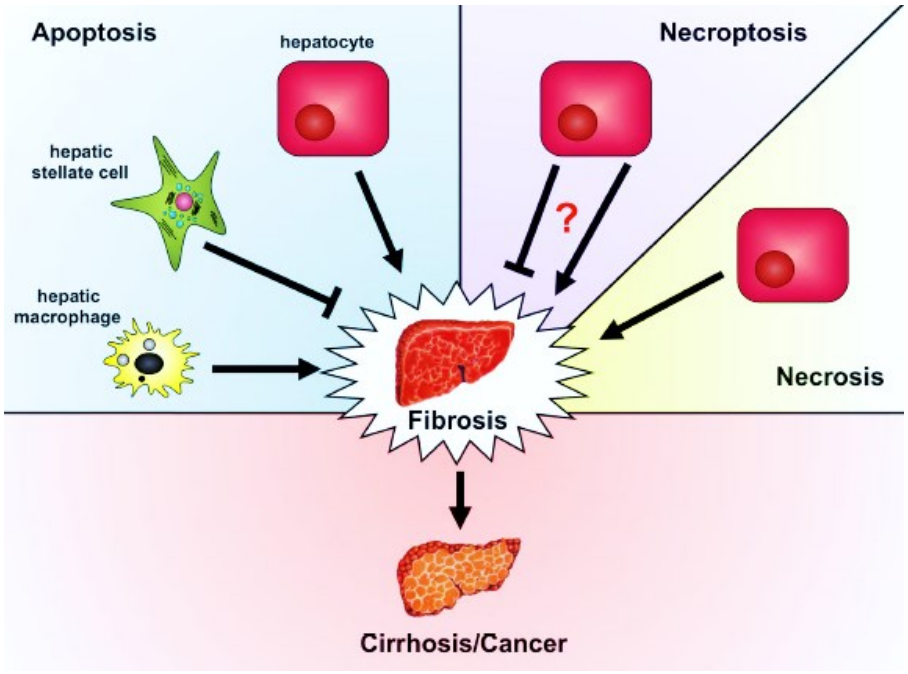

Figure 4 Cell death in liver cancer Cartoon of contributions from different cell death mechanisms to chronic liver disease and cancer (adapted from [86]).

The high amount of cell death contributes to liver disease and carcinogenesis in different ways. Especially necrotic or necroptotic damage leads to infiltration of immune cells via DAMP release. These immune cells then release cytokines enhancing hepatic stellate cell (HSC)-dependent fibrogenesis and hepatocyte or cholangiocyte proliferation. Uncontrolled levels of fibrosis induction and pro-proliferative pathways in hepatocytes, cholangiocytes or hepatic stem cells then lead to induction of PLC[69, 75, 86, 87]. There are several studies directly linking apoptosis to HCC development, however, for necroptosis this is much more controversial[69]. It has been reported that necroptosis is associated with ethanol-induced liver damage, cholestasis, NASH or fibrosis highlighting its importance in liver disease[88-90]. However, there is currently no evidence that necroptosis favors either HCC or ICC development.

1.3. Role of epigenetic in cellular fate and cancer

Epigenetic regulation is a fast and flexible mechanism to regulate gene expression upon external or internal stimuli but also to inherit information over several generations. In contrast to genetic alterations epigenetic regulation is reversible as no changes in the nucleotide sequences occur[91, 92]. The most important role of epigenetics lies in regulating the development of an organism. Usually a pluripotent

stem cell differentiates into a huge variety of other cell type via epigenetic regulation of its gene expression[93].

There are many different mechanisms of epigenetic regulation. One of them is the direct modification of the DNA at so called CpG-islands via DNA methyltransferases DNMT1, DNMT3A or DNMT3B. These enzymes methylate C^5 position of cytosines located 5' to guanosines. These CpG-islands are mainly found in the vicinity of promotor regions enabling them to affect the transcription of genes via regulating the binding of factors of the transcription machinery[94, 95].

Another important epigenetic characteristic is the chromatin appearance which is mostly affected by interaction with histones. Histones are proteins usually occurring in an octamer form bound to DNA (147 bp per octamer) due to their positive charge[96]. This charge can be regulated via modifying acetylation sites by histone acetyltransferases (HATs) or histone deacetylases (HDACs). Depending on the acetylation status of histones the chromatin occurs in an open and active form or in a condensed inactive form. However, histones can also be modified via methylation, ubiquitination or phosphorylation (Fig. 5). This can be either activating or inactivating depending on the site of modification within the histones and the target structure for these modifications[97-99].

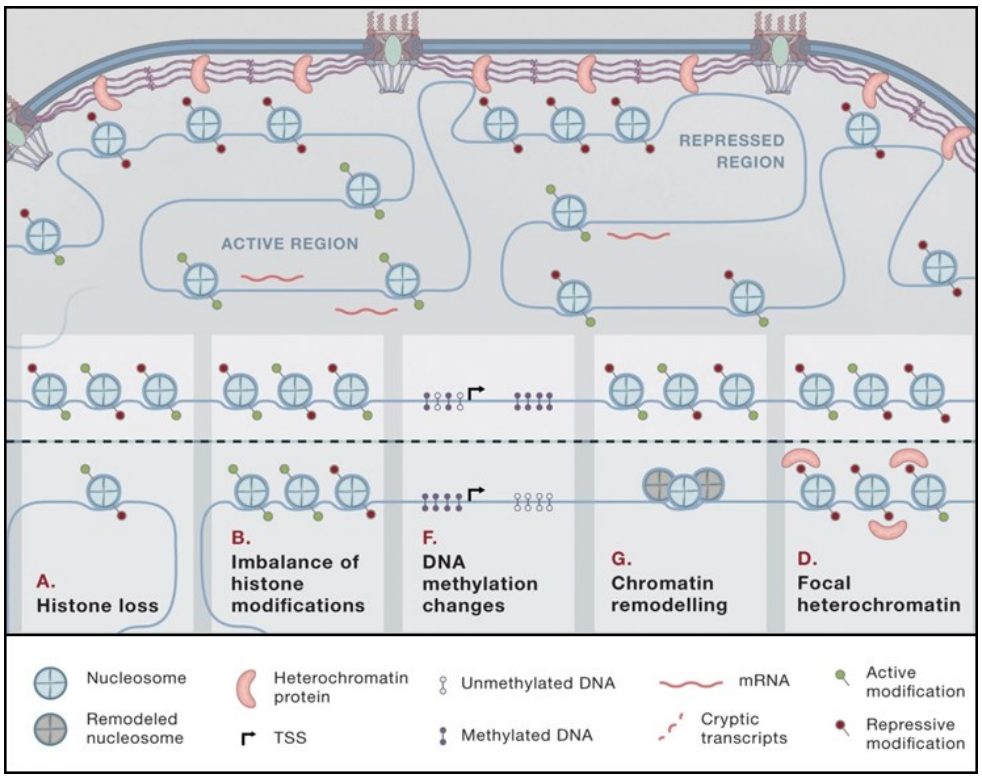

Figure 5 Epigenetic regulations in the cell Summary of the main regulations for epigenetic changes influencing gene expression (adapted from [100]).

One such target structure is the chromatin remodeling complex switch/sucrose non-fermentable (SWI/SNF) which is able to alter histone and chromatin structure and interaction thereby affecting gene transcription[96]. The SWI/SNF complex consists of several subunits and co-regulators which are frequently mutated in HCC and ICC[5].

It has been shown that lineage commitment through epigenetic regulations in hematopoietic cells is directly affected by environmental conditions. For example non-specialized macrophages gain different histone modifications after residing in different organs. Especially methylation of H3K4 in promotor and enhancer regions of pioneer transcription factors alter gene expression and pathways resulting in tissue-specific differentiation (Fig. 6)[101]. Other studies on macrophage specialization showed that transforming growth factor beta (TGFβ)/SMAD pathway or retinoic acid (RA)/GATA6 pathway activation via environmental signals influences lineage commitment[102-104].

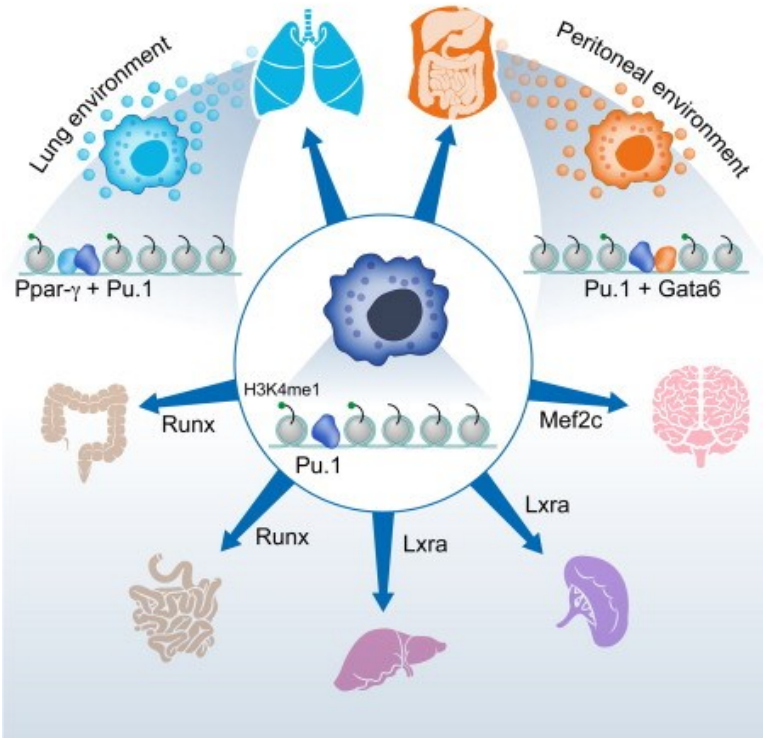

Figure 6 Environment-dependent fate decisions of macrophages Parental macrophages change their subtype via epigenetic regulation which depends on the microenvironment present in different organs (adapted from[101]).

It has been shown many years ago that epigenetics also plays an important role in cancer via activation of oncogenes or suppression of tumor suppressors which has also been reported for HCC and ICC[105-107]. Studies identified promotor hypermethylation for *cyclin-dependent kinase Inhibitor 2A* (*CDKN2A,* 62.5% HCC, 50% ICC), *Ras association domain family member 1* (*RASSF1A,* 60% HCC, 65%

ICC*)* or *cadherin 1* (*Cdh1,* 33% HCC, 43% ICC*)* pinpointing the importance as well as similarity of epigenetic dysregulation in both cancer types[108-111]. As mentioned earlier, the chromatin remodeling complex SWI/SNF and its pathway is highly deregulated in both tumor entities. Especially mutations in *ARID1A* which is a member of the SWI/SNF complex frequently occur in both tumor types. Further, mutations in the MLL family representing important histone methyltransferases are also increased in both tumor entities[5]. Interestingly, *IDH* which is frequently mutated in ICC leads to epigenetic silencing of *HNF4alpha* in hepatoblasts inhibiting hepatocyte differentiation and favoring ICC development.[33]

1.4. Aim of the study

Until now it is unknown which factors or circumstances favor the development of either HCC or ICC in chronically damaged liver of the same etiology.

The first aim of this study was to identify the cell of origin of HCC and ICC induced by the same oncogenes via hydrodynamic tail vein injection (HDTV) or *in vivo* liver electroporation (Epo), respectively. Then, we set out to analyze if somatic mutations might account for differences in tumor development. We further aimed to perform functional analyses if the conditions followed by HDTV or Epo might account for lineage commitment and to subsequently characterize these conditions. This characterization was focused on the inflammatory milieu as well as cell death occurrence in the liver. We focused on examining putative connections between the microenvironment and lineage commitment utilizing functional experiments.

Finally, the goal was to characterize a potential role of epigenetic regulation for HCC vs. ICC development and aimed to functionally probe epigenetically regulated candidate genes.

2. Material and Methods

2.1. Material

2.1.1. Chemicals

If not mentioned elsewhere, chemicals and solutions used in this study were purchased from the following companies: AppliChem, Biosciences, Carl Roth, Fermentas, Fluka, GE Healthcare, Invitrogen, Life Technologies, Merck, Millipore, Promega, Peqlab, Serva and Sigma Aldrich.

2.1.2. Enzymes

All restriction enzymes, DNAseI, calf intestinal alkaline phosphatase (CIP) or recombinant shrimp alkaline phosphatase (rSAP) and T4-DNA-ligase were purchased from NEB, dispase and collagenase were purchased from Roche or Serva, Platinum Pfx Polymerase was purchased from Invitrogen and proteinase K was purchased from Sigma Aldrich.

2.1.3. Kits

Table 1 Kits used in this study

Kit	Company
Mouse Gene 2.0 ST Array	Affymetrix
GeneChip WT PLUS Reagent Kit	Affymetrix
GeneChip Hybridization, Wash, and Stain Kit	Affymetrix
SureSelect Mouse AllExon XT Target Enrichment Kit	Agilent
TaqMan Reverse Transcriptase Kit	Applied Biosystems
PCR SYBR Green MasterMix	Applied Biosystems
DC-Protein Assay	Biorad
SimpleChIP kit	Cell Signaling
Q5 Site-Directed Mutagenesis Kit	NEB
KAPA Hyper Library Prep Kit	PEQLAB
Plasmid Maxi Kit	Qiagen
Qiaquick Gel Extraction Kit	Qiagen

RNeasy Mini Kit	Qiagen
QIAamp MicroKit	Qiagen
QIAGEN MinElute kit	Qiagen
QIAGEN PCR Cleanup kit	Qiagen
In Situ Cell Death Detection Kit Fluorescein	Roche
In Situ Cell Death Detection Kit TMR-Red	Roche
Accel-NGS 2S Plus DNA Library Kit	Swift Bioscience
PrimeScript RT Master Mix	Takara Clontech
SYBR Premix Ex Taq (Tli RNase H Plus)	Takara Clontech
Arcturus HistoGene LCM Frozen Section Staining Kit	Thermo Scientific
Qubit® dsDNA HS Assay Kit	Thermo Scientific
DAB solution	Zytomed

2.1.4. Buffers and solutions

Table 2 buffers and solutions used in this study

buffer/ solution	composition
ACK-buffer	150 mM NH_4Cl, 10 mM KHCO3, and 0.1 mM EDTA
Anesthesia	2 ml Ketamin (50 mg/ml), 500 µl Xylazin (20 mg/ml), ad 10 ml 0.9% NaCl
ATAC-lysis-buffer	10 mM Tris-HCl, pH 7.4, 10 mM NaCl, 3 mM $MgCl_2$, 0.1% IGEPAL CA-630
Cell-medium	500 ml DMEM, 5 ml Pen/Strep, 5 ml 100X MEM NEAA, 5ml 100X sodiumpyruvate, 50ml FCS
Digestion medium	1 ml HBS (10x), 10,000 units dispase, 1 units collagenase, ad 10 ml DMEM
gDNA extraction buffer	20 mM Tris-HCl (pH 8.0), 100 mM EDTA, 100 mM NaCl 1 % SDS, 0,5 mg/ml Proteinase K
HBS (10x)	7.5 mM Na_2HPO_4 (pH 7.0), 1.4 M NaCl, 250 mM HEPES, 60 mM Dextrose, 50 mM KCl
Laemmli- buffer (5x)	150 mM Tris-HCl (pH 6.8), 6 % SDS, 15 mM DTT, 30 % glycerol, 0.25 % bromphenolblue
LB-medium	1 l H20, 20 g LB-powder (Roth), 50 mg/l ampicillin
NP40 lysis buffer	50 mM TrisHCl (pH 7.5), 15 0mM NaCl, 0,5 % NP-40, 1x Complete mini® (Roche)
PBS (10x)	100 mM Na_2HPO_4*$2H_2O$, 20 mM KH_2PO_4, 1,37 M

	NaCl, 27 mM KCl (pH 7,4)
PBST	0.1 % Tween 20 in PBS
Permeabilization-buffer	5 % NGS, 0.2 % Triton X-100, 0.1 % Tween 20 in PBS
PFA in PBS	4 % PFA in PBS (pH 7.4)
SDS-running buffer (10x)	250 mM Tris Base, 1.92 M Glycine, 1 % SDS
Sodium citrate buffer	10 mM $C_6H_5Na_3O_7$ (pH 6.0)
TAE (50x)	2 M Tris Base (pH 8.5), 1 M glacial acetic acid, 50 mM EDTA
TBS (10x)	500 mM Tris-HCl, (pH 7.4), 1500 mM NaCl
TBST	0.1 % Tween 20 in TBS
Transfer buffer	48 mM Tris-HCl (pH 8.3), 39 mM Glycine, 20 % Methanol, 0,037 % SDS

2.1.5. Antibodies

Table 3 antibodies used in this study

Primary antibodies:

clone	antigen	species	company	conjugation	application
A-20	Tbx3	goat	Santa Cruz		ChIP
MABE972	Prdm5	ms	Merck		ChIP
30-F11	CD45	rat	BD	BV421	FC
HK1.4	Ly6C	rat	eBioscience	Alexa Fluor 488	FC
M1/70	CD11b	rat	eBioscience	PE	FC
53-6.7	CD8a	rat	eBioscience	PE	FC
17A2	CD3	rat	eBioscience	eFluor 660	FC
RB6-8C5	Ly-6G (Gr-1)	rat	eBioscience	PE-Cyanine7	FC
RM4-5	CD4	rat	eBioscience	APC	FC
BM8	F4/80	rat	BioLegend	APC	FC/IF
TROMA-III	K19	rat	DSHB		IHC/IF
GEN135-35-9	pRIPK3	rb	Genentech		IHC
1G6.1.4	RIPK3	rat	Genentech		IHC
C-19	HNF4α	goat	Santa Cruz		IHC
1A8	Ly6G	rat	BD		IHC
M5/114.15.2	MHCII	rat	Novus Biologicals		IHC

RA3-6B2	B220	rat	BD	IHC
SP7	CD3	rb	Zytomed	IHC
A2547	αSMA	ms	Sigma Aldrich	IHC
5A1E	cl. caspase 3	rb	Cell Signaling	WB
EPR9515(2)	pMLKL (S345)	rb	abcam	WB
hVIN-1	vinculin	ms	Sigma Aldrich	WB
11H10	tubulin	rb	Cell Signaling	WB
AC-74	beta-actin	ms	Sigma Aldrich	WB
orb32399	MLKL	rb	Biorbyt	WB

Secondary antibodies:

clone	antigen	species	company	conjugation	application
	anti-rat		Invitrogen	Alexa-Fluor 594	
	anti-goat		Santa Cruz	biotin	
	anti-polyvalent		Thermo Scientific	biotin	

2.1.6. Oligonucleotides

Table 4 oligonucleotides used in this study

qPCR Primer sequences	
Gene	Sequence
ß-actin fw	CCACCGATCCACACAGAGTA
ß-actin rev	GGCTCCTAGCACCATGAAGA
Tbx3 fw	CCACCTCCAACAACACGTTCT
Tbx3 rev	TAAGGAAACAGGCTCCCGAA
Prdm5 fw	TCAGAAAAGCGGCCTTATAACTG
Prdm5 rev	CCACTTGATCGAGCCTCTTGAAG
Rip3 fw	GCGGCCGCGGatggttaatcttcgtaatgag
Rip3 rev	GGGACGCGTctacttgtggaagggct
sgRNA sequences	
Gene	Sequence
p19Arf	GCACTGTGAGGATTCAGCGCG
shRNA sequences	
Tbx3_1	TGCTGTTGACAGTGAGCGACAGGCTGCTGTTGCTTTGAAATAGTGAAGC CACAGATGTATTTCAAAGCAACAGCAGCCTGGTGCCTACTGCCTCGGA

Tbx3_2	TGCTGTTGACAGTGAGCGCCACGACTATTGGACAAAGTATTAGTGAAGC
	CACAGATGTAATACTTTGTCCAATAGTCGTGTTGCCTACTGCCTCGGA
Prdm5_1	TGCTGTTGACAGTGAGCGACACAGGAAGATTCATGAGATATAGTGAAGC
	CACAGATGTATATCTCATGAATCTTCCTGTGCTGCCTACTGCCTCGGA
Prdm5_2	TGCTGTTGACAGTGAGCGCTCGACACAAGATGACACACAATAGTGAAG
	CCACAGATGTATTGTGTGTCATCTTGTGTCGAATGCCTACTGCCTCGGA
Ren	TGCTGTTGACAGTGAGCGCAGGAATTATAATGCTTATCTATAGTGAAGC
	CACAGATGTATAGATAAGCATTATAATTCCTATGCCTACTGCCTCGGA

Cloning of Fam72aMUT

Fam72a for	ggcgcgccGCCGCC ATGTCTACCAACAACTGTACTTTCAA
Fam72a rev	GGGACCGGTTCATCGAATATACTCTTCTGCTGA
Fam72aMUT for	CCACGTAATTTTTCCATGTAGTTC
Fam72aMUT rev	TAGCCTACAATGTTCCCAC

Cloning of Prdm5

AscI Prdm5 for	GGCGCGCCGCCGCCatgctgggcatgtacgt
NheI Prdm5 rev	GGGGCTAGCTTAGCTGTCAGCTACCCCA

Cloning of Tbx3

AscI Tbx3 for	ggcgcgccGCCGCCatgagcctctccatgagag
AgeI Tbx3 rev in PolyI:	GGGACCGGTTTAAGGGGACCCGCT

2.1.7. Plasmids

The sleeping beauty plasmids (SB13) were provided by David Largaespada. Transposon plasmids encoding c-Myc and Nras (pCaMIN) or c-Myc and AKT-1 (pCaMIA) were generated by Florian Heinzmann and Anja Hohmeyer, respectively, in our lab. Transposons encoding Fam72a and mutated Fam72a (259G>T), Tbx3 (Tbx3 OE) and Prdm5 (Prdm5 OE) were also cloned by Florian Heinzmann in our lab. The retroviral vector including TRE3G promotor, EGFP sequence, mirE shRNA backbone, PGK promotor, puromycin resistance cassette, IRES and an rtTA3 coding sequence (RT3GEPIR) was provided by Johannes Zuber. The plasmid encoding Cas9n and an sgRNA targeting *p19* (CCsgp19) based on the px330 plasmid was kindly provided by Wen Xue. The shRNA sequences targeting *Tbx3* or *Prdm5* were subcloned into RT3GEPIR or pCAMIN by Florian Heinzmann and Marco Seehawer, respectively.

2.1.8. Bacteria

For transfections and overnight cultures Subcloning efficiency DH5α *Escherichia coli* cells from Invitrogen were used.

2.1.9. Cell lines

For virus production the genetically modified human embryonic kidney cell line (HEK293T) Phoenix-AMPHO (ATCC:CRL-3213) was used. HCC or ICC cell lines used in this study were isolated from tumors of *p19*$^{-/-}$ mice after pCaMIN/SB13 delivery via hydrodynamic tail vein injection or *in vivo* liver electroporation. From each cell line single cell lines were generated via serial dilutions.

2.1.10. Mouse strains

Wildtyp mice (C57BL/6, CB17, C3H/HeN) and immunodeficient SCID/beige (CB17) as well as *Rag2*$^{-/-}$ (C57BL/6) knockout mice were purchased from Charles River or the Jackson Laboratory. *p19*$^{-/-}$ (C57BL/6) mice have been generated by Charles Sherr and were obtained from Scott W. Lowe. *AlbCre* x *MLKL*$^{fl/fl}$ (C57BL/6) were provided by Mihael Vucur and Tom Luedde. *5xTLR* KO mice (C57BL/6) were kindly provided by Thorsten Buch. *TLR 2/4* KO (C3H/HeN) mice were obtained from Alexander Weber. *AlbCre* mice were purchased from The Jackson Laboratory and crossed with the ROSA$^{mT/mG}$ mice (generated by Liqun Luo, obtained from Johannes Zuber) and were intercrossed with *p19*$^{-/-}$ mice by Lisa Hoenicke.

2.2. *In vivo* experiments

2.2.1. Mouse husbandry

All experimental mouse studies have been approved by the responsible local authority (Regierungspräsidium Tübingen), Baden-Württemberg. Mice were housed in type II long cages with food and water *ad libitum* under specific pathogen-free conditions according to guidelines of the University of Tübingen.

2.2.2. Hydrodynamic tail vein injection (HDTV)

For HDTV 25 µg transposon plasmid and 5 µg SB13 transposase plasmid were mixed and filled up with 0.9% sodium chloride solution to 10% of the mouse bodyweight. For experiments in wt mice, additional 10 µg of the Crispr/Cas9-sgp19 plasmid was added. Mice were fixed in a restrainer and the tail was warmed with water. Then the solution was injected into the tail vein of the mouse with a syringe and a 25G needle within 5 to 10 seconds.

2.2.3. In vivo liver electroporation (Epo)

Prior to Epo 25 µg transposon plasmid was mixed with 5 µg SB13 transposase plasmid and filled up with TE buffer to 50 µl. For experiments in wt mice 10 µg of Crispr/Cas9-sgp19 plasmid was added. Mice were anaesthetized with a mix of ketamine (100 mg/kg bodyweight) and xylazin (10 mg/kg bodyweight) and a small laparotomy below the thorax was conducted. The left lateral liver lobe was exposed and the plasmid solution was injected with a 30G needle into the liver capsule. The injected lobe was placed between tweezer of an electrode (CUY650P5, 5 mm diameter) and 2 electric pulses (75 V, 75 ms, 500 ms interval) were applied with a Square Wave Electroporator (CUY21SC, Nepa Gene, Japan). The liver lobe was placed back and the mouse was closed with resorbable suture material and individual stitches.

2.2.4. Bile duct ligation

Mice were anaesthetized and a laparotomy was performed as described earlier. The common bile duct was exposed with micro forceps and ligated with non-resorbable suture material. The liver was placed back and the mouse was closed with resorbable suture material and single stitches.

2.2.5. Liver perfusion

Mice were anaesthetized and liver perfusion medium (Invitrogen) was injected through the vena cava for 15 min. Afterwards it was exchanged with collagenase

(Serva) and Ca^{2+} supplemented medium for 15 min. Liver was harvested and hepatocytes were detached via gently shaking and purified via Percoll centrifugation.

2.2.6. Subcutaneous tumor cell injection

Cells were detached with 0.05% trypsin/EDTA working solution and washed 2 times with PBS and separated through a 100 µm mesh. Then they were counted using a counting chamber and diluted in sterile PBS to a concentration of $2x10^6$/100 µl. Mice were anaesthetized as described before and cells were injected into the left and right flank with a 30G needle.

2.3. Histological methods

2.3.1. Hematoxylin/eosin (H&E) and immunohistochemistry staining (IHC)

Collected tissue samples were fixed with 4% paraformaldehyde (PFA) o/n and embedded in paraffin. They were cut with a microtome into 4 µm thick slices and dried at 65°C o/n. They were hydrated via incubation in xylol, xylol/ ethanol (50%/50%), 90% ethanol, 70% ethanol, 50% ethanol and water for 3 min each. For H&E staining samples were incubated 8 min in hematoxylin (Gil II), rinsed with water and developed under running tap water for 10 min. Afterwards they were incubated in eosin Y solution for 3 minutes, washed with water and dehydrated via incubation in 90% ethanol, xylol/ ethanol (50%/50%) and xylol for 5 min each. Finally, samples were mounted with NeoMount and covered with a glass slide. For IHC antigen retrieval was performed after the hydration steps in boiling sodium citrate buffer (10 mM, pH 6.0, 0.5% Tween-20) in a rice cooker for 15 min. Then endogenous oxidases were saturated using 3% H_2O_2 for 5 min. The samples were circled with a PAP pen and blocked with blocking solution (Zytomed) or 5% BSA for 10 min and incubated with the primary antibody o/n at 4°C. Slides were washed with TBST and incubated with the secondary antibody for 1h at RT. After another washing step biotin-HRP solution (1:300, Dako) was added for 15 min and samples were washed again. DAB developing solution (Zytomed) was added until specific staining was visible under the microscope. Developing was then stopped via adding water and samples were counterstained with hematoxylin only and mounted as described before.

2.3.2. Native fluorescence staining

To detect native fluorescent signal in mouse livers samples were harvested and fixed with 4% PFA for 4 h at 4°C. Samples were then dehydrated in 30% sucrose solution at 4°C o/n and embedded in TissueTek (Sakura) at -80°C. Samples were cut with a cryotstat at -20°C into 6 µm slices and mounted with VECTASHIELD HardSet mounting medium with DAPI (Vector Labs).

2.3.3. Immunofluorescence staining (IF) on paraffin slides

Samples from ROSA$^{mT/mG}$ x *AlbCre x p19*$^{-/-}$ mice were fixed with 4%PFA and embedded in paraffin which quenched native tomato signal while native GFP signal was still visible. Samples were then cut and processed as described before until incubation with the primary antibody. Then AlexaFluor 594 coupled secondary antibody was added for 1 h at RT and slide was washed with PBST. Finally slides were mounted with VECTASHIELD HardSet mounting medium with DAPI (Vector Labs).

2.3.1. Immunofluorescence staining (IF) on cells

Cells were plated on Tissue Culture Chambers (Sarstedt) and incubated o/n. Then cells were fixed with 4% PFA at 4°C for 10 min, washed with PBST and permeabilized with permeabilization buffer (2.1 Materials) for 60 min at RT on a shaker. After three washing steps with PBST primary antibody was incubated in 1% NGS in PBST for 60 min at RT on a shaker. Samples were washed three times with PBST and fluorescent dye-labelled secondary antibody in 1% NGS in PBST was added for 60 min at RT under shaking. Samples were again washed three times with PBST and finally mounted with VECTASHIELD HardSet mounting medium with DAPI (Vector Labs).

2.3.2. Terminal deoxynucleotidyl transferase dUTP nick end labeling (TUNEL)

TUNEL staining on cryosections has been performed with the CellDeath Detection Kit Fluorescein (Roche) according to the manufacturer's protocol. For staining of

ROSA$^{mT/mG}$ x *AlbCre x p19*$^{-/-}$ mouse samples CellDeath Detection Kit TMR Red (Roche) was used. For quenching native tomato but retaining native GFP signal protocol was adjusted as following: Fixation step was reduced to 5 min, permeabilization step was reduced to 2 min and incubation duration was reduced to 15 min.

2.3.3. Laser capture microdissection (LCM)

For LCM procedure samples were directly embedded in TissueTek and frozen at -80°C. They were cut with a cryostat at -20°C and stained with Arcturus HistoGene LCM Frozen Section Staining Kit to maintain DNA quality. LCM was then performed using a Zeiss PALM MicroBeam and PALMRobo Software. From each sample material from at least 10 sections was collected.

2.4. Cell culture

2.4.1. Standard cell culture

Cells were maintained under sterile conditions in an incubator at 37°C and 7.5% CO^2 in modified DMEM media (2.1. Materials). When cells reached a confluency of 90% they were washed with PBS and detached using 0.05% trypsin/EDTA solution and 10% were plated on a new dish.

2.4.2. Establishing primary cell lines from tumors

Tumors were harvested under sterile conditions and chopped with a scalpel into small pieces. 1 ml of digestion medium (2.1 Materials) was added and incubated at 37°C for 30 min with constant shaking. Cell suspension was then filtered through a 100 µm nylon mesh and cells were washed 2 times with PBS. Finally, cells were plated onto gelatin (1%) coated plates and incubated under normal conditions.

2.4.3. Production of retroviral particles

Retroviral production was conducted using the Phoenix system. At 70% confluency Phoenix Ampho cells were treated with 25 µM chloroquine and incubated for 30 min at 37°C.Then, 25 µg of plasmid was mixed with 62.5 µl 2M $CaCl_2$ and filled up with water to 500 µl. 500 µl of HBS buffer was placed into a FACS tube and the plasmid mix was slowly dropped into the HBS buffer while constantly bubbling air into the buffer. The mix was incubated for 10 min and slowly transferred to the cells. After 12 h the media was refreshed. 24 h later the supernatant was harvested and filtered through a 0.45 µm filter.

2.4.4. Stable transduction of cells

Target cells were grown to 20% confluency and treated with 10 µg/ml polybrene for 15 min and 100 µl of viral supernatant was added. After 24 h this procedure has been repeated. After additional 24 h successfully transduced cells were selected with 4-6 µg/ml puromycin for 48 h.

2.4.5. Flow cytometry analysis

Liver samples were harvested and cut with a scalpel into small pieces. Then tissue was digested using collagenase (0.5mg/ml, Serva, NB 4G) in DMEM/HBS (1:1) for 30 min at 37°C. Afterwards cold medium was added and cells were separated using a 70 µm cell strainer and centrifuged at 800 rpm for 5 min. Erythrocytes were lysed with ACK buffer and cells were resuspended in 2%BSA/PBS and incubated with primary antibody for 30 min at 4°C. Then 1 µg/µl DAPI was added per sample and samples were measured with a FACSCanto (BD Biosciences). Data was analyzed with FlowJo (Tree Star).

2.5. Molecular biology techniques

2.5.1. Plasmid preparation from bacterial cultures

For high yield preparation 350 ml LB-medium including ampicillin was inoculated with the respective bacteria and incubated o/n at 37°C under constant shaking. Then MaxiPrep Kit from Qiagen has been used according to the protocol.
For low yield preparation 5 ml LB-medium including ampicillin were inoculated with bacteria and incubated o/n at 37°C under constant shaking. Then, bacteria were pelleted via centrifugation with 2,000 rpm for 5 min and resuspended in 200 µl buffer P1. 200 µl buffer P2 was added and incubated for 5 min to lyse the cells and neutralization was done via adding 200 µl buffer P3. The solution was mixed and cell debris was pelleted via centrifuging at 13,300 rpm for 10 min. 500 µl supernatant was transferred into new reaction tubes and DNA was precipitated with 400 µl isopropanol. Then samples were centrifuged at 13,300 rpm for 15 min to pellet DNA and pellet was washed with 70% ethanol at 13,300 rpm for 5 min. The pellet was air-dried and re-suspended in 30 µl water.

2.5.2. Digestion of specific DNA fragments with restriction enzymes

5 µg of genetic vectors or PCR products were digested with 0.5 µl of enzyme and the respective buffer (NEB) for 2 h at 37°C in a volume of 20 µl. If size separation was necessary the solution was run on an agarose gel (1.5%) at 120 V for 30 min and the correct band was cut out. Gel piece or digestion reaction was purified with QIAquick Gel Extraction Kit (Qiagen) according to manufacturer's protocol.

2.5.3. Dephosphorylation of DNA fragments

Backbone was dephosphorylated with 1 µl recombinant shrimp alkaline phosphatase (NEB) with CutSmart buffer (NEB) in a total volume of 20 µl and column purified as described before.

2.5.4. Ligation of DNA fragments

Ligation was performed using 0.5µl T4-ligase (NEB) and ligase buffer (NEB) over night with increasing temperature from 4°C to RT in a total volume of 10 µl and vector and insert according to the following formula: $m(insert) = \frac{bp(Insert)}{bp(vector)} * 6 * 100\ ng.$

2.5.5. Transformation of bacteria

Subcloning Efficiency DH5α cells were mixed with 1/10 (v/v) plasmid solution and incubated on ice for 30 min. They were heat-shocked at 42°C for 20 sec and incubated again for 2 min on ice and finally plated on LB-agar plates with ampicillin and incubated o/n at 37°C. Next day, single colonies were picked and used to inoculate 5 ml LB-medium with ampicillin which was incubated o/n at 37°C under constant shaking. Then plasmids were isolated as described earlier and sent for Sanger sequencing to Seqlab/Microsynth to check for integrity.

2.5.6. Polymerase chain reaction (PCR)

Polymerase chain reaction (PCR) was conducted with Platinum Pfx Polymerase (Invitrogen) to amplify DNA fragments. Additional restriction sites were added with specifically designed primers (Table 4). PCR was conducted according to the following protocol (X= melting temperature -3°C):

Table 5 PCR program for Pfx polymerase

PCR program		
94 °C	2 min	
94 °C	15 sec	} 25-35 cycles
X °C	30 sec	
68 °C	1 min per kb	
68 °C	5 min	
4 °C	∞	

2.5.7. Mutagenesis

Mutagenesis for Fam72a (259G>T) mutations was done with Q5 Site-Directed-Mutagenesis Kit (NEB) according to the manufacturers protocol.

2.5.8. Isolation of genomic DNA

Samples were harvested and minced with a homogenizer into small pieces. They were digested using 300 µl gDNA extraction buffer at 56°C o/n under constant shaking. Digestion was inactivated at 95°C for 5 min and cell debris was precipitated by adding 50 µl of 5 M NaCl and again incubating for 5 min at 95°C. Samples were centrifuged at 13,300 rpm for 10 min and supernatant was transferred into new reaction tubes. Then 2/3 (v/v) of isopropanol was added and centrifuged at 13,000 rpm and 4°C for 30 min to precipitate DNA. Pellet was washed with 500 µl 70% EtOH at 13,300 rpm for 10 min and finally resuspended in 100 µl water. Then 100 µl chloroform/phenol/isoamylalcohol (25:24:1) was added and phase separation was achieved using PhaseLockGel tubes at 13,300 rpm for 10 min at 4°C. Upper phase was transferred into new reaction tubes and DNA was precipitated with 10 µl 3 M NaOAc and 300 µl EtOH for 30 min at -20°C and centrifugation at 13,300 rpm for 15 min at 4°C. Pellet was then washed with 500 µl 70% EtOH and pellet was resuspended in water.

2.5.9. RNA Isolation

Samples were harvested and 1 ml Qiazol (Qiagen) was added. Tissue samples were homogenized with an electric homogenizer. Then 200 µl chloroform were added and vortexed for 15 sec and incubated for 3 min. Phase separation was achieved by centrifugation with 3,500 rpm for 15 min at 4°C. The RNA containing upper phase was transferred into a new reaction tube and RNA was precipitated with 1 ml isopropanol and pelleted via centrifugation with 3,000 rpm for 10 min at 4°C. Pellet was washed with 70% ethanol at 2,500 rpm for 5 min at 4°C and then air-dried. It was then resuspended in 87.5 µl water and DNA digestion has been performed adding 10 µl DNaseI buffer and 2.5 µl DNaseI (NEB) for 30 min at RT. Then 250 µl ethanol were added and the RNA was purified with the RNeasy Mini Kit from Qiagen according to the protocol.

2.5.10. Measuring DNA and RNA concentration

DNA or RNA concentration was measured with a NanoDrop1000 (PEQLAB) using 1 µl of the solution.

2.5.11. Quantitative Real-time-PCR (qRT-PCR)

First, cDNA synthesis has been performed with the TaqMan kit (Applied Biosystems) or the PrimeScript RT MasterMix (Takara) according to the respective protocol. Then qRT-PCR was conducted using the SYBR Green Mastermix (Applied Biosystems) or SYBR Premix Ex Taq (Takara) according to the protocol on a 7300 Real Time PCR System (Applied Biosystem). Data was analyzed with the 7500 software (Applied Biosystems) using the $2^{(-\Delta\Delta Ct)}$-method.

2.6. Biochemical methods

2.6.1. Protein Isolation

Samples were harvested and 500 µl NP40 buffer has been added. Tissues were additionally homogenized using an electric homogenizer. The mix was incubated on ice for 15 min while vortexing every 5 min. It was then centrifuged at 13,300 rpm for 30 min at 4°C and the protein containing supernatant was transferred into a new reaction tube.

2.6.2. Measuring protein concentration

Protein concentrations were measured with the DC Protein Assay from Biorad according to the manufacturer's protocol.

2.6.3. Sodium dodecyl sulphate polyacrylamide gel electrophoresis (SDS-PAGE)

To separate proteins according to their molecular weight SDS-PAGE has been performed using the Mini-PROTEAN Tetra Vertical Electrophoresis Cell device from Biorad. First SDS gels were cast according to the following table:

Table 6 composition of separating and stacking gel

separating gel		**stacking gel**	
Total	10 ml	Total	2.5 ml
water	4 ml	water	1.1 ml
Tris-HCl buffer (1.5M, pH8.8)	2.5 ml	Tris-HCl buffer (1M, pH 6.8)	315 µl
Acrylamide: Bis-acrylamide (37.5:1)	3.35 ml	Acrylamide: Bis-acrylamide (37.5:1)	1 ml
10% SDS	100 µl	10% SDS	25 µl
10% APS	50 µl	10% APS	12.5 µl
TEMED	15 µl	TEMED	7.5 µl

Gels were put into the chamber which was filled with 1x running buffer. Then 30 µg of protein was mixed with 1/5 (v/v) 5x Laemmli buffer and filled up to 30 µl. Samples were incubated at 95°C for 10 min and loaded on the gels. SDS-PAGE was run at 80V and maximum ampere until samples reached the separating gel. Then voltage was increased to 120 V.

2.6.4. Western Blot

Western blot was performed with a semi-dry or wet blot device. First, PVDF membranes were activated with MetOH for 1 min. Then, Whatman paper, PVDF membranes and gels were incubated in semi-dry or wet buffer, respectively, for 5 min. Blotting sandwich was arranged in the respective order according to the device. Semi-dry blot was run at 17 V for 35 min at RT and Wet blot at 100 V for 90 min at 4°C. Membranes were then incubated with blocking solution for 1 h at RT and then incubated with primary antibody o/n at 4°C. Next day, samples were washed three times with PBST for 5 min each and incubated with HRP-coupled secondary antibody for 1 h at RT. Membranes were again washed three times with PBST and specific signal were developed using Clarity Western ECL Substrate (Biorad) and a ChemiDoc Imaging System from Biorad.

2.7. Next Generation Sequencing (NGS) techniques

2.7.1. Whole exome sequencing (WES)

DNA from LCM purification was extracted using QIAamp MicroKit (Qiagen) according to the manufacturer's protocol. DNA was fragmented using an ultrasonicator and libraries were prepared with the KAPA Hyper Library Prep Kit (PEQLAB). Adapter ligation was performed with Agilent SureSelect Oligo-Mix followed by PreCapPCR according to the KAPA Hyper Library Prep Kit protocol. Library was enriched with AllExon XT Target Enrichment Kit (Agilent) and samples were run on a HiSeq2500.

2.7.2. Assay for Transposase-Accessible Chromatin (ATAC)-seq

50,000 cells were pelleted at 500g for 5 min at 4°C and washed with cold PBS. Nuclei were extracted with ATAC lysis buffer and centrifuged at 500g for 5 min at 4°C. Tagmentation was performed in 1x TD buffer (Illumina) and 2.5 µl Tn5 transposase (Illumina) in a total volume of 50 µl for 30 min at 37°C. DNA was purified using MinElute Kit (Qiagen) and libraries were PCR-amplified for 14 cycles using NEBNext High-Fidelity polymerase (NEB) and subsequently purified with PCR CleanUp Kit (Qiagen). Samples were then sequenced on a HiSeq2000.

2.7.3. Microarray gene expression profiling

RNA from cells was prepared with GeneChip WT PLUS Kit (Affymetrix) according to the manufacturer's protocol. Then GeneChip Hybridization, Wash and Stain Kit (Affymetrix) was used for further processing with Mouse Gene 2.0 ST Array (Affymetrix) according to the manufacturer's protocol. Chips were scanned with an Affymetrix GeneChip Scanner 3000 7G.

2.7.4. Chromatinimmunoprecipitation (ChIP)-seq

10 million cells were each aliquoted into 15 ml cell culture medium and cross-linked with 1% PFA for 10 min at RT. Then, 1 ml of 2 M glycine was added to quench the reaction for 5 min at RT. Cell Signaling SimpleChip Kit including Micrococcal

Nuclease was used to isolate and digest chromatin following manufacturer's protocol. Immunoprecipitations was conducted with equivalents of 40 million cells according to Cell Signaling ChIP protocol. ChIP-seq libraries were then generated using Accel-NGS 2S Plus DNA Library Kit (Swift Biosciences) with an adjusted protocol were DNA purification was achieved with phenol/chloroform/isoamylalcohol (25:24:1) purification and precipitation with ethanol o/n. Enrichment of libraries was conducted with Agencourt AMpure beads with a 1.1:1 ratio of beads to DNA. Libraries were then sequenced on a HiSeq2500 (Illumina).

3. Results

3.1. Hepatocyte-derived HCC and ICC can be induced by the same oncogenic drivers

Mosaic cancer mouse models are highly tractable non-germline genetically engineered mouse models. To study liver cancer in such models we used the well-established sleeping beauty (SB) transposon system[112-114]. This allows for stable integration of transposable elements into any host genome. These transposable elements can be genetically manipulated to encode for any gene of interest or shRNA cassettes to efficiently knockdown expression of specific genes via RNAi technology. As many human PLC patients harbor c-myc amplifications or activation of the MEK-ERK or PI3K pathway we used transposable elements encoding for c-myc and a constitutively active $Nras^{G12V}$ (pCaMIN) or c-myc and a constitutively active myristoylated AKT-1 (pCaMIA, Fig. 7a)[115-117]. We then delivered these plasmids into *p19*$^{-/-}$ mice via HDTV together with an SB13 to stably transfect hepatocytes. After 3 to 4 weeks we could observe outgrowth of multifocal tumor across the whole liver (Fig. 7b). Although this mostly resembles the situation in human patients many of them also only develop single (unilocular) tumors. To also induce such single tumors in our studies, we took advantage of another hepatocyte-specific delivery method, *in vivo* electroporation[118]. Indeed, Epo-induced delivery of pCaMIN or pCaMIA into livers of *p19*$^{-/-}$ mice allowed for outgrowth of single tumor nodules at the electroporated area after 4 to 6 weeks (Fig. 7c).

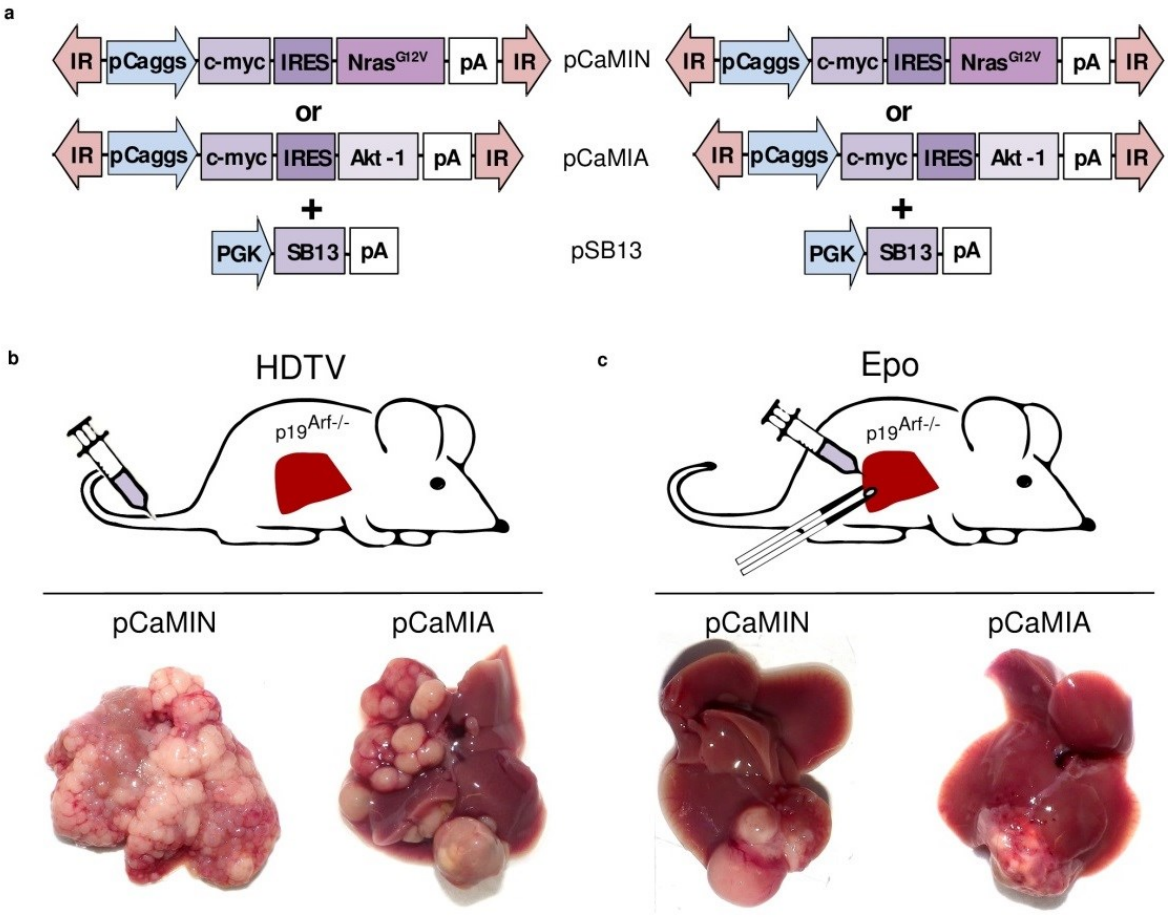

Figure 7 HDTV or Epo of c-myc/NrasG12V or c-myc/AKT-1 into *p19*$^{-/-}$ mice induces tumor development (a) Schematic presentation of transposon vectors including pCaggs promotor, c-myc, an IRES, Nras^{G12V} and a polyadenylation site (pA) flanked by inverted repeats (IR), upper panel (pCaMIN), vectors including pCaggs promotor, c-myc, an IRES, AKT-1 and a polyadenylation site (pA) flanked by inverted repeats (IR), middle panel (pCaMIA) or transposase vectors including phosphoglyceratkinase (PKG) promotor, SB13 coding sequence and a pA signal, lower panel. (b) Schematic presentation of HDTV (upper panel) which induces multifocal tumors with pCaMIN and pCaMIA (lower panel. (c) Schematic presentation of Epo (upper panel) which induces single tumors with pCaMIN and pCaMIA (lower panel).

Next, we sought to analyze the histopathology of the induced tumors. They were harvested, paraffin embedded and cut into 4 µm slides using a microtome. H&E staining of HDTV derived tumors showed typical HCC structures with solid or trabecular growth pattern and high steatosis (Fig 8a). Immunohistochemistry staining for the hepatocyte specific transcription factor HNF4alpha revealed strong nuclear signals while the biliary cell and cholangiocellular carcinoma specific marker K19 was totally absent (Fig. 8b and c). Taken together, HDTV injection of pCaMIA in all eleven mice and pCaMIN in all 14 mice induced pure HCC development (Fig. 8d). However, H&E staining of Epo induced tumor nodules revealed predominantly outgrowth of ICC with high amount of tumor stroma and glandular tumor cell formation (Fig. 8e).

HNF4alpha was mostly absent in these tumor while glandular structures were K19 positive (Fig. 8f and g). Out of 19 mice injected with pCaMIA via Epo one developed pure HCC, seven developed pure ICC and eleven developed mixed HCC-ICC tumors. In the pCaMIN cohort out of 8 mice one developed pure HCC, three developed mixed HCC-ICC tumors and four developed pure ICC (Fig. 8h).

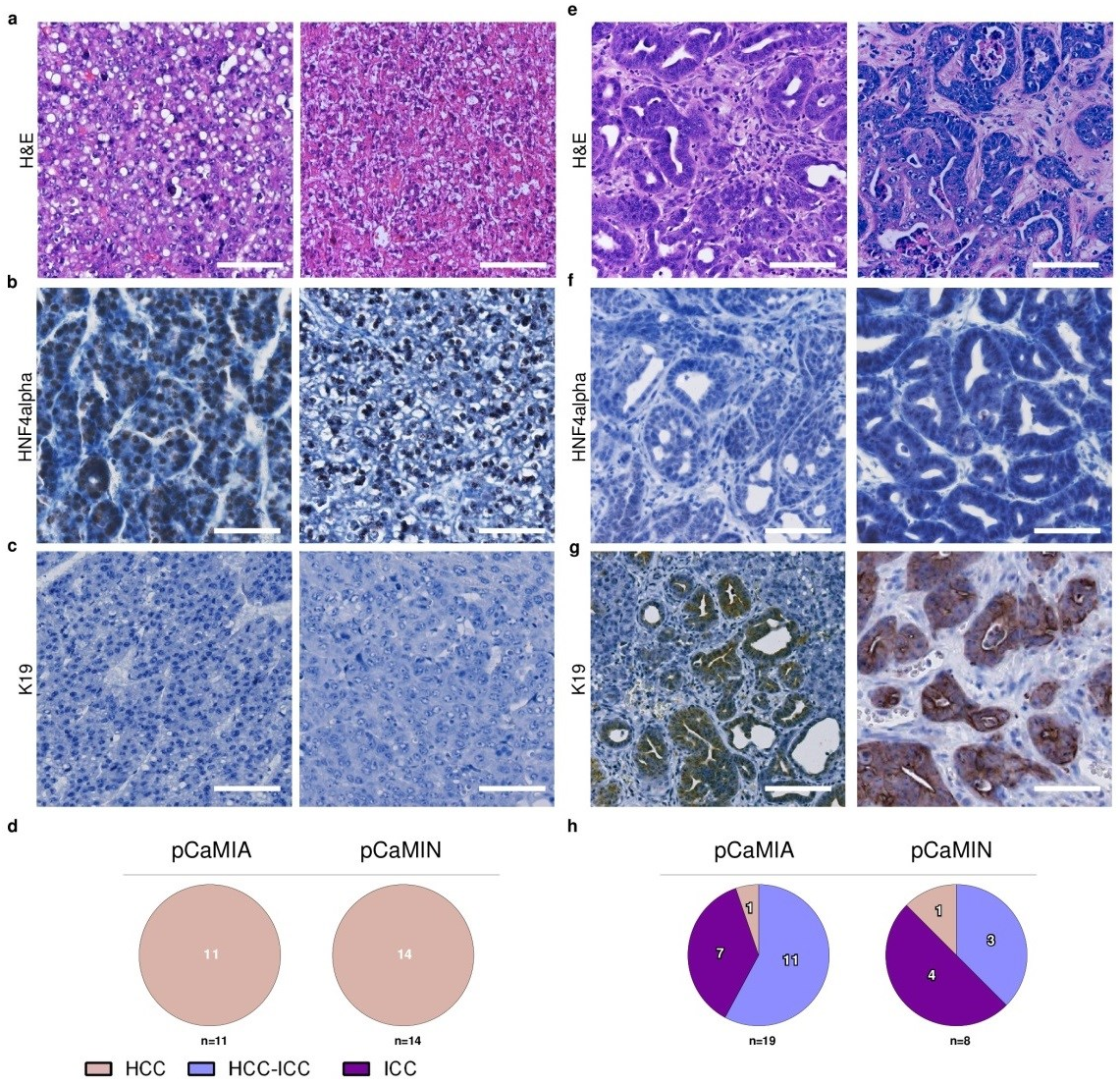

Figure 8 Delivery method dependent tumor type development (a-c) Representative photograph of (a) H&E (b) HNF4alpha IHC or (c) K19 IHC stained sections of liver tumors derived by HDTV of pCaMIA (left panel) or pCaMIN (right panel) after 4 weeks. Scale bar = 100 µm. (d) Histopathological classification of 11 pCaMIA and 14 pCaMIN HDTV derived tumors. (e-g) Representative photograph of (e) H&E (f) HNF4alpha IHC or (g) K19 IHC stained sections of liver tumors derived by Epo of pCaMIA (left panel) or pCaMIN (right panel) after 6 weeks. Scale bar = 100 µm. (d) Histopathological classification of 19 pCaMIA and 8 pCaMIN Epo derived tumors.

Several studies aimed to identify the cell of origin for HCC or ICC development, however, the results are still controversial. It has been shown that HDTV and Epo both target hepatocytes with high efficacy[118, 119]. However, to rule out the possibility

that the observed differences in the tumor type are due to targeting of other cells in the liver, we generated a lineage-tracing mouse model. We crossed ROSA$^{mT/mG}$ mice endogenously expressing membrane-tomato which switches to membrane-GFP expression upon Cre-recombination with *AlbCre* expressing Cre-recombinase under the hepatocyte specific albumin promotor[120-122]. These mice then were crossed into a *p19*$^{-/-}$ background to allow for tumor induction after intrahepatic transposon delivery (Fig. 9a). To test the functionality of these mice livers were harvested and cryosections of 6 µm were prepared for endogenous fluorescence imaging. While only hepatocytes had a green fluorescence all other cell types as bile duct cells or endothelial cells showed red fluorescence confirming the specificity of this lineage tracing model (Fig. 9b). We then delivered pCaMIN into these mice via HDTV or Epo and 4 or 6 weeks later tumors were collected. H&E and IHC stainings for HNF4alpha or K19 again showed HCC development upon HDTV and ICC development upon Epo, respectively (Fig. 9c). Endogenous fluorescence staining revealed that the HDTV derived tumors were all GFP positive (green) showing a hepatocytic origin. The Epo derived glandular tumors also showed pure GFP expression confirming that both tumor types derive from hepatocytes. Of note, the tumor stroma still showed tomato fluorescence (red) (Fig. 9d). To verify that the GFP positive glandular structures are indeed the K19 positive tumors we performed IF staining after quenching endogenous tomato signal. Indeed, the glandular structures showed endogenous GFP (green) expression co-localizing with K19 (red) signal (Fig. 9e).

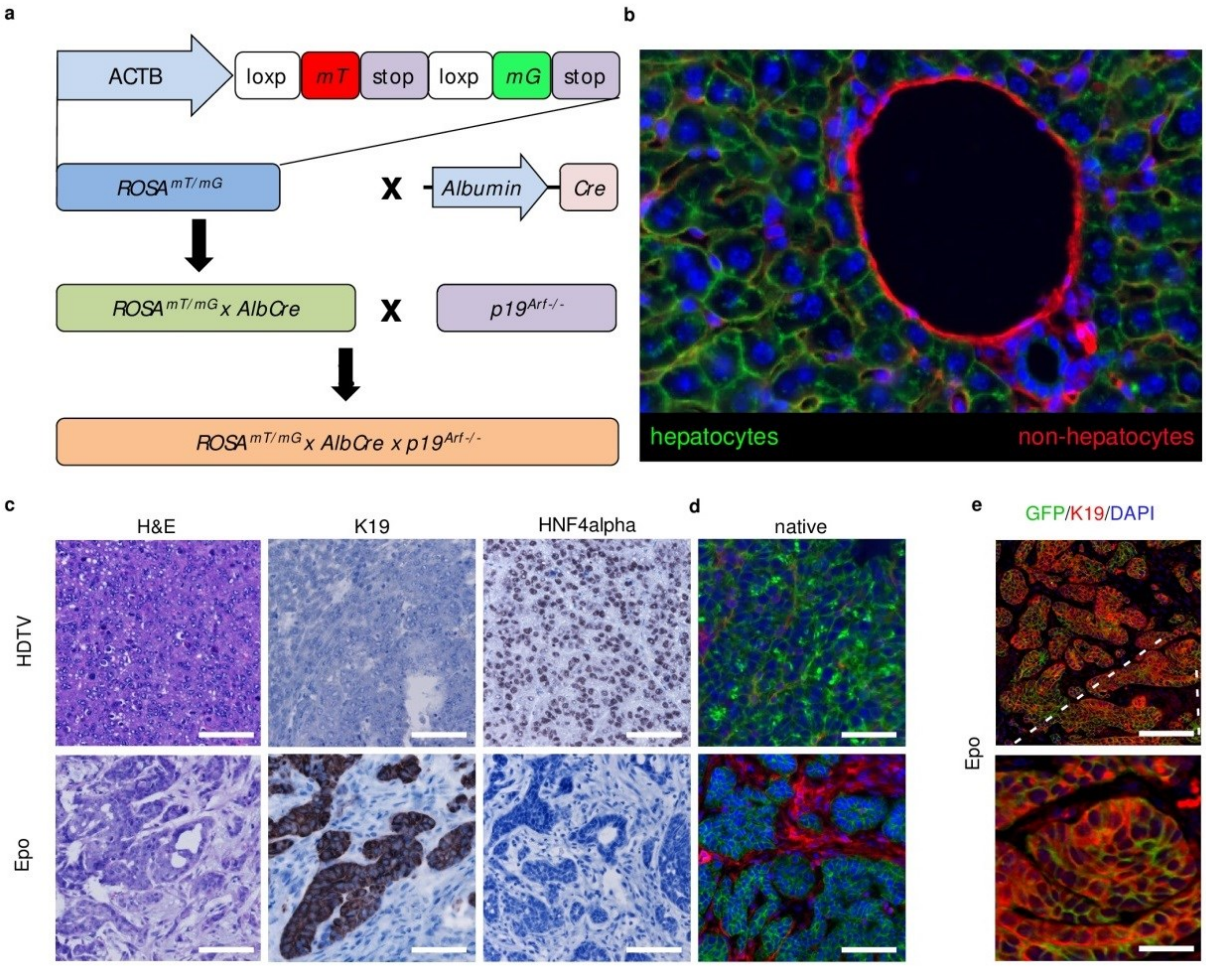

Figure 9 HCC and ICC both derive from adult hepatocytes (a) Crossing scheme to generate ROSA$^{mT/mG}$ x *Alb Cre* x *p19*$^{-/-}$ mice. (b) Representative photograph of native immunofluorescence of a liver from ROSA$^{mT/mG}$ x *Alb Cre* x *p19*$^{-/-}$ mice showing hepatocytes with GFP positive (green) membranes, bile duct and endothelial cells with tomato positive (red) membranes and DAPI (blue) stained nuclei. Scale bar, 100 µm (c and d) Photographs of H&E, K19 IHC, HNF4alpha IHC and native immunofluorescence stainings from liver tumors derived by pCaMIN HDTV (upper panel) or Epo (lower panel) in ROSA$^{mT/mG}$ x *Alb Cre* x *p19*$^{-/-}$ mice. Scale bar, 100 µm (e) IHC staining of K19 (red) on liver tumors derived by pCaMIN Epo in from R ROSA$^{mT/mG}$ x *Alb Cre* x *p19*$^{-/-}$ mice co-localized with GFP positive (green) tumors and counter stained nuclei with DAPI (blue). Scale bar, 100 µm (upper panel), 20 µm (lower panel).

3.2. Lineage commitment in PLC is independent of somatic mutations

Although HCC and ICC share similarities in their mutational landscape there are mutations which predominantly occur in HCC (e.g. *TERT* or *CTNNB1*) or ICC (e.g. *IDH1/2*, *FGFR2*-fusions), respectively[5]. To analyze if somatic mutations might influence the decision for HCC or ICC development in our model we aimed to perform whole exome sequencing (WES). First, mice were electroporated with pCaMIN and derived tumors were harvested. One half of every tumor was snap-

frozen and the other half was conducted for histopathological analysis. To minimize inter-specimen background signal in the WES we selected tumors which had mixed HCC and ICC compartments to directly compare both tumor types. The according snap-frozen parts were cut with a cryostat into 6 µm slices and stained with a fast stain protocol to minimize DNA degradation. Then we performed laser capture microdissection (LCM) to separate normal tissue (n=1), HCC tissue (n=3) and ICC glands (n=3) and performed WES using a low-input protocol (Fig. 10a). We identified 12 somatic mutations occurring in at least one of the tumor samples as mutations in the hydrase function gene *Car7* or the glycoprotein gene *Dag1*, however, they were found in HCC and ICC samples. In contrast, mutations in *Smc3* were found in two ICC samples but were absent in HCC and *Fam72a* mutations were found in two HCC samples but were absent in ICC (Fig. 10b). Nevertheless, interrogation of the online databases COSMIC and cBioPortal did not reveal any correlation of these mutations to either HCC or ICC. We further cloned *Fam72a* cDNA into our transposable elements via AscI and AgeI and introduced the same mutation found in the WES (259G>T) with a mutagenesis kit. This mutated *Fam72a* or a control vector was then co-delivered with pCaMIN via electroporation into *p19*$^{-/-}$ mice (Fig. 10c). The developed tumors were then stained for K19 which revealed ICC development in control as well as mutated *Fam72a* injected mice (Fig. 10d).

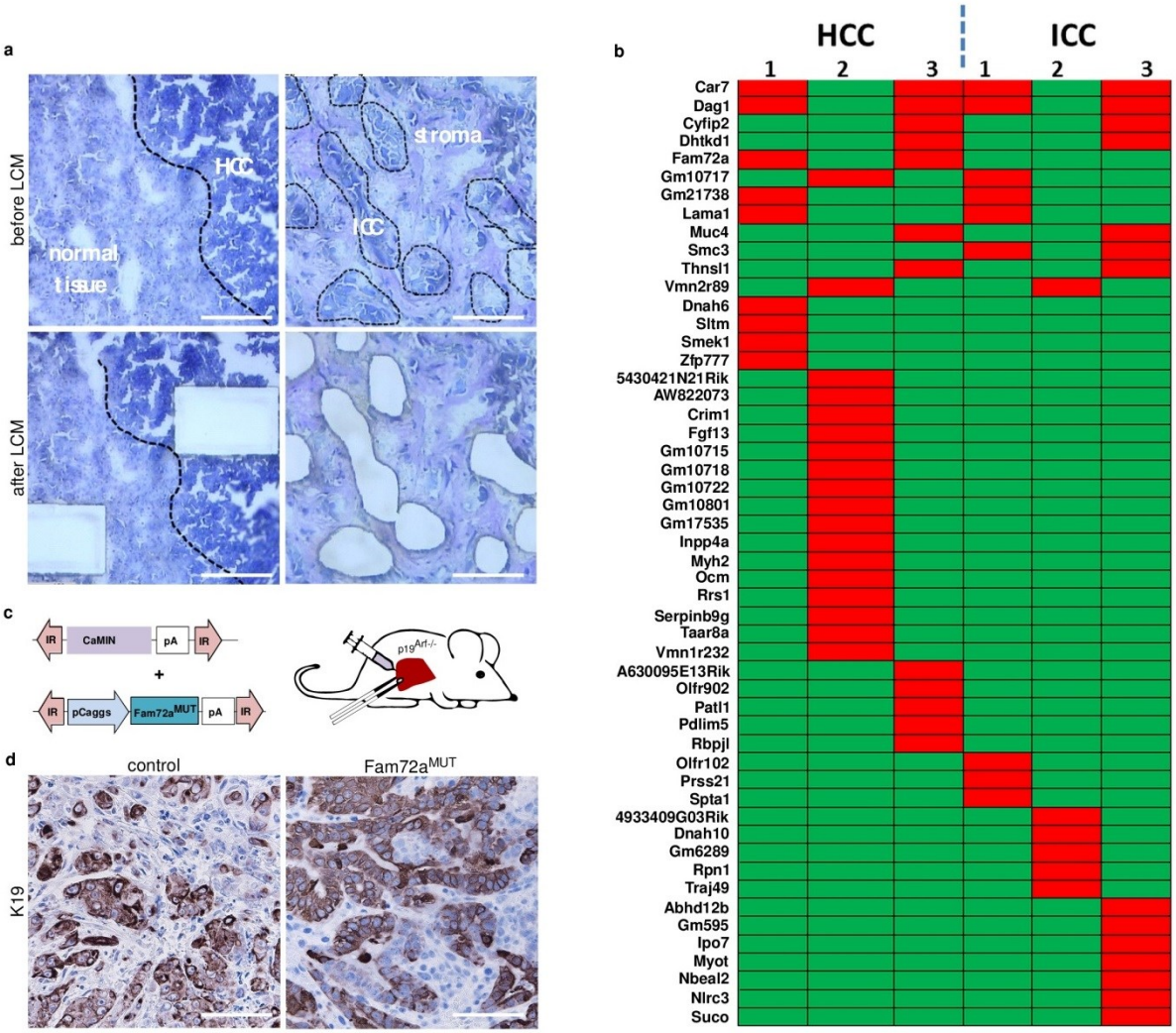

Figure 10 Somatic mutations do not determine liver tumor phenotype (a) Representative photographs of normal and HCC tissue (left panel) or ICC glands (right panel) before and after LCM of mixed HCC/ICC tumors derived from pCaMIN Epo of *p19*$^{-/-}$ mice. (b) Overview of mutated (red) and non-mutated (green) genes identified by WES of LCM purified tumor material from three different mixed HCC/ICC tumors. (c) Schematic representation of pCaMIN vector and transposon vector encoding for mutated *Fam72a* (259G>T, Fam72a^{MUT}) co-delivered via Epo into *p19*$^{-/-}$ mice. (d) Representative photographs of K19 IHC of tumors derived by pCaMIN plus control transposon or pCaMIN plus Fam72a^{MUT} transposon via Epo of *p19*$^{-/-}$ mice. Scale bar, 100 µm.

3.3. Physicochemical conditions of oncogene plasmid delivery method determine the tumor type

We could show that HCC and ICC can derive from the same cell of origin and that no specific mutations determine the lineage commitment. So we reasoned that transposon integration levels due to the different delivery methods, HDTV or Epo, might differ and influence the cell fate. We isolated genomic DNA from HDTV or Epo induced tumors and performed qRT-PCR with transposon specific primers which bind in the CAG promotor and c-myc in the transposable element. As a reference we used

β-actin primers which bind the exon and the intron to ensure detection of genomic DNA. We could show that the Epo method induced a 1.44-fold increased integration compared to the HDTV (Fig. 11a). To equalize the integration levels we used another version of the sleeping beauty transposase SB10 which has been reported to have lower transposition efficiency. We electroporated *p19*$^{-/-}$ mice with pCaMIN and SB10 and harvested the outgrown tumors. We again isolated genomic DNA and performed transposon specific qRT-PCR. Indeed, integration levels were equal to HDTV with SB13, however, histopathology and HNF4alpha and K19 stainings of Epo/SB10 derived tumors still showed ICC characteristics (Fig. 11a and b). We hypothesized that the electroporation procedure itself might play a significant role. To test this we first applied HDTV with pCaMIN and two hours later performed a mock electroporation in the same mouse and collected outgrown tumors after two to three weeks (Fig. 11c). We observed multifocal tumor development across the whole liver and a distinct tumor at the electroporated area (Fig. 11d). Strikingly, when we performed histopathological analysis with H&E, HNF4alpha and K19 stained tumor sections we could observe ICC outgrown at the electroporated area (Fig. 11e) while the HDTV induced multifocal tumors were clearly identified as HCC (Fig. 11f).

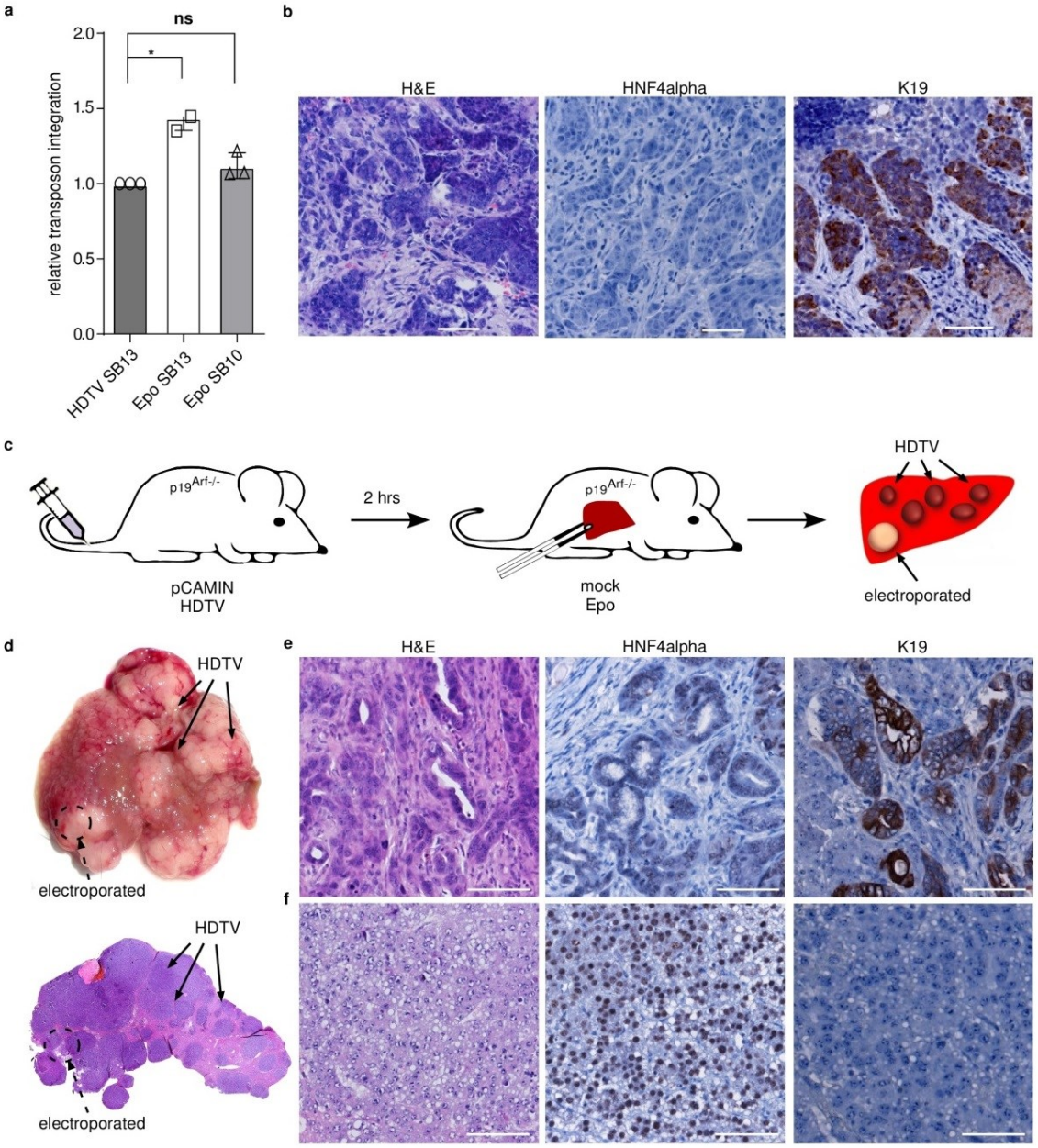

Figure 11 Epo-associated conditions favor ICC development (a) qRT-PCR data for transposon specific integration from genomic DNA isolated from HDTV or Epo induced tumors with pCaMIN and SB13 or Epo pCaMIN SB10. n=3 each (b) Representative photographs of H&E, HNF4alpha IHC and K19 IHC staining from Epo pCaMIN SB10 induced tumors still showed ICC phenotype. Scale bar, 100 µm (c) Cartoon of functional validation experiment to determine the influence of Epo-associated conditions on HDTV induced HCC. (d) Macroscopic overview of HDTV derived tumors (arrows) with highlighted electroporated area (dashed circle) (e) Representative photographs of H&E, HNF4alpha IHC and K19 IHC staining from tumors in mock electroporated area two hours after HDTV. Scale bar, 100 µm (f) Representative photographs of H&E, HNF4alpha IHC and K19 IHC staining from tumors after HDTV. Scale bar, 100 µm

3.4. Immune cell composition during the pre-tumorigenic phase does not impact tumor phenotype

At this point we had proved that the electroporation conditions themselves are sufficient to switch HCC development to ICC development. To further characterize these pre-tumorigenic conditions we wanted to know when tumor onset starts to define the pre-tumorigenic phase. So we performed time series analysis after pCaMIN injection via HDTV or Epo. Five days after delivery we could observe microtumors which already show ICC characteristic in the Epo treated mice and HCC characteristic in the HDTV treated mice using HNF4alpha and K19 IHC stainings (Fig. 12a, indicated by arrowheads). Based on this we focused on the three day time point after transposon delivery for analyses of the pre-tumorigenic stage. We first analyzed livers for any macroscopic signs. HDTV induced tissue damage across the whole liver while Epo only focally led to tissue damage. H&E sections of livers, however, revealed large eosinophilic areas of tissue damage and high amount of infiltrating immune cells in damaged areas in both conditions (Fig. 12b).

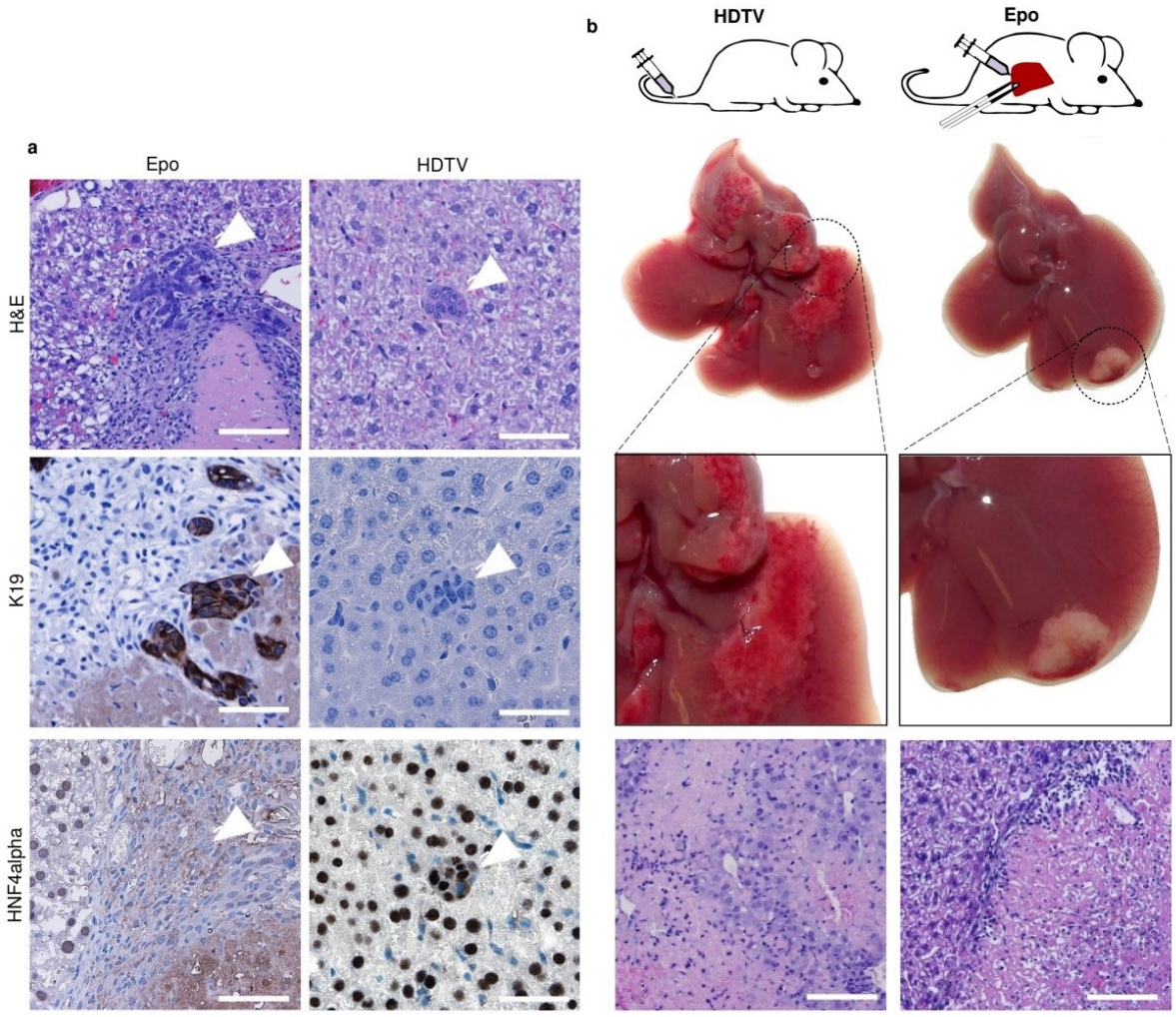

Figure 12 Characterization of pre-tumorigenic phase upon HDTV or Epo (a) Representative photographs of H&E, HNF4alpha IHC and K19 IHC staining from tumors five days after Epo (left panel) or HDTV (right panel) already showing microcarcinomas (white arrowheads). Scale bar, 100 µm (b) Macroscopic and microscopic photographs of liver tissue three days after HDTV (left panel) or Epo (right panel) revealed hepatic damage and immune cell infiltrations. Scale bar, 100 µm

It has been shown in different studies that liver specific stellate cells and Kupffer cells play important roles in liver damage[29]. To quantify these cell types in the pre-tumorigenic phase we performed IHC staining for alpha smooth muscle actin (aSMA) a marker for activated stellate cells. However, there were no differences between HDTV and Epo treated mice (Fig. 13a). We further conducted IF for F4/80 a Kupffer cell marker. Again no differences between HDTV and Epo could be observed (Fig 13b). To also functionally test the role of Kupffer cells in liver tumor lineage commitment we took advantage of clodronate which are small liposomes specifically killing macrophages and Kupffer cells. To test their efficiency we first treated mice with lipopolysaccharide (LPS) to induce macrophage and Kupffer cell infiltration and

additionally administered clodronate or control liposomes. Then we harvested the livers after one day and digested the tissue with collagenase and filtered the cell suspension through a nylon mesh to prepare single cell solutions. The cells were then stained with CD45 and F4/80 antibodies to specifically label Kupffer cells and analyzed via flow cytometry analysis. While the Kupffer cell population from mice treated with control liposomes was 9.19% the population from clodronate treated mice was reduced to 3.95% (Fig. 13c, upper panel). We then pre-treated another cohort of mice three days before pCaMIN Epo with control or clodronate liposomes and continued the treatment for 2 weeks. After additional 4 weeks we collected the tumors and analyzed IHC staining for HNF4alpha and K19, however, both groups showed ICC histopathology (Fig. 13c, lower panel).

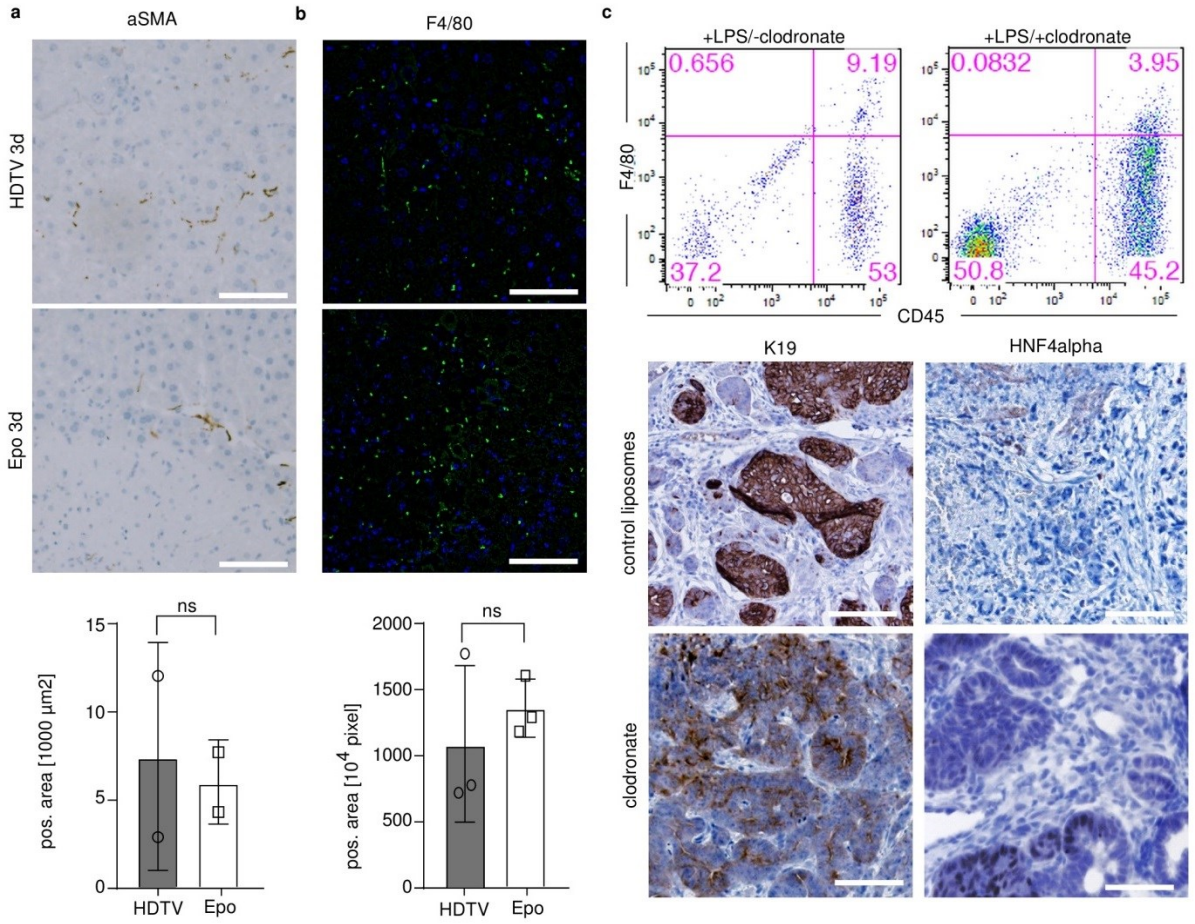

Figure 13 Amounts of Kupffer cells and stellate cells are equal after HDTV or Epo (a) Representative photographs and quantification of aSMA IHC on livers three days after HDTV (upper panel) or Epo (middle panel). n=2 each, scale bar, 100 µm (b) Representative photographs and quantification of F4/80 (green) on livers three days after HDTV (upper panel) or Epo (middle panel) with nuclei counter stained with DAPI (blue). n=3 each, scale bar, 100 µm (c) Flow cytometry analysis of single cell suspension from digested liver tissue from mice treated with LPS and control liposomes (upper left panel) or LPS and clodronate (upper right panel) with F4/80 and CD45 specific antibodies to detect Kupffer cells. K19 IHC and HNF4alpha IHC from liver tumors of mice

treated with control liposomes (middle panel) or clodronate (lower panel) before and after Epo pCaMIN revealed ICC phenotype. Scale bar, 100 µm

Then, we also expanded our analyses to other types of immune cells. We performed IHC stainings for T-cells (CD3), monocytes and neutrophilic granulocytes (Ly6G), B-cells (B220) and antigen-presenting cells (MHCII) (Fig. 14a and b). Quantifications of stained area per field of view showed an overall higher number of Ly6G and MHCII positive cells, however, no difference between HDTV and EPO treated mice was detectable (Fig. 14c). For further analysis of subpopulations of immune cells we performed flow cytometry analysis. We characterized T-cells ($CD45^+$, $CD3^+$), helper T-cells ($CD45^+$, $CD3^+$, $CD8^-$, $CD4^+$) and killer T-cells ($CD45^+$, $CD3^+$, $CD8^+$, $CD4^-$) as well as monocytic immature myeloid cells (moIMC, $CD11b^+$, $Gr1^{low}$, $Ly6C^+$, $F4/80^-$) neutrophilic immature myeloid cells (NeuIMC, $CD11b^+$, $Gr1^+$, $Ly6C^-$, $F4/80^-$) and macrophages (macr., $CD11b^+$, $Gr1^-$, $Ly6C^-$, $F4/80^+$). Again, we did not see any difference between HDTV and Epo treated mice (Fig. 14d and e).

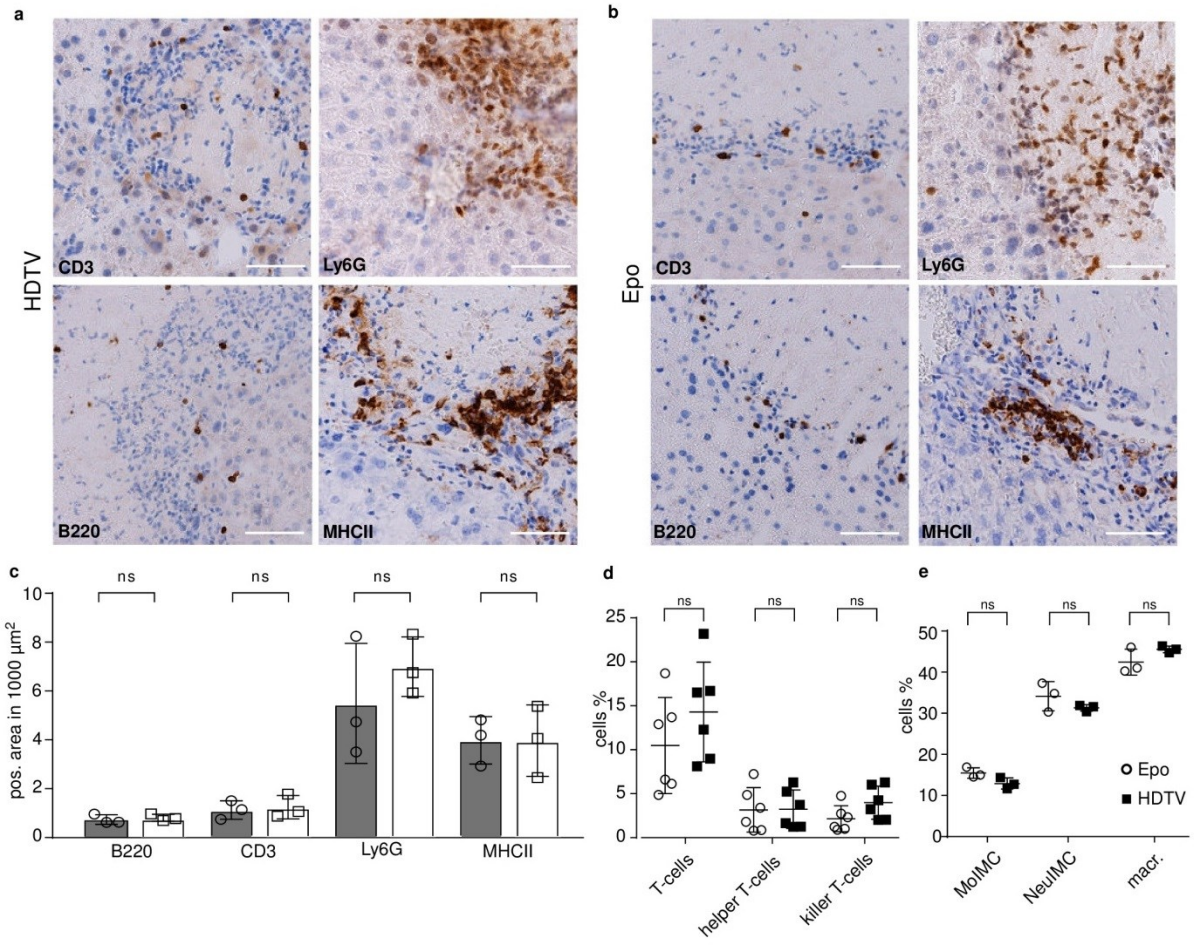

Figure 14 Immune cell populations in the liver do not differ between HDTV or Epo treated mice (a) Representative photographs of CD3 IHC, Ly6G IHC, B220 IHC and MHCII IHC of damaged liver tissue of mice treated with pCaMIN HDTV after three days. Scale bar, 100 µm (b) Representative photographs of CD3 IHC,

Ly6G IHC, B220 IHC and MHCII IHC of damaged liver tissue of mice treated with pCaMIN Epo after three days. Scale bar, 100 µm (c) Quantification of positive stained areas of samples from (a) and (b) did not show any significant difference between HDTV and Epo. n=3 each (d) Flow cytometry analyses for T-cells ($CD45^+$, $CD3^+$), helper T-cells ($CD45^+$, $CD3^+$, $CD8^-$, $CD4^+$) and killer T-cells ($CD45^+$, $CD3^+$, $CD8^+$, $CD4^-$) from mouse liver three days after HDTV or Epo, respectively. n=6 each (e) Flow cytometry analyses for monocytic immature myeloid cells (mo iMC, $CD11b^+$, $Gr1^{low}$, $Ly6C^+$, $F4/80^-$) granulocytic immature myeloid cells (gr iMC, $CD11b^+$, $Gr1^+$, $Ly6C^-$, $F4/80^-$) and macrophages ($CD11b^+$, $Gr1^-$, $Ly6C^-$, $F4/80^+$) from mouse liver three days after HDTV or Epo, respectively. n=3 each

3.5. Hepatocyte cell death influences tumor fate

As we could not detect any differences regarding intrahepatic immune cell infiltrations we put our attention towards the damaged liver tissue itself. It is known that hepatic cell death is a major factor in liver disease and liver tumor development so we quantified the amount of dying cells in the affected tissue[69, 88-90, 123]. We performed TUNEL assay on cryosections of HDTV or Epo treated mice 3 days after pCaMIN delivery. There was a high amount of TUNEL positive cells in the HDTV (69%±16%, green, indicated by white arrowhead) but also in the Epo treated livers (70%±18%, green, indicated by white arrowhead, Fig. 15a). To validate that dying cells were hepatocytes we repeated this assay in the ROSA$^{mT/mG}$ x *AlbCre x p19*$^{-/-}$ mice. Indeed, TUNEL positive (red) cells were hepatocytes shown by GFP positive (green) membranes (Fig. 15b). Although the amount of dying cells in both methods is equal there is still the possibility that the type of cell death might be different as TUNEL detects all types of cell death[124]. To prove this we extracted protein lysates from HDTV or Epo-treated mice after three days and performed western blot for the apoptosis marker cleaved caspase 3 and the necroptosis marker pMLKL. Lysates from HDTV-treated mice clearly showed cleaved caspase 3 staining while they had a low signal for pMLKL (Fig. 9c, left panel). The opposite was true for lysates from Epo-treated mice which had low levels of cleaved caspase 3 and higher levels of pMLKL (Fig. 15c, right panel). Additionally we conducted IHC for RIPK3 and activated pRIPK3, another marker for necroptosis. While HDTV-treated mouse liver did not show any signal livers from Epo-treated mice showed clear staining for both (Fig. 15d). Upregulation of *Ripk3* was also confirmed via qRT-PCR from livers where Epo treatment induced a 2.17-fold increase compared to HDTV (Fig. 15e). Necroptotic cells are known to secrete high levels of DAMP´s so we sought to analyze these signatures in our mouse models[75, 76]. We performed a qRT-PCR based array for 84

different cytokines and receptors where we identified five down-regulated and 14 up-regulated candidates in Epo vs HDTV-treated livers (Fig. 15f). We then wanted to know if this Epo-induced cytokine pattern is dependent on the Epo-induced necroptosis induction. As necrostatin-1 (Nec-1) is a potent inhibitor of necroptosis we pre-treated mice three days daily before applying pCaMIN Epo. Nec-1 treatment reduced the amount of TUNEL positive cells (Fig. 15 g and h) although there was a slight induction of apoptosis shown by an increase in cleaved caspase 3 signal (Fig. 15i). Nevertheless, induction of necroptosis was efficiently decreased shown by the strong reduction of pMLKL intensity (Fig. 15j). We again performed the qRT-PCR based cytokine array and could show that out of the 14 Epo-induced candidates 12 could be reduced upon Nec-1 treatment (Fig. 15k). Analysis of immune cell infiltration via IHC staining further showed a significant reduction of Ly6G positive cells in Nec-1-treated compared to control mice (Fig. 15l). We pre-treated another cohort of mice with control or Nec-1 three days before pCaMIN Epo and continued the treatment for two weeks. After additional four weeks we collected the tumors and performed HNF4alpha and K19 IHC. Strikingly, the amount of K19 positive staining was greatly reduced in Nec-1 treated group while the number of HNF4alpha positive cells was significantly increased in the tumor tissue (Fig. 15m and n).

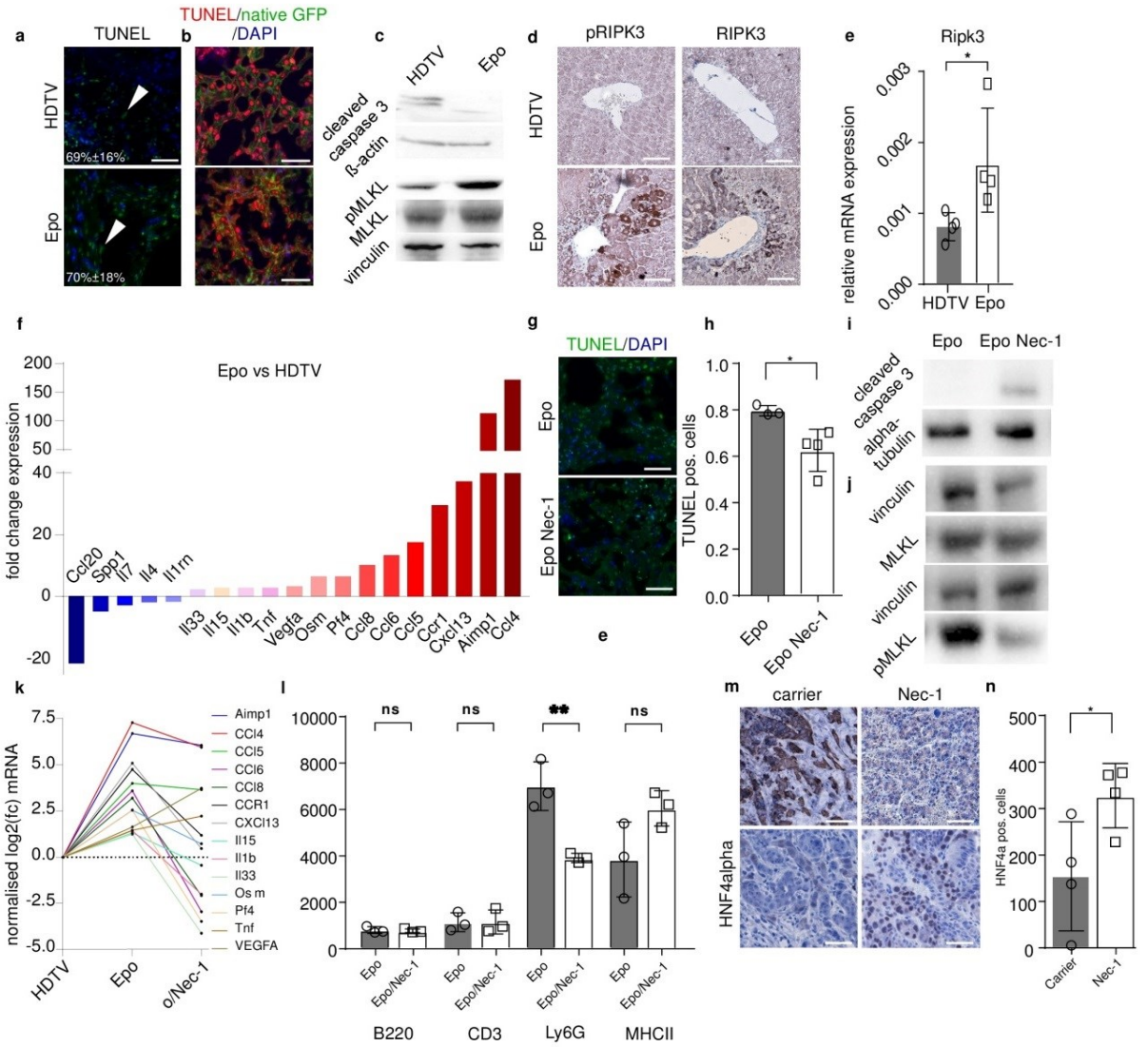

Figure 15 Necroptosis induction upon liver electroporation (a) Representative photograph of TUNEL (green, positive cells are indicated by white arrowheads) staining and quantification of damaged liver tissue of mice three days after HDTV (upper panel) or Epo (lower panel). Scale bar, 100 µm (b) Representative photograph of TUNEL (red) staining on livers from ROSA$^{mT/mG}$ x *Alb Cre* x *p19*$^{-/-}$ mice three days after HDTV (upper panel) or Epo (lower panel) showing co-localization with GFP positive (green) hepatocytes. Scale bar, 100 µm (c) Western Blot on lysates from liver of HDTV (left panel) or Epo (right panel) treated mice after three days for cleaved caspase 3, pMLKL, MLKL and the corresponding controls. n=3 pooled lysates per lane (d) IHC for pRIPK3 and RIPK3 on livers from mice three days after HDTV (upper panel) or Epo (lower panel), Scale bar, 100 µm (e) qRT-PCR for *Ripk3* from livers of mice three days after HDTV or Epo showed a significant upregulation in Epo treated livers. n=4 each (f) Fold-change expression of genes which are <-1.5-fold decreased or >1.5-fold increased in Epo vs HDTV treated livers in qRT-PCR based cytokine and receptor array. n=2 each (g) Representative photographs of TUNEL (green) staining on livers of mice pre-treated with control (upper panel) or Nec-1 (lower panel) three days before Epo harvested three days after Epo. Scale bar, 100 µm (h) Quantification of TUNEL positive cells from (g) showed significant reduction in the Nec-1 pre-treated group compared to control. n=3 (control) and 4 (Nec-1) (h) Western Blot on lysates from liver of control treated (left panel) or Nec-1 treated (right panel) mice three days after Epo for cleaved caspase 3, pMLKL, MLKL and the corresponding controls. n=3 pooled lysates per lane (k) Normalized log2 fold-change expression of Epo-associated upregulated genes from (f) in Epo or Nec-1 pre-treated plus Epo treated mice compared to HDTV treated mice. n=2 each (l) Quantifications of positive areas for

B220, CD3 Ly6G or MHCII IHC staining on livers of Epo or Nec-1 pre-treated plus Epo treated mice after three days. n=3 each (m) Representative photograph of K19 and HNF4alpha IHC on tumor samples derived from Epo pCaMIN of mice treated with control (left panel) or Nec-1 (right panel). Scale bar, 100 µm (n) Quantification of HNF4alpha positive cells per field of view in tumor tissues from (m) showed significant induction in the Nec-1 treated group. n=4 each

Although Nec-1 is a potent necroptosis inhibitor it also has some additional effects. Due to its ability to block the interaction of RIPK1 and RIPK3 it can influence all downstream pathways of these targets[125]. To analyze the role of necroptosis more specifically we took advantage of a genetic model. Mice with hepatocyte specific Cre expression (*AlbCre*) were crossed with floxed *MLKL* mice ($MLKL^{fl/fl}$). MLKL is the most downstream target in the necroptosis cascade. Efficient Cre-recombination induced knockout of hepatocyte MLKL was validated via western blot. Therefore, livers of *AlbCre* positive or negative mice were perfused and hepatocytes were purified. Western blot analysis of protein lysates from these cells showed total absence of MLKL in the *AlbCre* positive cells while *AlbCre* negative cells still showed a signal (Fig. 16a). We then conducted Epo in the $MLKL^{fl/fl}$ *x* $AlbCre^{+/-}$ mice and prepared protein lysates from whole tissue of electroporated liver areas. While there was a weak band for MLKL we could not detect any pMLKL compared to *MLKL* wt mice (Fig. 16b). As we proved functionality of these mice we aimed for further functional and tumor development studies. However, transformed hepatocytes have to be p19 deficient to allow for efficient tumor development. To achieve a *p19* knockout in these cells we used the CRISPR/Cas9 technology. For functionality testing we co-delivered a plasmid encoding for Cas9n and an sgRNA against *p19* included in a CRISPR cassette (CCsgp19) together with pCaMIN and SB13 into wt mice. We could show that these mice also developed tumors after four to six weeks which was slightly increased compared to complete $p19^{-/-}$ mice (Fig. 16c). So, we electroporated $MLKL^{fl/fl}$ *x* $AlbCre^{+/-}$ or $MLKL^{fl/fl}$ *x* $AlbCre^{-/-}$ with pCaMIN and CCsgp19 and harvested livers after three days. We again performed IHC stainings to quantify different immune cell types, however, we could not detect any difference in B220, CD3, Ly6G or MHCII positive cells (Fig. 16d). When we performed the qRT-PCR based cytokine array we could see that from the Epo-specific cytokines *Pf4, CCL8, CCL6, CCL5, CCR1 and Aimp1* were reduced in $MLKL^{fl/fl}$ x $AlbCre^{+/-}$ mice compared to $MLKL^{fl/fl}$ *x* $AlbCre^{-/-}$ (Fig. 16e, green bars). Furthermore we set up another cohort of mice for tumor development. The tumors were analyzed for HNF4alpha and K19 IHC which showed that hepatocyte specific knockdown significantly increases the number

of HNF4alpha positive HCC cells in the tumors (Fig. 16f and g). To exclude the possibility that the Cre expression might be the reason for this switch we also electroporated *MLKL* wt x *AlbCre*$^{+/-}$ mice and analyzed the developing tumors. However, they were mostly HNF4alpha negative and K19 positive proving an ICC phenotype (Fig 16h). To validate that necroptosis directly impacts the tumor phenotype we used the bile duct ligation (BDL) method which was reported to induce necroptosis in the liver[90, 126]. Ten days after BDL or sham operation livers were harvested and analyzed for necroptosis induction. We could detect pRIPK3 protein expression by IHC in BDL conducted mice as well as induction of pMLKL by western blot (Fig. 16i and j). Therefore we performed BDL or sham operation in a second cohort and additionally conducted HDTV with pCaMIN and SB13. Tumors were then harvested and analyzed for HNF4alpha or K19 expression to determine tumor phenotype. While sham operated mice harbored pure HCC tumors BDL treated mice showed poorly differentiated K19 positive HNF4alpha weakly positive tumors classified as tumors with mixed hepatobiliary features (Fig. 16k).

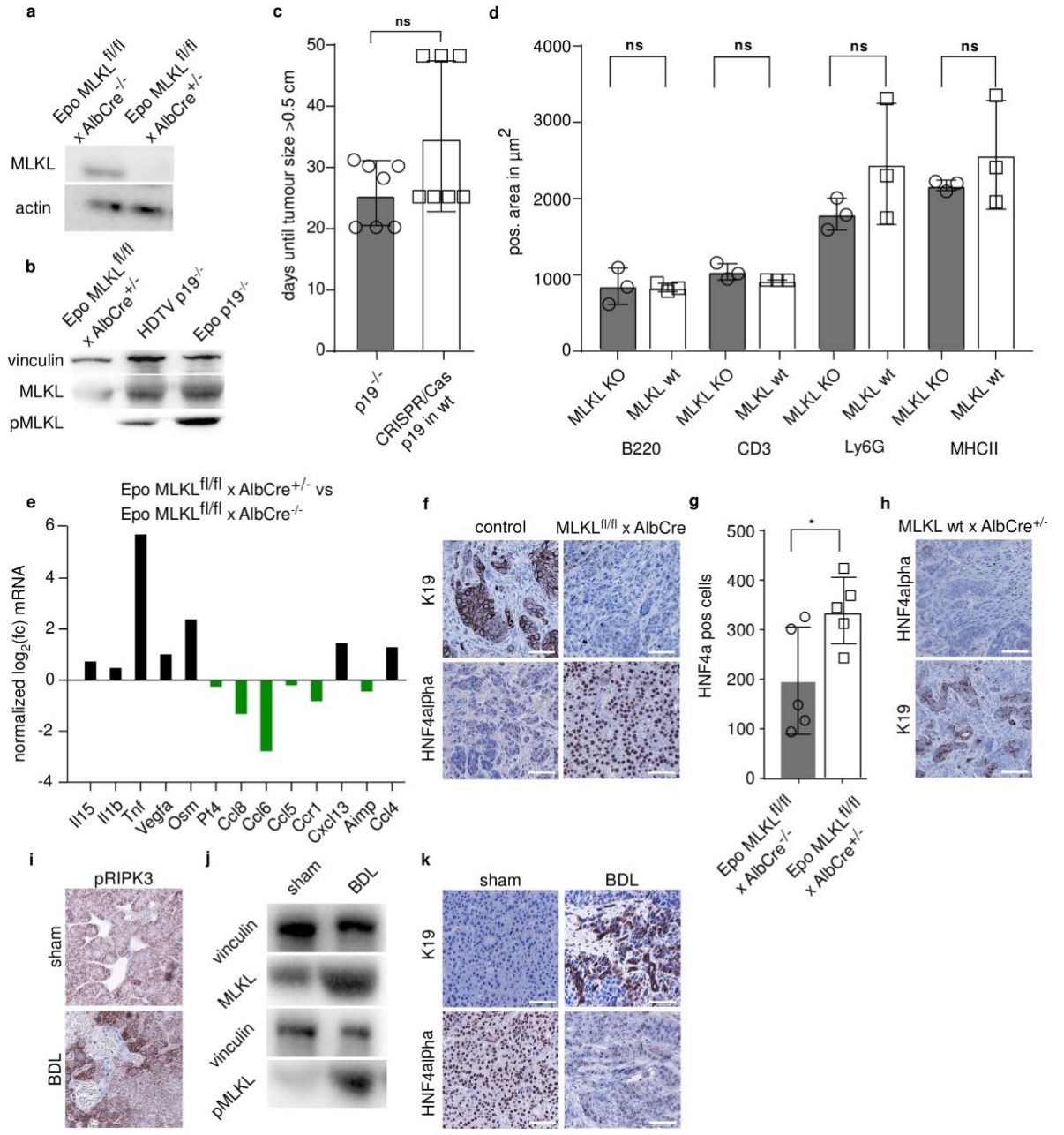

Figure 16 Genetic inhibition of necroptosis induces an ICC to HCC development switch (a) Western blot for MLKL with lysates from purified hepatocytes of *MLKLfl/fl x AlbCre+/-* and *MLKLfl/fl x AlbCre-/-* mice proving efficiency of Cre-recombinase induced knockout. n=2 each (b) Western blot for pMLKL and MLKL with lysates from *MLKLfl/fl x AlbCre+/-* mice after Epo compared to HDTV or Epo of *p19*$^{-/-}$ mice (middle and left part of the blot is the same depicted in Fig. 9c). n=3 each, 2 individual experiments (c) Duration until tumor development until 0.5 cm diameter in *p19*$^{-/-}$ mice treated with pCaMIN Epo or wt mice with pCaMIN plus CCsgp19 Epo. n=7 each (d) Quantifications of positive areas for B220, CD3 Ly6G or MHCII IHC stainings on livers of Epo treated *MLKLfl/fl x AlbCre+/-* and *MLKLfl/fl x AlbCre-/-* mice after three days. n=3 each (e) Normalized log2 fold-change expression of Epo-associated upregulated genes from Fig. 9f in Epo treated *MLKLfl/fl x AlbCre+/-* and *MLKLfl/fl x AlbCre-/-* mice after three days. Down-regulated genes are marked in green. n=2 each (f) Representative photographs of K19 and HNF4alpha IHC on tumors derived from Epo pCaMIN treated *MLKLfl/fl x AlbCre-/-* (left panel) and *MLKLfl/fl x AlbCre+/-* (right panel) mice. Scale bar, 100 µm (g) Quantification of HNF4alpha positive cells per field of view in tumors from samples in (f). n=5 each (h) Representative photographs of HNF4alpha and K19 IHC on tumors derived from Epo pCaMIN treated *MLKL wt x AlbCre +/-* mice (i) Representative photographs of pRIKP3

on liver sections of sham-operated (upper panel) or BDL-treated (lower panel) *p19*$^{-/-}$ mice after 10 days. Scale bar, 100 µm (j) Western blot for MLKL and pMLKL with liver lysates from sham-operated or BDL-treated *p19*$^{-/-}$ mice after 10 days. n=3 pooled lysates per lane (k) Representative photograph of K19 and HNF4alpha IHC on sections of liver tumors derived from sham-operated plus pCaMIN HDTV-injected (left panel) or BDL-treated plus pCaMIN HDTV-injected mice. Scale bar, 100 µm

Next, we were interested if these findings also reflect the situation in human liver cancer patients. We pre-selected 84 genes defining an apoptosis signature and 10 genes defining a necroptosis signature (Appendix) and analyzed a cohort of human HCC and ICC expression data regarding these signatures. We found that HCC samples had an overall up-regulation of pro-apoptotic genes while anti-apoptotic gens were down-regulated compared to ICC samples. The opposite was true for necroptosis-related genes which were higher in ICC samples compared to HCC (Fig. 17a). Of note, expression of one main regulator of necroptosis, *RIPK3*, was significantly higher in ICC samples compared to HCC (Fig. 17b).

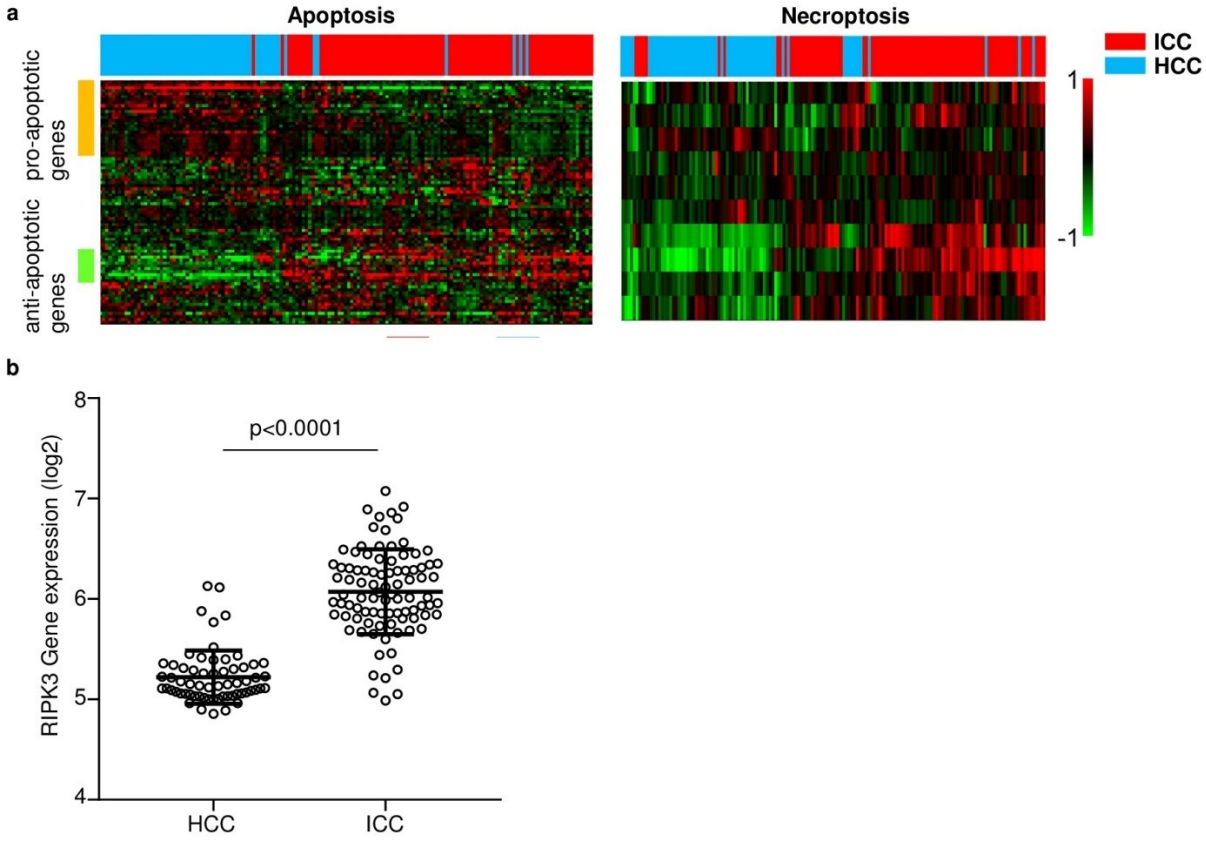

Figure 17 Human HCC and ICC tumors harbor distinct transcriptomic cell death signatures (a) Transcriptome data from human HCC and ICC were analyzed regarding pre-selected gene signatures (84 apoptosis-related genes and 10 necroptosis-related genes). HCC samples showed higher expression (red) of pro-apoptotic genes and lower expression (green) of anti-apoptotic genes compared to ICC samples (left panel). Necroptosis-related genes were higher in ICC samples (right panel). (b) qRT-PCR of the same cohort for *RIPK3* showed significant upregulation in ICC samples compared to HCC.

3.6. Toll-like-receptors are necessary for lineage commitment in liver tumorigenesis

We identified that necroptosis is the predominant type of cell death occurring after electroporation which can also influence lineage commitment in liver tumor development. Further we showed that necroptosis is accompanied by a specific cytokine pattern in the microenvironment. The most prominent receptor classes for DAMPs are the toll-like-receptors (TLRs). They are widely expressed on immune cells, however, some subclasses can also be found on nearly every cell type[75, 76, 127]. To analyze the role of TLRs in our tumor model system we used mice which are deficient for *TLR 2, 3, 5, 7* and 9 (*TLR5x* KO)[128]. We conducted these mice and syngeneic wt mice to Epo to test if the genotype alone affects necroptosis induction. Western blot with protein lysates of livers three days after electroporation showed that there is still induction of necroptosis in these mice (Fig. 18a). IHC analysis of B220, CD3, Ly6G and MHCII positive cells did not show any difference between *TLR5x* KO or wt mice (Fig. 18b). qRT-PCR based cytokine array showed that from the Epo-specific pattern *Il1b, Pf4, CCL8, CCL6, CCR1* and *Aimp1* were reduced (Fig. 18c). Interestingly out of these six candidates five were also reduced when hepatocytic necroptosis was inhibited (compare Fig. 18c, green bars and Fig. 17e, green bars). Again, we electroporated a second cohort which we used for tumor development studies. IHC analyses for HNF4alpha and K19 revealed that in the *TLR5x* KO mice tumors consisted of significantly more HNF4alpha positive HCC parts than the syngeneic wt mice (Fig. 18 d and e). To specify which TLRs are the most important ones for this switch we also performed tumor development studies in *TLR 2* and *4* double KO mice. As before the amount of HNF4alpha positive HCC parts was increased in tumors of KO mice compared to the wt group. As TLR 4 and 2 can be expressed on hepatocytes as well as immune cells we aimed to narrow down the important host cell. We electroporated SCID/beige mice which lack the majority of the adaptive and immune system and again found an increase in HNF4alpha positive tumor cells compared to syngeneic controls (Fig. 18g).

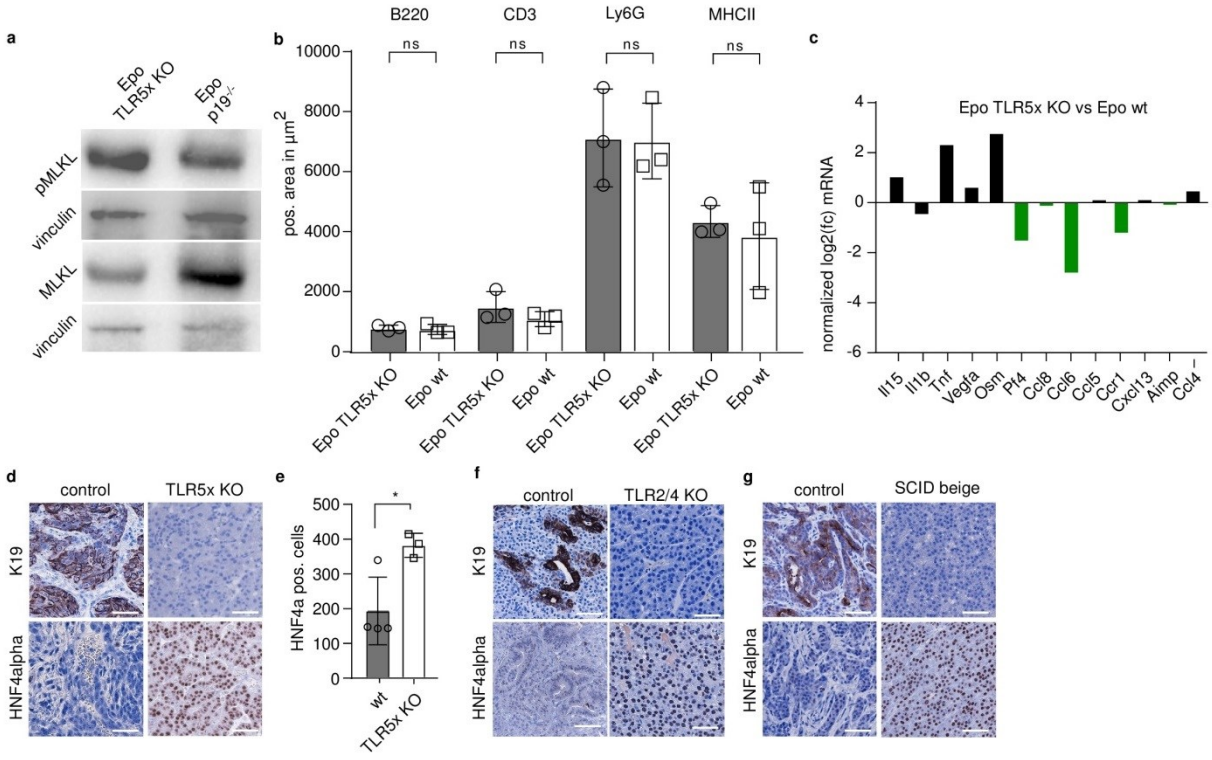

Figure 18 Toll-like-receptors contribute to cell fate decision in liver tumorigenesis (a) Western blot for pMLKL and MLKL with liver lysates from *TLR5x* KO and *p19*$^{-/-}$ mice three days after Epo. n=3 pooled lysates per lane (b) Quantifications of positive areas for B220, CD3 Ly6G or MHCII IHC stainings on livers of Epo *TLR5x* KO and wt mice after three days. n=3 each (c) Normalized log2 fold-change expression of Epo-associated upregulated genes from Fig. 9f in Epo treated *TLR5x* KO and mice after three days. Down-regulated genes which are also identified in Fig. 11e are marked in green. n=2 each (d) Representative photographs of K19 IHC and HNF4alpha IHC on sections of liver tumor derived by pCaMIN Epo of control (left panel) or *TLR5x* KO (right panel) mice. Scale bar, 100 µm (e) Quantifications of HNF4alpha positive cells per field of view in tumor sections from (d). n=4 (wt) or 3 (*TLR5x* KO) (f) Representative photographs of K19 IHC and HNF4alpha IHC on sections of liver tumor derived by pCaMIN Epo of control (left panel) or *TLR2/4* KO (right panel) mice. Scale bar, 100 µm (g) Representative photographs of K19 IHC and HNF4alpha IHC on sections of liver tumor derived by pCaMIN Epo of control (left panel) or *TLR2/4* KO (right panel) mice. Scale bar, 100 µm

3.7. Lineage commitment in liver tumorigenesis is epigenetically regulated

After having identified a role of the microenvironment for determining cell fate decisions in liver tumorigenesis we next sought to address by which cell intrinsic mechanisms ICC vs. HCC outgrowth is regulated. It has already been reported for other cell types that the microenvironment can influence the cellular fate via epigenetic regulations[101]. As we could already exclude the influence of somatic mutations between HCC and ICC tumors in our model we hypothesized that epigenetic regulations might play an important role. First, we aimed to validate that the HCC or ICC phenotypes are stably imprinted in the tumor cells. We performed

HDTV or Epo with pCaMIN in *p19*$^{-/-}$ mice and harvested the outgrown tumors. We digested them with collagenase/dispase and took the cells into culture. Via serial dilutions we then selected single cell clones from each tumor type. To verify that we only culture ICC cells from the Epo derived tumors we performed K19 IF staining. We only continued with K19 positive cells while all HCC cells from HDTV induced tumors were K19 negative (Fig. 19 a). We then injected the cells into the flanks of immunocompromised *Rag2*$^{-/-}$ mice (Fig. 12b). While the HCC cell grew as solid, K19 negative tumors ICC cells induced tumors with stromal parts and K19 positive cells (Fig. 19b and c). As stability of the tumor phenotype was verified we analyzed the epigenetic landscape of these cells. From each tumor type we used two single cell clones from male and two single cell clones from female mice and performed ATAC-seq. This technique allows analyzing the accessibility of chromatin regions due to its conformation[129, 130]. Density heatmap of differentially accessible chromatin regions clearly showed that all HCC cells clustered together while all ICC cells clustered with the opposite accessibility of 108 different chromatin regions (Fig. 19d). K-means clustering of normalized ATAC fragment confirmed that all HCC cells can be nicely separated from ICC cells (Fig. 19e). With the same cell lines we then conducted transcriptome analyses using microarrays. Again, all tumor specific cells clustered together when we analyzed differentially expressed genes between HCC and ICC (Fig. 19f). These data clearly indicate that ICC and HCC cells which derived from the same cell of origin (Fig. 9d and e) harbor different epigenetic and transcriptomic signatures.

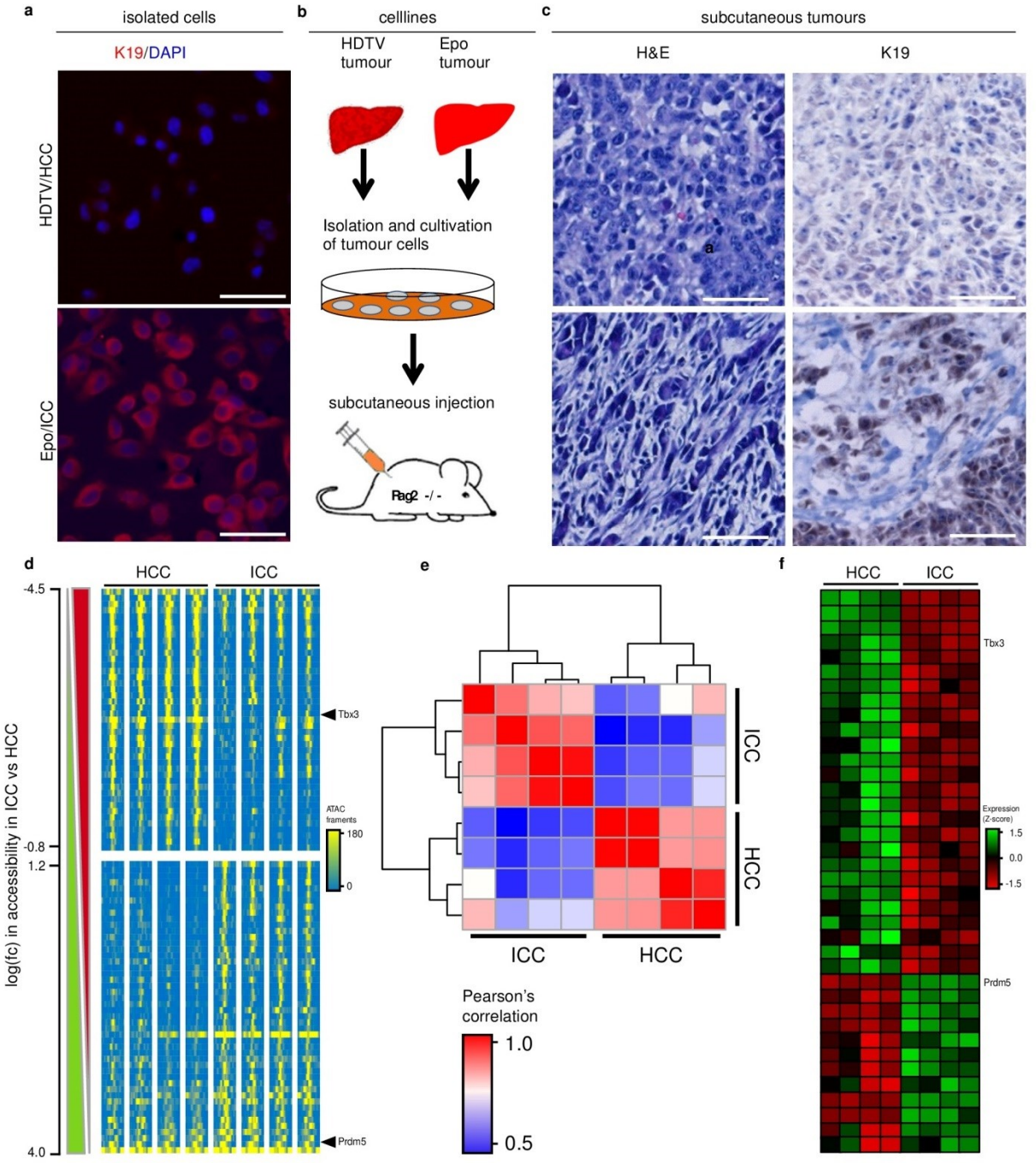

Figure 19 Epigenetic signatures of tumor phenotype in HCC and ICC cells (a) Representative photograph of K19 (red) IF staining on cells isolated from pCaMIN HDTV (upper panel) or pCaMIN Epo (lower panel) –induced tumors. Scale bar, 100 µm (b) Cartoon showing experimental setup to examine capability of tumor cells to regrow with similar phenotype (c) Representative photographs of H&E or K19 IHC stainings of tumors derived by injection of HCC cells (upper panel) or ICC cells (lower panel) subcutaneously into *Rag2*$^{-/-}$ mice. Scale bar, 100 µm (d) ATAC-seq density heatmap of differentially accessible chromatin regions in HCC (left panel) or ICC (right panel) cell lines. Peaks are ranked according to ICC vs HCC fold-change. Data for each gene are represented as smoothed normalized fragment pseudo-counts ± 1kb around the center of peaks. n=4 single cell clone lines each (e) Bi-clustering of pairwise Pearson's correlations of ATAC-seq data from (d). (f) Heatmap depicting data from transcriptome analysis of HCC (left panel) and ICC (right panel) cell lines. Up-regulated genes are presented in red down-regulated genes are presented in green. n=4 single cell clone lines each

An open accessible chromatin region is no guarantee for transcriptional activity as there are many other factors which influence transcription.[91, 97] To identify genes with correlations between chromatin accessibility and gene expression we conducted comparative analyses of ATAC-seq and transcriptome data. We found that the chromatin region of the transcription factor *Tbx3* was inaccessible in ICC cells while it was accessible in HCC cells (Fig. 20a, left panel). This correlated with gene expression which was higher in HCC cells compared to ICC cells which we also validated via qRT-PCR (Fig. 20a, right panel, Fig. 20b). Furthermore, analysis of a large cohort of HCC and ICC patients also showed that human HCC tumors express significantly higher amounts of *Tbx3* compared to ICC tumors (Fig. 20c). Another candidate from the comparative analysis was the transcription factor *Prdm5* which showed accessible regions in ICC cells while the HCC cells did not (Fig. 20d, left panel). Again, this correlated with gene expression which was significantly higher in ICC cells compared to ICC which was also validated via qRT-PCR (Fig. 20d, right panel, Fig. 20e). Using the same cohort of human patients we could also show that human ICC tumors had a significantly higher expression of *Prdm5* compared to human HCC tumors (Fig. 20f).

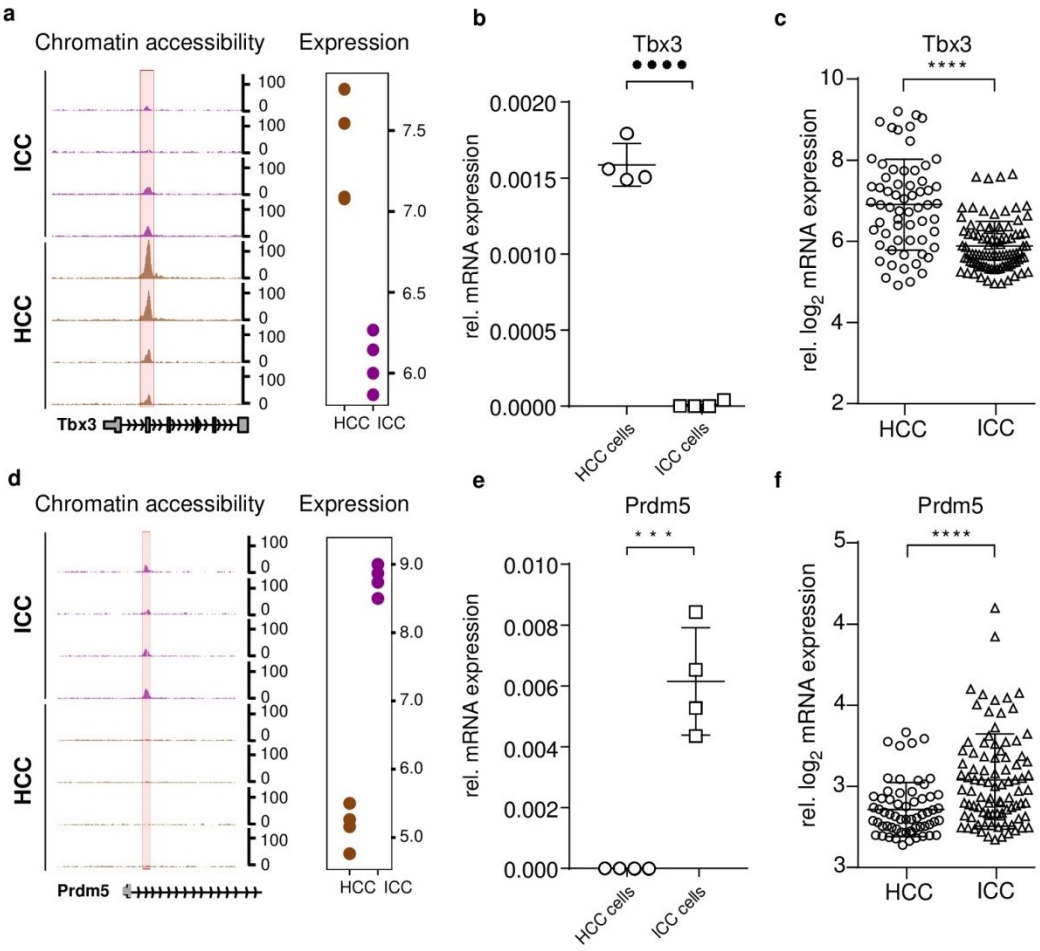

Figure 20 *Tbx3* and *Prdm5* are enriched in HCC and ICC, respectively (a) Correlation between ATAC-fragment counts (left panel) and gene expression (right panel) of *Tbx3* in HCC and ICC cells. n=4 single cell clone lines each (b) qRT-PCR data for *Tbx3* in HCC and ICC cells. Data is presented as relative mRNA expression. n=4 single cell clone lines each (c) qRT-PCR data for *Tbx3* in human HCC and ICC tumor samples. Data is presented as relative log2 mRNA expression. n=199 (d) Correlation between ATAC-fragment counts (left panel) and gene expression (right panel) of *Prdm5* in HCC and ICC cells. n=4 single cell clone lines each (b) qRT-PCR data for *Prdm5* in HCC and ICC cells. Data is presented as relative mRNA expression. n=4 single cell clone lines each (c) qRT-PCR data for *Prdm5* in human HCC and ICC tumor samples. Data is presented as relative log2 mRNA expression. n=199

3.8. Prdm5 and Tbx3 are key regulators of PLC lineage commitment

Although we could prove a direct correlation of Prdm5 and Tbx3 epigenetic regulation and mRNA expression to ICC and HCC, respectively, we aimed to functionally test their impact on our tumor mouse models. First, we cloned shRNAs against *Tbx3* or *Prdm5* with XhoI and EcoRI into a retroviral vector consisting of a TRE3G promotor, GFP-coding sequence, mirE shRNA backbone, PGK promotor, puromycin resistance cassette, an IRES and an rtTA3 coding sequence (RT3GEPIR). After verification of

correct insertion of the shRNAs via Sanger sequencing vectors were transfected into Phoenix-Ampho cells via $CaPO_3$ method. After cells secreted virus into the supernatant it was collected and used for infection of HCC cells (shRNA against *Tbx3*) or ICC cells (shRNA against *Prdm5*). Infected cells were selected with puromycin and shRNA expression was induced by adding doxycycline. After three days cells were harvested and RNA was isolated and conducted for qRT-PCR. For each gene the two shRNAs with the best knockdown were chosen (Fig. 21a shTbx3_1 and shTbx3_2 and Fig. 21b shPrdm5_1 and shPrdm5_2) and subcloned via XhoI/AscI and XhoI/MluI into pCaMIN. For additional overexpression of *Tbx3* or *Prdm5*, respectively, we also cloned cDNA of *Tbx3* (Tbx3 OE) or *Prdm5* (Prdm5 OE) via AscI/AgeI or AscI/NheI into transposable elements. To mimic a high expression of *Tbx3*, as found in HCC cells, we first electroporated pCaMIN including a control shRNA (pCaMINshRen) into *p19*$^{-/-}$ mice. Immunohistopathology of derived tumors showed growth of solid undifferentiated HNF4alpha and K19 negative tumors (Fig. 21c, left panel). When Tbx3 OE was co-delivered with pCaMINshPrdm5_1 via Epo into *p19*$^{-/-}$ mice outgrown tumors were still K19 negative but were more differentiated and had a slight induction of HNF4alpha positive cells (Fig. 21c, right panel). We then wanted to mimic the expression of *Prdm5* as found in ICC cells in our HDTV model. We co delivered pCaMIN together with Prdm5 OE and analyzed outgrown tumors, however, there were still pure K19 negative, HNF4alpha positive HCC (Fig. 21d, left part). We then aimed to analyze the function of Tbx3 in HCC lineage commitment so we performed HDTV of pCaMINshTbx3_1 into *p19*$^{-/-}$. Histopathologic analysis of the derived tumors again showed K19 negative, HNF4alpha positive HCC (Fig. 21d, middle part). Similar to the experiments before in the Epo model we also co-delivered pCaMINshTbx3_1 and Prdm5 OE into *p19*$^{-/-}$ mice via HDTV. Livers were again subjected to histopathological analysis which showed that these mice had tumors which were clearly HNF4alpha negative, K19 positive ICC with high amount of stromal parts (Fig. 21d, right panel). These results suggest that Tbx3 and Prdm5 act in concert to determine lineage commitment in liver tumorigenesis.

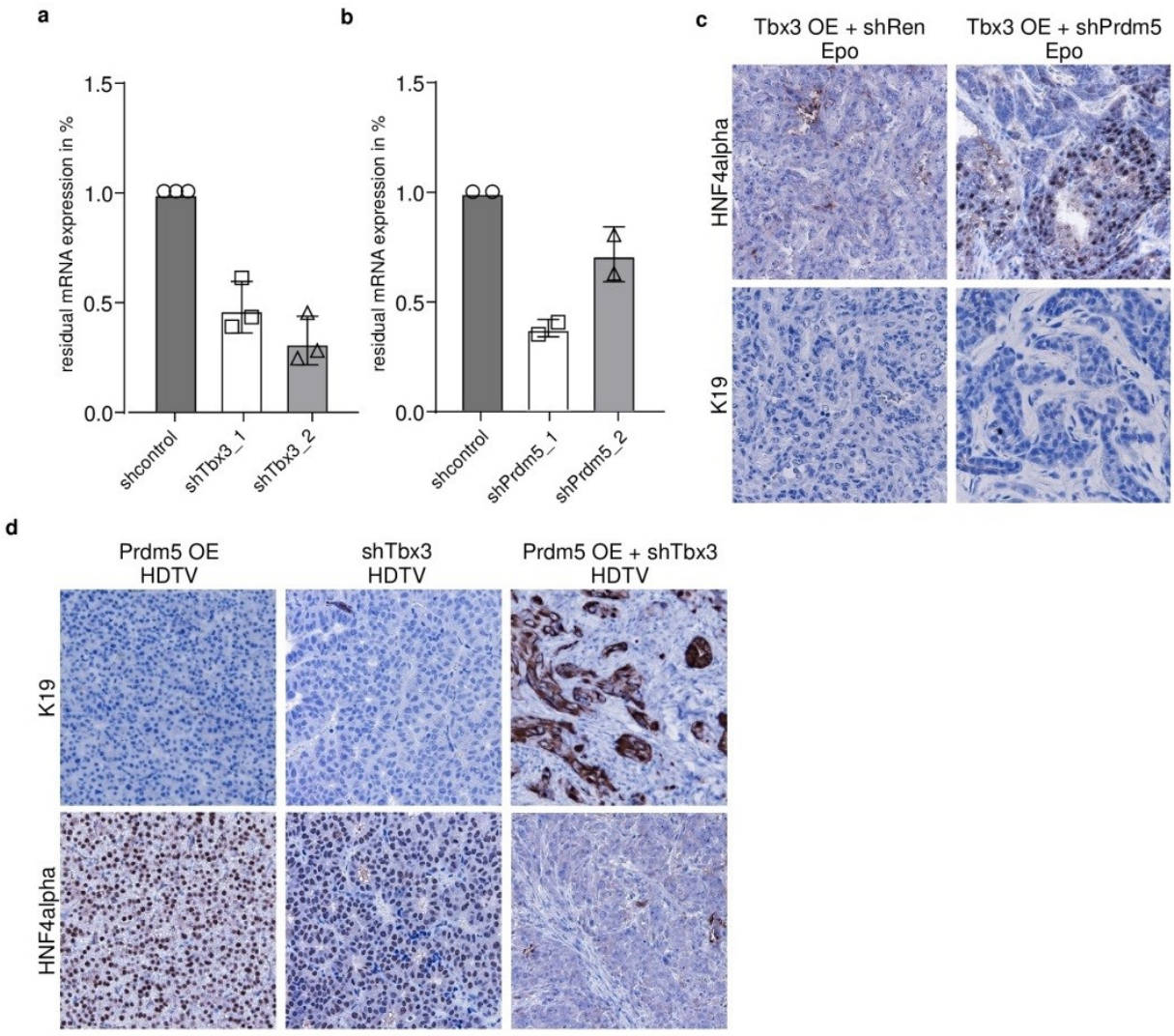

Figure 21 Functional validation of Tbx3 and Prdm5 (a) Knockdown efficiency testing via qRT-PCR of HCC cells stably transfected with control or 2 independent shRNA against *Tbx3*. Data are presented as residual mRNA expression compared to control. n=3 each (b) Knockdown efficiency testing via qRT-PCR of ICC cells stably transfected with control or 2 independent shRNA against *Prdm5*. Data are presented as residual mRNA expression compared to control. n=3 each (c) Representative photographs of HNF4alpha and K19 IHC on sections of liver tumors induce by Tbx3 OE plus pCaMINshRen (left panel) or Tbx3 OE plus pCaMINshPrdm5 Epo of *p19*$^{-/-}$ mice. Scale bars, 100 µm (d) Representative photographs of HNF4alpha and K19 IHC on sections of liver tumors induce by Prdm5 OE plus pCaMINshRen (left panel), pCaMINshTbx3 or Prdm5 OE plus pCaMINshTbx3 HDTV of *p19*$^{-/-}$ mice. Scale bars, 100 µm

After showing the importance of Tbx3 and Prdm5 in tumor fate decision we aimed to examine pathways which were affected by these transcription factors. As there are no publications showing the direct binding of Tbx3 or Prdm5 to specific gene regions in mice we performed ChIP-seq analyses. We chose two of the HCC single cell clone lines and two of the ICC single cell clone lines each. All chromatin interactors were cross-linked and chromatin was isolated and immunoprecipitation was performed with Tbx3 or Prdm5 antibody, respectively. Then, libraries were prepared and

sequenced and annotated peaks for each gene were plotted on a heatmap. This heatmap was nicely in concordance with the ATAC-seq heatmap generated earlier with these cell lines proving the robustness of both analyses (Fig. 22a and b). To gain further insights into direct and indirect targets of Tbx3 or Prdm5, respectively, we also performed functional experiments. The HCC cell lines were stably infected with *Tbx3* or control shRNAs and ICC cell lines with *Prdm5* or control shRNAs as described before. Then, RNA was isolated and microarray analyses were performed. These data were correlated to the ChIP-seq results to identify gene which were directly or indirectly up- or down-regulated upon *Tbx3* or *Prdm5* knockdown, respectively (Fig. 22c and d). Interestingly, among the most regulated genes for Tbx3 are developmental genes like *Hhip, Dkk1* or *Daam2* while for Prdm5 cell morphogenesis genes like *Cdh6*, *Twist1* or *Snai2* are highly regulated.

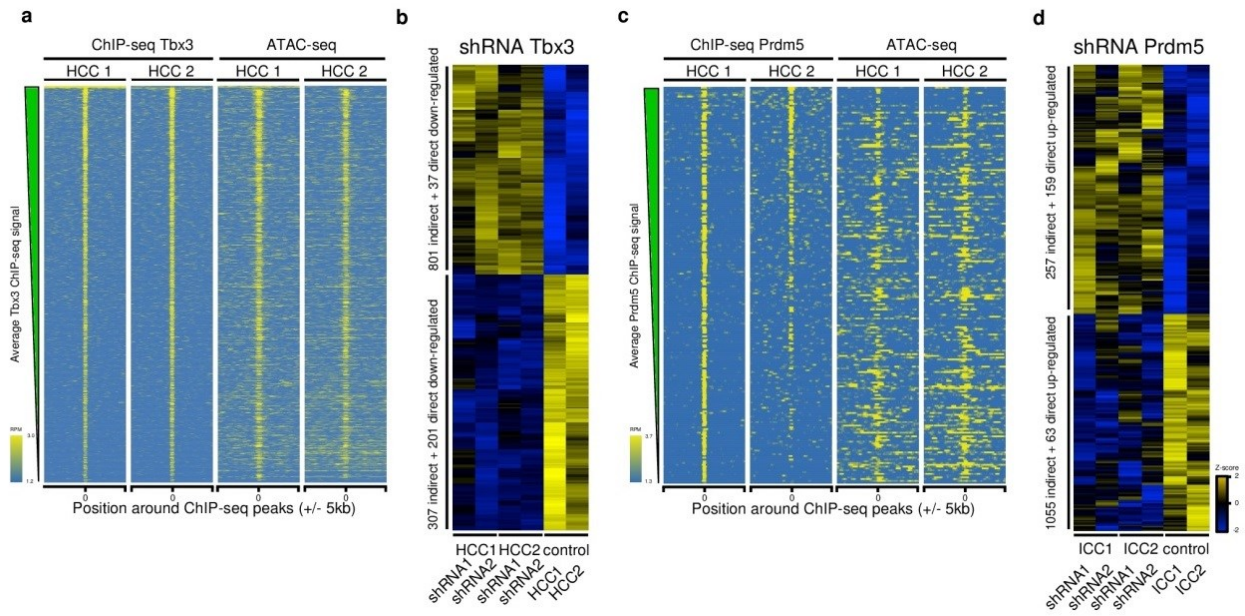

Figure 22 Direct and indirect targets of Tbx3 and Prdm5 transcription factors (a) Correlation of ChIP-seq data (left panel) for Tbx3 and ATAC-seq data (right panel) in HCC cells. Data are presented as normalized read per million mapped reads and ranked according to average Tbx3 ChIP-seq signal. n=2 cell lines each (b) Heatmap of differentially expressed genes for up (yellow) and down (blue) –regulated genes either directly or indirectly in HCC cells with stable *Tbx3* knockdown compared to HCC cells with stable control shRNA expression. n=4 (2 cell lines with 2 different shRNAs each) or 2 (1 control shRNA in duplicate) (c) Correlation of ChIP-seq data (left panel) for Prdm5 and ATAC-seq data (right panel) in ICC cells. Data are presented as normalized read per million mapped reads and ranked according to average Prdm5 ChIP-seq signal. n=2 cell lines each (b) Heatmap of differentially expressed genes for up (yellow) and down (blue) –regulated genes either directly or indirectly in ICC cells with stable *Prdm5* knockdown compared to ICC cells with stable control shRNA expression. n=4 (2 cell lines with 2 different shRNAs each) or 2 (1 control shRNA in duplicate)

Using the correlated ChIP-seq and microarray data we performed functional over-representation analyses with MSigDB canonical pathways which revealed regulation of pathways like Biological oxidation or developmental biology for Tbx3 while for Prdm5 Extracellular matrix organization, collagen formation or Erbb signaling could be identified. Interestingly, there was nearly no overlap of annotated pathway between Tbx3 and Prdm5 (Fig. 23a). Finally, we sought to address how Tbx3 and Prdm5 might be epigenetically regulated during pre-tumorigenic phase to impact the tumor cell fate. So we performed HDTV or Epo with *p19*$^{-/-}$ mice and took liver samples three days later. We isolated RNA and performed a qRT-PCR based array to detect expression of epigenetic modifiers. We found nine significantly up-regulated genes in Epo-treated mice from different enzyme classes like histone deacetylases (*Hdac5*), histone acetyltransferases (*Ncoa1*) or histone lysine methyltransferases (*Ehmt1*) (Fig. 23b). However, functional validation of these candidates needs to be done in the future.

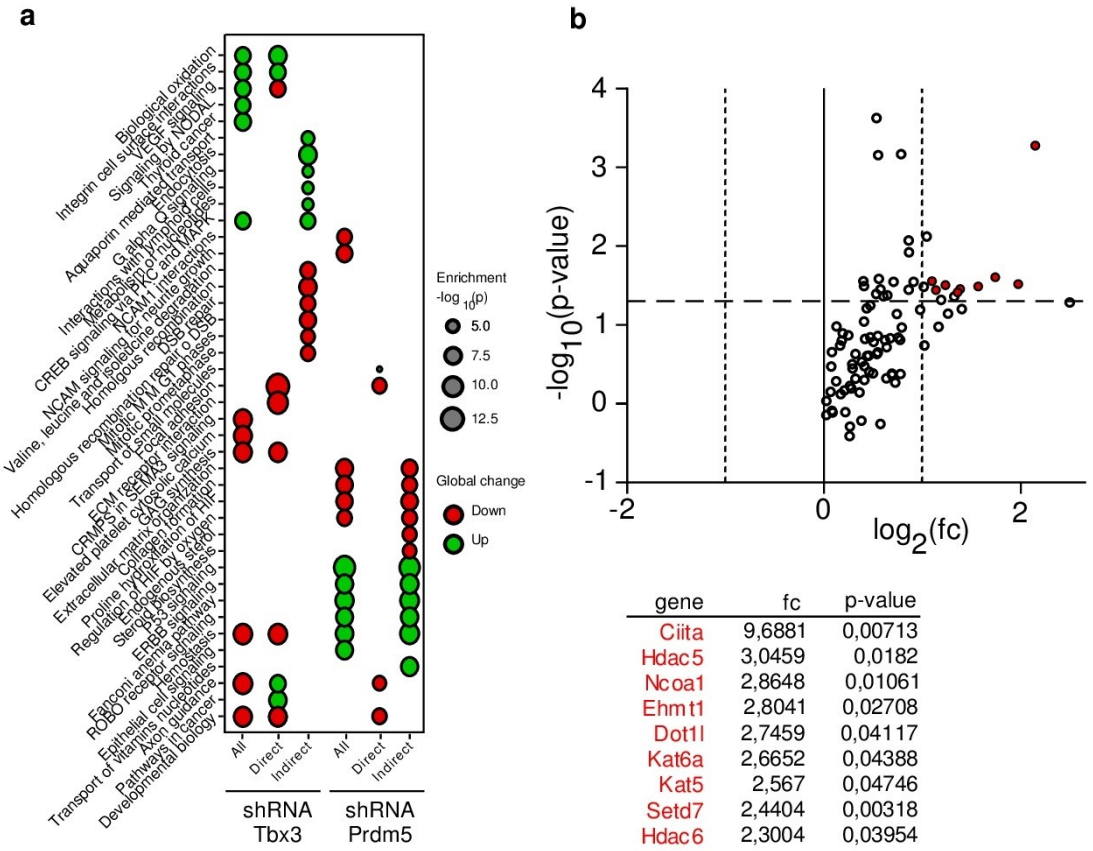

gene	fc	p-value
Ciita	9,6881	0,00713
Hdac5	3,0459	0,0182
Ncoa1	2,8648	0,01061
Ehmt1	2,8041	0,02708
Dot1l	2,7459	0,04117
Kat6a	2,6652	0,04388
Kat5	2,567	0,04746
Setd7	2,4404	0,00318
Hdac6	2,3004	0,03954

Figure 23 Tbx3 and Prdm5 downstream signaling (a) Functional overrepresentation analysis of pathways using MSigDB canonical pathways using expression data from Fig. 15b and d. Down-regulated pathways are drawn as red up-regulated pathways are drawn as green circles. Size of the circles correlates to the p-value (b) Volcano-plot of qRT-PCR based array for chromatin modifiers using RNA from Epo vs HDTV-treated livers after three days. n=3 each

4. Discussion

Primary liver cancer, predominantly represented by HCC and ICC, with its increasing incidences and high mortality rates, represents a major health problem[1, 4]. Epidemiological data revealed that chronic liver inflammation and liver damage are important risk factors for both cancer types, however, up to now it remained unclear why some patients with such conditions develop HCC while others develop ICC[5, 8]. It has been shown in different studies that both cancer types can evolve from liver progenitor cells or from hepatocytes[46, 47, 49].

Over the last years more and more mouse models to study either HCC or ICC were developed. Mostly genetically engineered mouse models were used to study the role of single genes or genetic interactions. Other models took advantage of chemically- or inflammation-induced chronic liver damage which finally results in liver cancer development[131]. Models pioneered in the Zender laboratory utilize transposon vectors together with intrahepatic delivery methods to transform hepatocytes in their natural environment[113, 114, 118]. These models have the advantage of being relatively fast and highly flexible.

In mosaic mouse models the use of defined driving oncogenes or combinations of oncogenic drivers usually triggers the outgrowth of either pure HCC or ICC. For example activation of the Wnt/β-catenin pathway which is often seen in human HCC and forced induction of the pathway also results in HCC in mice.[132, 133] Conversely, Kras or Notch signaling, which is activated in human ICCs, also induces ICC development in mosaic mouse models[49, 50, 134-136]. These data suggest that oncogenic mutations can direct cell fate decisions in liver tumorigenesis. However, data obtained within the scope of the cancer genome project revealed a shared mutational landscape of many HCC and ICC, making it unlikely that phenotype-specific mutations are the sole determinant of lineage commitment in liver cancer[34-37]. For example, besides mutations in the *TP53* tumor suppressor, HCC and ICC share recurrent mutations in *ARID1A, PIK3CA, MLL3, BAP1* and others[34-37]. Interestingly, in my thesis work we could show that overexpression of c-myc together with an $Nras^{G12V}$ mediated induction of the MEK-ERK signaling pathway or c-myc together with a constitutive active form of AKT1 can either lead to HCC, ICC or mixed tumors depending on the model of gene delivery. This led to the suggestion that other

factors than mutations also impact lineage commitment which is further supported by the fact that no additional somatic mutations occurred in our HCC or ICC model. Of note, lineage commitment in our model is determined at an early time point of tumorigenesis (5 days after oncogene delivery) while the spontaneous acquisition is a rather slow process.

It has been under debate for several years which cells represent the cell of origin for HCC or ICC development. It has been shown via different lineage tracing models that HCC can derive from LPC or hepatocytes and that ICC can derive from LPC, cholangiocytes or hepatocytes[43, 49, 137]. However, it was not yet shown, that both cancer types can derive from the same cells in one model driven by the same oncogenes. Using the *AlbCre* hepatocyte-specific lineage tracing mouse model we could show that in our system HCC as well as ICC derived from adult hepatocytes. It has to be mentioned that some studies reported that in the *AlbCre* mouse an activity of Cre-recombinase was not only observed in hepatocytes but also in bile duct cells[138]. However, in concordance with our results, other showed hepatocyte-specific Cre-expression[139]. Furthermore it has been shown, that transformation via Epo only affects hepatocytes[118]. Nevertheless, to validate our results in another lineage-tracing model one could make use of a hepatocyte-specific adeno-associated virus expressing Cre under the Ttr promotor[140]. This virus which has been reported to express Cre exclusively in hepatocytes could be delivered into the ROSA$^{mT/mG}$ mice. Subsequently fluorescence analysis of Epo-induced ICC could validate hepatocytic origin of ICC tumors. However, our finding supports the theory that hepatocytes harbor a high grade of plasticity. Still, we do not know if hepatocytes first undergo dedifferentiation into PLC-like cells as it has been reported in other studies[46]. Interestingly, one study showed that hepatic injury is already sufficient for this dedifferentiation so it is likely that this may also occur upon Epo-treatment[52]. Immunohistochemistry analysis of stem cell markers as Nanog, Oct4 or Nestin could be conducted and analyzed to identify putative dedifferentiation of cells[141].

Many studies have shown that the microenvironmental conditions play a major role in tumor development. Using a sequential application of oncogene delivery via HDTV and a mock Epo clearly showed that environmental conditions due to Epo favor

development of ICC. The most prominent condition during the pre-tumorigenic phase in the HDTV as well as Epo model was the high amount of tissue damage.

It is known that hepatic cell death is a prerequisite of liver cancer development[69]. It usually leads to proliferative compensation of other LPC or hepatocytes. Dying cells can release DAMP´s or other factors recruiting immune cells or directly interacting with normal or already transformed cells. Interestingly, in this study the type of hepatic cell death strongly depends on the oncogene delivery method. HDTV predominantly induces apoptosis which is reported in numerous studies to play major roles in HCC development. For example hepatocyte specific knockout of the BCL-2 family member *myeloid cell leukemia sequence 1 (MCL1)* leads to high amounts of apoptosis-mediated liver damage subsequently resulting in HCC development[142]. Further, hepatocyte specific inhibition of the kinase *TGF-β–activated kinase 1 (Tak1)* showed high levels of cleaved caspase 3 again resulting in liver damage and HCC development[143]. It has to be mentioned that in these studies hepatic cell death is the driver of carcinogenesis while in our study it only seems to be a bystander of the delivery method. Chemical or genetic inhibition of apoptosis in our HCC model might help to answer the question if an apoptotic microenvironment is necessary for tumor development in general or even especially for HCC development.

In contrast, induction of necroptosis could be observed after applying Epo to mouse livers. It is widely accepted and in accordance with our data that under physiological conditions hepatocytes do not express RIPK3 making them unlikely to undergo necroptosis. However, in line with our findings it has been reported that upon APAP, concanavalin A or high-fat-diet induced liver damage hepatocytes are able to induce *Ripk3* expression[144, 145]. Necroptosis has not yet been directly linked to PLC development, however, there are several studies showing its importance in liver diseases which often subsequently develop into liver cancers. For example, increased levels of necroptosis have been described in liver disease patients. It was shown that expression of *RIPK3* is induced in patients with ethanol-induced liver injury, cholangitis or NASH[88-90]. It is conceivable that the increased incidence of ICC might be, at least in part, due to the rising numbers of patients suffering from NASH. At least our study showed that necroptosis signatures are enriched in ICC patients. This data suggests that an anti-necroptotic therapy in liver disease patients might be able to reduce ICC induction or at least switch ICC to HCC development which is less invasive and for which more therapeutic options exist. Nevertheless, studies have to

be done in the future where liver disease patients with or without necroptosis marker need to be monitored for HCC or ICC development to draw a distinct correlation between necroptosis and ICC induction in humans.

Another prominent observation in the microenvironment in the pre-cancerous phase of our PLC mouse models was the high amount of infiltrating immune cells. It is known from several studies that especially liver-resident immune cells as Kupffer cells and stellate cells highly impact development of primary liver cancers[30, 31]. However, this is mostly mediated by the induction of chronic liver damage or fibrosis which are pre-conditions for tumor development. It was also shown that Kupffer cell-released tumor necrosis factor α (TNFα) directly induces biliary proliferation[32]. Other direct interactions of immune cells with oncogenically transformed cells have also been reported. For example it has been shown that immature myeloid precursor cells can inhibit NK cells which in turn promotes HCC development[146]. Interestingly, in the here presented study the composition of immune cell infiltrates seems to be irrelevant as no differences in numbers of any population could be observed between HDTV and Epo induction. This is quite interesting as necroptotic cells are known to release high amounts of pro-inflammatory DAMPs. Until now only few of them are known as IL-33, HMGB1 or ATP[75]. It is likely that they also play a major role in the Epo model, however, quantifications of these factors for example via western blot or functional studies using blocking antibodies during oncogenesis need to be done for validation. Nonetheless knockout of the most important DAMP receptors, the group of TLRs, was sufficient to favor HCC development over ICC. TLRs are especially widely expressed on cells of the immune system[127]. We further showed that in SCID/beige mice, which lack major parts of the innate and adaptive immune system predominantly also HCC develops after Epo-induced transformation. This suggests that TLRs on immune cells might be important mediators in the underlying mechanism that a necroptotic environment favors ICC development. However, it cannot be excluded that TLRs on hepatocytes also contribute. It is known that TLR4 is expressed on hepatocytes and TLR2 can be expressed upon hepatocyte damage[147, 148]. Notably, knockout of these two TLRs is already sufficient to prevent necroptosis associated ICC development. Further, activated TLRs are known to be able to induce necroptosis[76]. Although there was an induction of necroptosis in *TLR5x* KO mice, there is still the possibility that hepatocyte-TLR-induced necroptosis

contributes to DAMP release which activates immune cell TLRs. This issue could be answered via bone marrow transplantation experiments from TLR knockout mice into wt mice or vice versa with subsequent Epo-induced tumorigenesis. Another approach would be to use hepatocyte or immune cell-specific TLR knockout mice for tumor development experiments.

TLRs are also important in the activation of immune cells and not only in their attraction. Based on our results of quantifications of immune cells this might be more important in this study. This is supported by the fact that SCID/beige mice preferably develop HCC upon Epo-induced transformation. To characterize activity or maturation of immune cells flow cytometry with fluorescently labelled antibodies specific for maturation or activity markers could be conducted on liver lysates after applying HDTV or Epo. Functional experiments using immune cell-specific knockout mice or immune cell depleting treatments in HDTV- and Epo-induced tumor development and subsequent analysis of the tumor phenotype might also help to identify a putative role of immune cell activation. However, it has to be mentioned that in this study we used combinations with strong oncogenic drivers which are already sufficient to induce tumor development within the same time also in the absence of an intact immune system. So it remains possible that the role of immune cells in lineage commitment might be underestimated in this study as usually PLC develops due to inflammatory conditions[69]. To also analyze the influence of necroptosis in hepatocyte damage- or inflammatory-driven liver cancer mouse models utilizing DEN, CCl_4 or concanavalin A could be used[131]. In these models first chronic liver damage and inflammation occurs which subsequently induces HCC development. In parallel to the liver-damaging treatment chronic necroptosis induction could be applied. In such a setting long-term necroptosis-dependent immune reactions could be analyzed regarding the influence on HCC to ICC developmental switch. This would better reflect the situation in human patients were liver cancer develops over a long time with a more chronic necroptosis.

Another hint suggesting that the activation status of immune cells influences lineage commitment comes from analyses of the cytokine milieu. We could show that necroptosis is associated with a distinct cytokine pattern and main sources for cytokine production are activated immune cells. In this study it was not addressed which distinct cytokine might be the most potent one to direct lineage commitment or how this regulations might be conducted. However, to identify these regulations is not

only important for understanding basic mechanisms but also holds high potential for a therapeutic modulation of cytokine effects. Indeed, it has been shown that single cytokines can regulate cancer development. For example interleukin 6 (IL-6) was reported to activate β-catenin pathway promoting HCC induction[149]. Although the cytokine analysis in Epo vs HDTV showed the highest regulation for CCL4, it is not much affected upon chemically or genetically inhibition of necroptosis. So, it is more likely that Epo-specific cytokines which were down-regulated upon necroptosis inhibition or TLR knockout, such as CCL6, CCL8, Pf4, or Aimp1 are important for lineage commitment. There are several possibilities to narrow down which distinct cytokines affect hepatocyte lineage commitment. First, hepatocytes could be isolated from HDTV or Epo-treated livers and expression of known cytokine-receptors could be analyzed. Further, phospho-proteomics could be conducted to identify activation of specific intracellular pathways which could be matched upstream to a cytokine receptor. Then functional experiments via blocking antibodies or applying recombinant cytokines in combination with HDTV or Epo of oncogenes could help to validate the results. Additionally, shRNA-mediated knockdown of cytokine-receptor downstream targets could also be applied simultaneously to oncogene delivery as well as over-activation via mutated cDNAs for genetic validation.

Of course, not only the identification of the cytokine but also the determination of the cells which produce them might hold therapeutic potential. For example CCL8 is produced by macrophages or T-cells, however it is likely that also other cell types produce CCL8 as there is not much known about its sources yet[150, 151]. As SCID/beige mice lack functional T-cells and have impaired macrophages CCL8 might be an important regulator[152]. However, clodronate-mediated macrophage depletion did not switch ICC to HCC making macrophages the main regulatory cells more unlikely. CCL6 is also produced by macrophages as well as neutrophils which have decreased activity in SCID/beige mice[153-155]. Interestingly neutrophils also express multiple TLRs[156]. So there is the possibility that neutrophil derived CCL6 influences lineage commitment of liver cancer. Importantly, CCL6 could only be identified in rodents but not in humans so the human ortholog still needs to be identified for therapeutic use. Activated platelets are the only known source for Pf4 making them a putative candidate for lineage commitment, too. They also harbor TLR expression and it has been reported that SCID/beige mice have an impaired platelet function making platelet-derived Pf4 another putative regulator[157, 158]. About Aimp1 there is

not much known yet. It has been suggested that it is released from dying cells, however, there is no information about a specific immune cell population which releases Aimp1[159]. Nevertheless, to identify the source population or populations more functional experiments using depleting antibodies or knockout mice in our HCC and ICC models are needed.

A key remaining question is which signaling pathways within the hepatocyte transduce the cytokine-mediated lineage commitment signals. As the information for tumor entity was heritable in tumor cells shown in cell transplantation experiments it is likely that epigenetic events might play an important role. Indeed, we found tumor type specific epigenetic signatures using chromatin accessibility analyses. It has been shown earlier that HCC and ICC harbor different epigenetic landscapes, however, in these studies it was not known from which cell types these tumors derived[34, 108, 109]. This is especially important as the normal epigenetic landscape between different cell types is already quite distinct. Also, the oncogenic drivers in these samples were quite diverse between all samples which made interpretation of the results difficult.

It has been shown for cells in the hematopoietic lineage that environmental conditions can influence epigenetic landscape[101, 102]. One study used transplantation of bone marrow-derived macrophages into recipient mice and analyzed settled macrophages from different organs a few months later. Interestingly, they showed that epigenetic signatures from these transplanted macrophages were highly similar to distinct tissue-resident macrophages from control mice. How the interaction between the microenvironment and the macrophages could be conducted need to be remained. However, they found that especially some pioneer transcription factors have an altered methylation of the histone H3K4. Similar to this we could identify different chromatin accessibilities in gene regions of two pioneer transcription factors Tbx3 and Prdm5.

Tbx3 is known to play important roles in cell stemness and especially in cell differentiation of LPC into hepatocytes or cholangiocytes. Deletion of *Tbx3* reduces differentiation of hepatoblasts into hepatocytes but favors cholangiocytic differentiation[160, 161]. This correlates with the fact that in our study chromatin availability and expression of *Tbx3* was significantly higher in HCC cells than in ICC as well as HCC patients compared to ICC. On the other hand, forced expression of

Tbx3 in our Epo-induced ICC model shifted tumor development towards phenotype of undifferentiated tumor. However, it remains unknown if forced *Tbx3* expression only compensates necroptosis-associated cholangiocytic lineage differentiation or if it also able to switch already established ICC. This question could for example be addressed using inducible *Tbx3* constructs using the TRE/doxycycline system. This would allow switching on *Tbx3* expression via doxycycline food in mice already bearing ICC tumors.

Importantly, knockdown of *Tbx3* alone was not sufficient to switch HCC to ICC development. This might be explained with less efficient knockdown of *Tbx3* as one study also showed that heterozygous knockout of *Tbx3* had a much smaller developmental effect on the liver compared to homozygous knockout[160]. Experiments using the CRISPR/Cas9 system could be conducted to induce complete *Tbx3* knockout which might already be sufficient to alter tumor phenotype.

Another pioneer transcription factor we identified using comparative analysis of ATAC-seq and microarray data was *Prdm5*. Prdm5 is known to attract histone methyltransferases or deacetylases and thus alter chromatin structure of bound genome regions[162]. Interestingly, expression of *Prdm5* is associated with decreased activation of Wnt/β-catenin pathway which is usually activated in HCC[163]. This correlates with our findings that ICC cells as well as ICC patients have higher expression levels compared to HCC cells or patients, respectively.

Nonetheless, forced expression of *Prdm5* in our HDTV-based HCC model did not change the type of the tumor. One explanation for this observation could be that Prdm5 usually functions in concert with other transcriptions factors which might be less active in this scenario. However, simultaneous expression of *Prdm5* together with *Tbx3* knockdown was able to switch HCC- to ICC development. This was in line with the observation that downstream signaling pathways either related to Tbx3 or Prdm5 are quite distinct with only small overlaps. Interestingly, amongst positively related pathways to Prdm5 are collagen formation and extracellular matrix interaction which are important for interactions of tumor and stroma cells which are highly abundant in ICC[3].

Nevertheless, which exact downstream signaling events underlie the observed lineage commitment phenotype is still unknown. Taking advantage of our ChIP-seq and microarray data shRNA libraries could be generated and delivered together with a fluorescence marker into mice either via Epo or HDTV. Developing tumors could

then be harvested and sorted via flow cytometry with additional staining of K19 to differentiate between HCC and ICC tumor cells. Finally distribution of shRNAs could be calculated to identify main pathways for Tbx3 or Prdm5-mediated lineage commitment.

A remaining question is how Tbx3 and Prdm5 itself are regulated during the early phases of tumor initiation. Our study suggested some candidates of chromatin remodeling proteins which are differentially regulated between HDTV and Epo in the pre-tumorigenic phase. However, functional validation of these candidates via additional overexpression or shRNA mediated knockdown of these regulators needs to be done in the future. To perform a more unbiased analysis oncogene delivery together with a marker gene should be performed and cells could be sorted via FACS at different time points. Transcriptome analyses or ATAC-seq might give insights into the dynamic and regulatory network of early epigenetic regulation. A more direct way would be a CRISPR-ChAP-MS analysis[164]. Here, sgRNAs specifically binding regions of Tbx3 or Prdm5, respectively, could be co-delivered with a Cas9 encoding plasmid. Then, bound Cas9 could be precipitated together with the chromatin and other bound factors. Subsequently, these factors could be analyzed via mass spectrometry to identify direct regulators of early Tbx3 or Prdm5 regulation. These putative candidates then need to be genetically validated if they indeed alter expression of Tbx3 or Prdm5.

Our here presented findings on microenvironment dependent changes of the ICC or HCC defining epigenetic landscapes are likely to also have important implications for the treatment of HCC and ICC. It is well established that HCC and ICC behave quite different regarding therapeutic responses towards classical cytotoxic chemotherapies or molecularly targeted therapies. It has been shown that HCC represents a primarily chemoresistant tumor and so far no cytotoxic therapy could improve survival of patients with advanced HCC[165]. In contrast, ICC responds to cytotoxic therapy with the substances Gemcitabine and Cisplatin, resulting in a significantly increased survival of patients with advanced ICC[28]. Conversely, it was shown that treatment with the multikinase inhibitors sorafenib, lenvatinib and cabozantinib can moderately but significantly increase the overall survival of patients with advanced HCC, however, ICC do not respond to therapies with multikinase inhibitors[20, 22, 166, 167]. It is tempting to speculate that chromatin structural changes and epigenetic regulation

may contribute to these distinct patterns of sensitivity/resistance towards liver cancer therapies and may also contribute to acquired resistance in treated tumors. There are studies which show that HCC after a therapy using transarterial chemoembolization (TACE) with Doxorubicin show increased characteristics of cholangiocellular morphology[168, 169]. TACE is described to induce hepatic and tumor necrosis, however, there are no studies further characterizing the exact type of cell death[170]. Such an analysis could unravel the underlying mechanisms. If induction of necroptosis was observed, it would support our here presented theory of lineage commitment. Of course, only a direct correlation of TACE-induced necroptosis and subsequent ICC development could exactly validate it. Further, studies using anti-necroptotic drugs during or after TACE might have therapeutic potential to reduce a switch to the more invasive ICC. Additionally, epigenetic analyses of tumors before and after TACE might be useful to support the here presented mechanism. Also combination therapies involving epigenetic modulators such as histone-deacetylase (HDAC) or methyltransferase inhibitors should be explored in order to break primary or secondary therapy resistance of liver cancer. Likewise, as ICC is highly metastatic while HCC most often show local destructive growth within the liver, such therapies may have potential to decrease metastasis in liver cancer.

5. Acknowledgements

First of all, I would like to thank my supervisor Lars Zender for the opportunity to perform this study in his lab, for his scientific guidance and input.
Further, I am grateful to Klaus Schulze-Osthoff for being a referent for my PhD thesis.
I want to specially thank Florian Heinzmann who not only taught me many things in the lab but also conducted much of the presented work in collaboration. Jule Harbig, Luana D'Artista, Sabrina Klotz, Tae-Won Kang and Lisa Hönicke also deserve my gratitude for supporting this project.
Additionally, I am very thankful to Elke Rist, Pearl Schiemann, Carolin Fellmeth and Dominique Quetting for assistance with mouse husbandry, histology and general lab organization.
A special thank also goes to all our collaboration partners from Bischof Lab, Zuber Lab, Wang Lab, Heikenwälder Lab and Luedde Lab as well as Thomas Longerich, Bence Sipos, and Thorsten Buch for their great help completing this project.
The whole Zender Lab deserves a really big thanks for providing great working conditions and a great atmosphere also outside the lab.
Finally, I want to thank my family and friends for always supporting me in any situation during this exciting and sometimes exhausting time.

6. References

1. Lozano, R. *et al.* Global and regional mortality from 235 causes of death for 20 age groups in 1990 and 2010: a systematic analysis for the Global Burden of Disease Study 2010. *Lancet* **380**, 2095-2128 (2012).

2. Llovet, J.M. *et al.* Hepatocellular carcinoma. *Nat Rev Dis Primers* **2**, 16018 (2016).

3. Rizvi, S. & Gores, G.J. Pathogenesis, diagnosis, and management of cholangiocarcinoma. *Gastroenterology* **145**, 1215-1229 (2013).

4. Collaborators, G.B.D.C.o.D. Global, regional, and national age-sex specific mortality for 264 causes of death, 1980-2016: a systematic analysis for the Global Burden of Disease Study 2016. *Lancet* **390**, 1151-1210 (2017).

5. Marquardt, J.U., Andersen, J.B. & Thorgeirsson, S.S. Functional and genetic deconstruction of the cellular origin in liver cancer. *Nat Rev Cancer* **15**, 653-667 (2015).

6. El-Serag, H.B. Hepatocellular carcinoma. *N Engl J Med* **365**, 1118-1127 (2011).

7. Ghouri, Y.A., Mian, I. & Rowe, J.H. Review of hepatocellular carcinoma: Epidemiology, etiology, and carcinogenesis. *J Carcinog* **16**, 1 (2017).

8. Farazi, P.A. & DePinho, R.A. Hepatocellular carcinoma pathogenesis: from genes to environment. *Nat Rev Cancer* **6**, 674-687 (2006).

9. Schulz, P.O. *et al.* Association of nonalcoholic fatty liver disease and liver cancer. *World J Gastroenterol* **21**, 913-918 (2015).

10. Zeuzem, S. Decade in review-HCV: hepatitis C therapy-a fast and competitive race. *Nat Rev Gastroenterol Hepatol* **11**, 644-645 (2014).

11. Zender, L. & Malek, N.P. [Diagnostics and treatment of cholangiocellular carcinoma]. *Internist (Berl)* **57**, 1191-1205 (2016).

12. Palmer, W.C. & Patel, T. Are common factors involved in the pathogenesis of primary liver cancers? A meta-analysis of risk factors for intrahepatic cholangiocarcinoma. *J Hepatol* **57**, 69-76 (2012).

13. Welzel, T.M. *et al.* Risk factors for intrahepatic and extrahepatic cholangiocarcinoma in the United States: a population-based case-control study. *Clin Gastroenterol Hepatol* **5**, 1221-1228 (2007).

14. Shaib, Y.H., El-Serag, H.B., Davila, J.A., Morgan, R. & McGlynn, K.A. Risk factors of intrahepatic cholangiocarcinoma in the United States: a case-control study. *Gastroenterology* **128**, 620-626 (2005).

15. Honjo, S. *et al.* Genetic and environmental determinants of risk for cholangiocarcinoma via Opisthorchis viverrini in a densely infested area in Nakhon Phanom, northeast Thailand. *Int J Cancer* **117**, 854-860 (2005).

16. Watanabe, T. *et al.* Synchronous development of HCC and CCC in the same subsegment of the liver in a patient with type C liver cirrhosis. *World J Hepatol* **1**, 103-109 (2009).

17. Marrero, J.A. *et al.* Alpha-fetoprotein, des-gamma carboxyprothrombin, and lectin-bound alpha-fetoprotein in early hepatocellular carcinoma. *Gastroenterology* **137**, 110-118 (2009).

18. Llovet, J.M., Schwartz, M. & Mazzaferro, V. Resection and liver transplantation for hepatocellular carcinoma. *Semin Liver Dis* **25**, 181-200 (2005).

19. European Association For The Study Of The, L., European Organisation For, R. & Treatment Of, C. EASL-EORTC clinical practice guidelines: management of hepatocellular carcinoma. *J Hepatol* **56**, 908-943 (2012).

20. Llovet, J.M. *et al.* Sorafenib in advanced hepatocellular carcinoma. *N Engl J Med* **359**, 378-390 (2008).

21. Bruix, J. *et al.* Regorafenib for patients with hepatocellular carcinoma who progressed on sorafenib treatment (RESORCE): a randomised, double-blind, placebo-controlled, phase 3 trial. *Lancet* **389**, 56-66 (2017).

22. Abou-Alfa, G.K. *et al.* Cabozantinib in Patients with Advanced and Progressing Hepatocellular Carcinoma. *N Engl J Med* **379**, 54-63 (2018).

23. El-Khoueiry, A.B. *et al.* Nivolumab in patients with advanced hepatocellular carcinoma (CheckMate 040): an open-label, non-comparative, phase 1/2 dose escalation and expansion trial. *Lancet* **389**, 2492-2502 (2017).

24. Tshering, G., Dorji, P.W., Chaijaroenkul, W. & Na-Bangchang, K. Biomarkers for the Diagnosis of Cholangiocarcinoma: A Systematic Review. *Am J Trop Med Hyg* **98**, 1788-1797 (2018).

25. Cho, S.Y. *et al.* Survival analysis of intrahepatic cholangiocarcinoma after resection. *Ann Surg Oncol* **17**, 1823-1830 (2010).

26. Choi, S.B. *et al.* The prognosis and survival outcome of intrahepatic cholangiocarcinoma following surgical resection: association of lymph node metastasis and lymph node dissection with survival. *Ann Surg Oncol* **16**, 3048-3056 (2009).

27. Endo, I. *et al.* Intrahepatic cholangiocarcinoma: rising frequency, improved survival, and determinants of outcome after resection. *Ann Surg* **248**, 84-96 (2008).

28. Valle, J. *et al.* Cisplatin plus gemcitabine versus gemcitabine for biliary tract cancer. *N Engl J Med* **362**, 1273-1281 (2010).

29. Fujita, T. & Narumiya, S. Roles of hepatic stellate cells in liver inflammation: a new perspective. *Inflamm Regen* **36**, 1 (2016).

30. Okabe, H. *et al.* Hepatic stellate cells may relate to progression of intrahepatic cholangiocarcinoma. *Ann Surg Oncol* **16**, 2555-2564 (2009).

31. Ju, C. & Tacke, F. Hepatic macrophages in homeostasis and liver diseases: from pathogenesis to novel therapeutic strategies. *Cell Mol Immunol* **13**, 316-327 (2016).

32. Yuan, D. *et al.* Kupffer Cell-Derived Tnf Triggers Cholangiocellular Tumorigenesis through JNK due to Chronic Mitochondrial Dysfunction and ROS. *Cancer Cell* **31**, 771-789 e776 (2017).

33. Saha, S.K., Parachoniak, C.A. & Bardeesy, N. IDH mutations in liver cell plasticity and biliary cancer. *Cell Cycle* **13**, 3176-3182 (2014).

34. Farshidfar, F. *et al.* Integrative Genomic Analysis of Cholangiocarcinoma Identifies Distinct IDH-Mutant Molecular Profiles. *Cell Rep* **18**, 2780-2794 (2017).

35. Jiao, Y. *et al.* Exome sequencing identifies frequent inactivating mutations in BAP1, ARID1A and PBRM1 in intrahepatic cholangiocarcinomas. *Nat Genet* **45**, 1470-1473 (2013).

36. Guichard, C. *et al.* Integrated analysis of somatic mutations and focal copy-number changes identifies key genes and pathways in hepatocellular carcinoma. *Nat Genet* **44**, 694-698 (2012).

37. Fujimoto, A. *et al.* Whole-genome sequencing of liver cancers identifies etiological influences on mutation patterns and recurrent mutations in chromatin regulators. *Nat Genet* **44**, 760-764 (2012).

38. Farazi, P.A. *et al.* Differential impact of telomere dysfunction on initiation and progression of hepatocellular carcinoma. *Cancer Res* **63**, 5021-5027 (2003).

39. Tannapfel, A. *et al.* Frequency of p16(INK4A) alterations and K-ras mutations in intrahepatic cholangiocarcinoma of the liver. *Gut* **47**, 721-727 (2000).

40. Chan-On, W. *et al.* Exome sequencing identifies distinct mutational patterns in liver fluke-related and non-infection-related bile duct cancers. *Nat Genet* **45**, 1474-1478 (2013).

41. Sia, D., Villanueva, A., Friedman, S.L. & Llovet, J.M. Liver Cancer Cell of Origin, Molecular Class, and Effects on Patient Prognosis. *Gastroenterology* **152**, 745-761 (2017).

42. Mu, X. *et al.* Hepatocellular carcinoma originates from hepatocytes and not from the progenitor/biliary compartment. *J Clin Invest* **125**, 3891-3903 (2015).

43. Guest, R.V. *et al.* Cell lineage tracing reveals a biliary origin of intrahepatic cholangiocarcinoma. *Cancer Res* **74**, 1005-1010 (2014).

44. Cardinale, V., Carpino, G., Reid, L., Gaudio, E. & Alvaro, D. Multiple cells of origin in cholangiocarcinoma underlie biological, epidemiological and clinical heterogeneity. *World J Gastrointest Oncol* **4**, 94-102 (2012).

45. Komuta, M. *et al.* Clinicopathological study on cholangiolocellular carcinoma suggesting hepatic progenitor cell origin. *Hepatology* **47**, 1544-1556 (2008).

46. Tschaharganeh, D.F. *et al.* p53-dependent Nestin regulation links tumor suppression to cellular plasticity in liver cancer. *Cell* **158**, 579-592 (2014).

47. Tschaharganeh, D.F. *et al.* Yes-associated protein up-regulates Jagged-1 and activates the Notch pathway in human hepatocellular carcinoma. *Gastroenterology* **144**, 1530-1542 e1512 (2013).

48. Fitamant, J. *et al.* YAP Inhibition Restores Hepatocyte Differentiation in Advanced HCC, Leading to Tumor Regression. *Cell Rep* (2015).

49. Sekiya, S. & Suzuki, A. Intrahepatic cholangiocarcinoma can arise from Notch-mediated conversion of hepatocytes. *J Clin Invest* **122**, 3914-3918 (2012).

50. Zender, S. *et al.* A critical role for notch signaling in the formation of cholangiocellular carcinomas. *Cancer Cell* **23**, 784-795 (2013).

51. Fan, B. *et al.* Cholangiocarcinomas can originate from hepatocytes in mice. *J Clin Invest* **122**, 2911-2915 (2012).

52. Schaub, J.R., Malato, Y., Gormond, C. & Willenbring, H. Evidence against a stem cell origin of new hepatocytes in a common mouse model of chronic liver injury. *Cell Rep* **8**, 933-939 (2014).

53. Schlageter, M., Terracciano, L.M., D'Angelo, S. & Sorrentino, P. Histopathology of hepatocellular carcinoma. *World J Gastroenterol* **20**, 15955-15964 (2014).

54. Schmuck, R.B., de Carvalho-Fischer, C.V., Neumann, C., Pratschke, J. & Bahra, M. Distal bile duct carcinomas and pancreatic ductal adenocarcinomas: postulating a common tumor entity. *Cancer Med* **5**, 88-99 (2016).

55. Galluzzi, L. *et al.* Molecular mechanisms of cell death: recommendations of the Nomenclature Committee on Cell Death 2018. *Cell Death Differ* **25**, 486-541 (2018).

56. Roos, W.P., Thomas, A.D. & Kaina, B. DNA damage and the balance between survival and death in cancer biology. *Nat Rev Cancer* **16**, 20-33 (2016).

57. Brumatti, G., Salmanidis, M. & Ekert, P.G. Crossing paths: interactions between the cell death machinery and growth factor survival signals. *Cell Mol Life Sci* **67**, 1619-1630 (2010).

58. Shamas-Din, A., Kale, J., Leber, B. & Andrews, D.W. Mechanisms of action of Bcl-2 family proteins. *Cold Spring Harb Perspect Biol* **5**, a008714 (2013).

59. Luna-Vargas, M.P.A. & Chipuk, J.E. Physiological and Pharmacological Control of BAK, BAX, and Beyond. *Trends Cell Biol* **26**, 906-917 (2016).

60. Llambi, F. *et al.* BOK Is a Non-canonical BCL-2 Family Effector of Apoptosis Regulated by ER-Associated Degradation. *Cell* **165**, 421-433 (2016).

61. Lee, E.F. *et al.* Physiological restraint of Bak by Bcl-xL is essential for cell survival. *Genes Dev* **30**, 1240-1250 (2016).

62. Li, P. *et al.* Cytochrome c and dATP-dependent formation of Apaf-1/caspase-9 complex initiates an apoptotic protease cascade. *Cell* **91**, 479-489 (1997).

63. Liu, X., Kim, C.N., Yang, J., Jemmerson, R. & Wang, X. Induction of apoptotic program in cell-free extracts: requirement for dATP and cytochrome c. *Cell* **86**, 147-157 (1996).

64. Tait, S.W. & Green, D.R. Mitochondria and cell death: outer membrane permeabilization and beyond. *Nat Rev Mol Cell Biol* **11**, 621-632 (2010).

65. Julien, O. & Wells, J.A. Caspases and their substrates. *Cell Death Differ* **24**, 1380-1389 (2017).

66. Shalini, S., Dorstyn, L., Dawar, S. & Kumar, S. Old, new and emerging functions of caspases. *Cell Death Differ* **22**, 526-539 (2015).

67. Enari, M. *et al.* A caspase-activated DNase that degrades DNA during apoptosis, and its inhibitor ICAD. *Nature* **391**, 43-50 (1998).

68. Sakahira, H., Enari, M. & Nagata, S. Cleavage of CAD inhibitor in CAD activation and DNA degradation during apoptosis. *Nature* **391**, 96-99 (1998).

69. Luedde, T., Kaplowitz, N. & Schwabe, R.F. Cell death and cell death responses in liver disease: mechanisms and clinical relevance. *Gastroenterology* **147**, 765-783 e764 (2014).

70. Kaiser, W.J. *et al.* Toll-like receptor 3-mediated necrosis via TRIF, RIP3, and MLKL. *J Biol Chem* **288**, 31268-31279 (2013).

71. Upton, J.W., Kaiser, W.J. & Mocarski, E.S. DAI/ZBP1/DLM-1 complexes with RIP3 to mediate virus-induced programmed necrosis that is targeted by murine cytomegalovirus vIRA. *Cell Host Microbe* **11**, 290-297 (2012).

72. Galluzzi, L., Kepp, O., Krautwald, S., Kroemer, G. & Linkermann, A. Molecular mechanisms of regulated necrosis. *Semin Cell Dev Biol* **35**, 24-32 (2014).

73. Li, J. *et al.* The RIP1/RIP3 necrosome forms a functional amyloid signaling complex required for programmed necrosis. *Cell* **150**, 339-350 (2012).

74. Murphy, J.M. *et al.* The pseudokinase MLKL mediates necroptosis via a molecular switch mechanism. *Immunity* **39**, 443-453 (2013).

75. Pasparakis, M. & Vandenabeele, P. Necroptosis and its role in inflammation. *Nature* **517**, 311-320 (2015).

76. Takeuchi, O. & Akira, S. Pattern recognition receptors and inflammation. *Cell* **140**, 805-820 (2010).

77. Kolb, J.P., Oguin, T.H., 3rd, Oberst, A. & Martinez, J. Programmed Cell Death and Inflammation: Winter Is Coming. *Trends Immunol* **38**, 705-718 (2017).

78. Paoli, P., Giannoni, E. & Chiarugi, P. Anoikis molecular pathways and its role in cancer progression. *Biochim Biophys Acta* **1833**, 3481-3498 (2013).

79. Das, G., Shravage, B.V. & Baehrecke, E.H. Regulation and function of autophagy during cell survival and cell death. *Cold Spring Harb Perspect Biol* **4** (2012).

80. Guicciardi, M.E., Malhi, H., Mott, J.L. & Gores, G.J. Apoptosis and necrosis in the liver. *Compr Physiol* **3**, 977-1010 (2013).

81. Faubion, W.A. *et al.* Toxic bile salts induce rodent hepatocyte apoptosis via direct activation of Fas. *J Clin Invest* **103**, 137-145 (1999).

82. Asselah, T. *et al.* In vivo hepatic endoplasmic reticulum stress in patients with chronic hepatitis C. *J Pathol* **221**, 264-274 (2010).

83. Merquiol, E. *et al.* HCV causes chronic endoplasmic reticulum stress leading to adaptation and interference with the unfolded protein response. *PLoS One* **6**, e24660 (2011).

84. Iredale, J.P. *et al.* Mechanisms of spontaneous resolution of rat liver fibrosis. Hepatic stellate cell apoptosis and reduced hepatic expression of metalloproteinase inhibitors. *J Clin Invest* **102**, 538-549 (1998).

85. Xia, X. *et al.* Cholangiocyte injury and ductopenic syndromes. *Semin Liver Dis* **27**, 401-412 (2007).

86. Hammerich, L. & Tacke, F. Eat more carrots? Dampening cell death in ethanol-induced liver fibrosis by beta-carotene. *Hepatobiliary Surg Nutr* **2**, 248-251 (2013).

87. Maeda, S., Kamata, H., Luo, J.L., Leffert, H. & Karin, M. IKKbeta couples hepatocyte death to cytokine-driven compensatory proliferation that promotes chemical hepatocarcinogenesis. *Cell* **121**, 977-990 (2005).

88. Gautheron, J. *et al.* A positive feedback loop between RIP3 and JNK controls non-alcoholic steatohepatitis. *EMBO Mol Med* **6**, 1062-1074 (2014).

89. Roychowdhury, S., McMullen, M.R., Pisano, S.G., Liu, X. & Nagy, L.E. Absence of receptor interacting protein kinase 3 prevents ethanol-induced liver injury. *Hepatology* **57**, 1773-1783 (2013).

90. Afonso, M.B. *et al.* Activation of necroptosis in human and experimental cholestasis. *Cell Death Dis* **7**, e2390 (2016).

91. Bird, A. Perceptions of epigenetics. *Nature* **447**, 396-398 (2007).

92. Feinberg, A.P. Phenotypic plasticity and the epigenetics of human disease. *Nature* **447**, 433-440 (2007).

93. Kiefer, J.C. Epigenetics in development. *Dev Dyn* **236**, 1144-1156 (2007).

94. Bird, A. DNA methylation patterns and epigenetic memory. *Genes Dev* **16**, 6-21 (2002).

95. Chaudry, S.F. & Chevassut, T.J.T. Epigenetic Guardian: A Review of the DNA Methyltransferase DNMT3A in Acute Myeloid Leukaemia and Clonal Haematopoiesis. *Biomed Res Int* (2017).

96. Suganuma, T. & Workman, J.L. Signals and combinatorial functions of histone modifications. *Annu Rev Biochem* **80**, 473-499 (2011).

97. Turner, B.M. Defining an epigenetic code. *Nat Cell Biol* **9**, 2-6 (2007).

98. Blancafort, P., Jin, J. & Frye, S. Writing and rewriting the epigenetic code of cancer cells: from engineered proteins to small molecules. *Mol Pharmacol* **83**, 563-576 (2013).

99. Ordog, T., Syed, S.A., Hayashi, Y. & Asuzu, D.T. Epigenetics and chromatin dynamics: a review and a paradigm for functional disorders. *Neurogastroenterol Motil* **24**, 1054-1068 (2012).

100. Sen, P., Shah, P.P., Nativio, R. & Berger, S.L. Epigenetic Mechanisms of Longevity and Aging. *Cell* **166**, 822-839 (2016).

101. Lavin, Y. *et al.* Tissue-resident macrophage enhancer landscapes are shaped by the local microenvironment. *Cell* **159**, 1312-1326 (2014).

102. Okabe, Y. & Medzhitov, R. Tissue-specific signals control reversible program of localization and functional polarization of macrophages. *Cell* **157**, 832-844 (2014).

103. Abutbul, S. *et al.* TGF-beta signaling through SMAD2/3 induces the quiescent microglial phenotype within the CNS environment. *Glia* **60**, 1160-1171 (2012).

104. Butovsky, O. *et al.* Identification of a unique TGF-beta-dependent molecular and functional signature in microglia. *Nat Neurosci* **17**, 131-143 (2014).

105. Feinberg, A.P. & Vogelstein, B. Hypomethylation of Ras Oncogenes in Primary Human Cancers. *Biochem Bioph Res Co* **111**, 47-54 (1983).

106. Feinberg, A.P. & Vogelstein, B. Hypomethylation Distinguishes Genes of Some Human Cancers from Their Normal Counterparts. *Nature* **301**, 89-92 (1983).

107. Sandhu, D.S., Shire, A.M. & Roberts, L.R. Epigenetic DNA hypermethylation in cholangiocarcinoma: potential roles in pathogenesis, diagnosis and identification of treatment targets. *Liver International* **28**, 12-27 (2008).

108. Zhang, C.S. *et al.* CpG island methylator phenotype association with upregulated telomerase activity in hepatocellular carcinoma. *International Journal of Cancer* **123**, 998-1004 (2008).

109. Yang, B., House, M.G., Guo, M.Z., Herman, J.G. & Clark, D.P. Promoter methylation profiles of tumor suppressor genes in intrahepatic and extrahepatic cholangiocarcinoma. *Modern Pathol* **18**, 412-420 (2005).

110. Matsumura, T., Makino, R. & Mitamura, K. Frequent down-regulation of E-cadherin by genetic and epigenetic changes in the malignant progression of hepatocellular carcinomas. *Clin Cancer Res* **7**, 594-599 (2001).

111. Tischoff, I. *et al.* Allele loss and epigenetic inactivation of 3p21.3 in malignant liver tumors. *International Journal of Cancer* **115**, 684-689 (2005).

112. Carlson, C.M., Frandsen, J.L., Kirchhof, N., McIvor, R.S. & Largaespada, D.A. Somatic integration of an oncogene-harboring Sleeping Beauty transposon models liver tumor development in the mouse. *Proc Natl Acad Sci U S A* **102**, 17059-17064 (2005).

113. Dauch, D. *et al.* A MYC-aurora kinase A protein complex represents an actionable drug target in p53-altered liver cancer. *Nat Med* **22**, 744-753 (2016).

114. Rudalska, R. *et al.* In vivo RNAi screening identifies a mechanism of sorafenib resistance in liver cancer. *Nat Med* **20**, 1138-1146 (2014).

115. Calvisi, D.F. *et al.* Inactivation of Ras GTPase-activating proteins promotes unrestrained activity of wild-type Ras in human liver cancer. *J Hepatol* **54**, 311-319 (2011).

116. Calvisi, D.F. *et al.* Ubiquitous activation of Ras and Jak/Stat pathways in human HCC. *Gastroenterology* **130**, 1117-1128 (2006).

117. Zender, L. *et al.* Cancer gene discovery in hepatocellular carcinoma. *J Hepatol* **52**, 921-929 (2010).

118. Gurlevik, E. *et al.* Adjuvant gemcitabine therapy improves survival in a locally induced, R0-resectable model of metastatic intrahepatic cholangiocarcinoma. *Hepatology* **58**, 1031-1041 (2013).

119. Hickman, M.A. *et al.* Gene expression following direct injection of DNA into liver. *Hum Gene Ther* **5**, 1477-1483 (1994).

120. Muzumdar, M.D., Tasic, B., Miyamichi, K., Li, L. & Luo, L. A global double-fluorescent Cre reporter mouse. *Genesis* **45**, 593-605 (2007).

121. Postic, C. *et al.* Dual roles for glucokinase in glucose homeostasis as determined by liver and pancreatic beta cell-specific gene knock-outs using Cre recombinase. *J Biol Chem* **274**, 305-315 (1999).

122. Iverson, S.V., Comstock, K.M., Kundert, J.A. & Schmidt, E.E. Contributions of new hepatocyte lineages to liver growth, maintenance, and regeneration in mice. *Hepatology* **54**, 655-663 (2011).

123. Wang, H. *et al.* Mixed lineage kinase domain-like protein MLKL causes necrotic membrane disruption upon phosphorylation by RIP3. *Mol Cell* **54**, 133-146 (2014).

124. Grasl-Kraupp, B. *et al.* In situ detection of fragmented DNA (TUNEL assay) fails to discriminate among apoptosis, necrosis, and autolytic cell death: a cautionary note. *Hepatology* **21**, 1465-1468 (1995).

125. Degterev, A. *et al.* Identification of RIP1 kinase as a specific cellular target of necrostatins. *Nat Chem Biol* **4**, 313-321 (2008).

126. Afonso, M.B. *et al.* miRNA-21 ablation protects against liver injury and necroptosis in cholestasis. *Cell Death Differ* **25**, 857-872 (2018).

127. Kiziltas, S. Toll-like receptors in pathophysiology of liver diseases. *World J Hepatol* **8**, 1354-1369 (2016).

128. Conrad, M.L. *et al.* Maternal TLR signaling is required for prenatal asthma protection by the nonpathogenic microbe Acinetobacter lwoffii F78. *J Exp Med* **206**, 2869-2877 (2009).

129. Buenrostro, J.D., Giresi, P.G., Zaba, L.C., Chang, H.Y. & Greenleaf, W.J. Transposition of native chromatin for fast and sensitive epigenomic profiling of open chromatin, DNA-binding proteins and nucleosome position. *Nat Methods* **10**, 1213-1218 (2013).

130. Buenrostro, J.D., Wu, B., Chang, H.Y. & Greenleaf, W.J. ATAC-seq: A Method for Assaying Chromatin Accessibility Genome-Wide. *Curr Protoc Mol Biol* **109**, 21 29 21-29 (2015).

131. He, L., Tian, D.A., Li, P.Y. & He, X.X. Mouse models of liver cancer: Progress and recommendations. *Oncotarget* **6**, 23306-23322 (2015).

132. Lee, S.A. *et al.* Integration of genomic analysis and in vivo transfection to identify sprouty 2 as a candidate tumor suppressor in liver cancer. *Hepatology* **47**, 1200-1210 (2008).

133. Tward, A.D. *et al.* Distinct pathways of genomic progression to benign and malignant tumors of the liver. *Proc Natl Acad Sci U S A* **104**, 14771-14776 (2007).

134. Che, L. *et al.* Jagged 1 is a major Notch ligand along cholangiocarcinoma development in mice and humans. *Oncogenesis* **5**, e274 (2016).

135. Cigliano, A., Wang, J., Chen, X. & Calvisi, D.F. Role of the Notch signaling in cholangiocarcinoma. *Expert Opin Ther Targets* **21**, 471-483 (2017).

136. Ikenoue, T. *et al.* A novel mouse model of intrahepatic cholangiocarcinoma induced by liver-specific Kras activation and Pten deletion. *Sci Rep* **6**, 23899 (2016).

137. Holczbauer, A. *et al.* Modeling pathogenesis of primary liver cancer in lineage-specific mouse cell types. *Gastroenterology* **145**, 221-231 (2013).

138. Geisler, F. *et al.* Liver-specific inactivation of Notch2, but not Notch1, compromises intrahepatic bile duct development in mice. *Hepatology* **48**, 607-616 (2008).

139. Weisend, C.M., Kundert, J.A., Suvorova, E.S., Prigge, J.R. & Schmidt, E.E. Cre Activity in Fetal albCre Mouse Hepatocytes: Utility for Developmental Studies. *Genesis* **47**, 789-792 (2009).

140. Malato, Y. *et al.* Fate tracing of mature hepatocytes in mouse liver homeostasis and regeneration. *J Clin Invest* **121**, 4850-4860 (2011).

141. Luo, W. *et al.* Embryonic stem cells markers SOX2, OCT4 and Nanog expression and their correlations with epithelial-mesenchymal transition in nasopharyngeal carcinoma. *PLoS One* **8**, e56324 (2013).

142. Weber, A. *et al.* Hepatocyte-specific deletion of the antiapoptotic protein myeloid cell leukemia-1 triggers proliferation and hepatocarcinogenesis in mice. *Hepatology* **51**, 1226-1236 (2010).

143. Inokuchi, S. *et al.* Disruption of TAK1 in hepatocytes causes hepatic injury, inflammation, fibrosis, and carcinogenesis. *Proc Natl Acad Sci U S A* **107**, 844-849 (2010).

144. Deutsch, M. *et al.* Divergent effects of RIP1 or RIP3 blockade in murine models of acute liver injury. *Cell Death Dis* **6**, e1759 (2015).

145. Roychowdhury, S. *et al.* Receptor interacting protein 3 protects mice from high-fat diet-induced liver injury. *Hepatology* **64**, 1518-1533 (2016).

146. Eggert, T. *et al.* Distinct Functions of Senescence-Associated Immune Responses in Liver Tumor Surveillance and Tumor Progression. *Cancer Cell* **30**, 533-547 (2016).

147. Jia, L. *et al.* Hepatocyte Toll-like receptor 4 regulates obesity-induced inflammation and insulin resistance. *Nat Commun* **5**, 3878 (2014).

148. Ojaniemi, M. *et al.* TLR-2 is upregulated and mobilized to the hepatocyte plasma membrane in the space of Disse and to the Kupffer cells TLR-4 dependently during acute endotoxemia in mice. *Immunol Lett* **102**, 158-168 (2006).

149. Bergmann, J. *et al.* IL-6 trans-signaling is essential for the development of hepatocellular carcinoma in mice. *Hepatology* **65**, 89-103 (2017).

150. Severa, M. *et al.* The transcriptional repressor BLIMP1 curbs host defenses by suppressing expression of the chemokine CCL8. *J Immunol* **192**, 2291-2304 (2014).

151. Agrati, C. *et al.* Activated V gamma 9V delta 2 T cells trigger granulocyte functions via MCP-2 release. *J Immunol* **182**, 522-529 (2009).

152. Boehle, A.S., Dohrmann, P., Leuschner, I., Kalthoff, H. & Henne-Bruns, D. An improved orthotopic xenotransplant procedure for human lung cancer in SCID bg mice. *Ann Thorac Surg* **69**, 1010-1015 (2000).

153. Coelho, A.L. *et al.* The chemokine CCL6 promotes innate immunity via immune cell activation and recruitment. *J Immunol* **179**, 5474-5482 (2007).

154. Orlofsky, A., Berger, M.S. & Prystowsky, M.B. Novel expression pattern of a new member of the MIP-1 family of cytokine-like genes. *Cell Regul* **2**, 403-412 (1991).

155. Takeuchi, K., Wood, H. & Swank, R.T. Lysosomal elastase and cathepsin G in beige mice. Neutrophils of beige (Chediak-Higashi) mice selectively lack lysosomal elastase and cathepsin G. *J Exp Med* **163**, 665-677 (1986).

156. Prince, L.R., Whyte, M.K., Sabroe, I. & Parker, L.C. The role of TLRs in neutrophil activation. *Curr Opin Pharmacol* **11**, 397-403 (2011).

157. Ding, N. *et al.* Toll-like receptor 4 regulates platelet function and contributes to coagulation abnormality and organ injury in hemorrhagic shock and resuscitation. *Circ Cardiovasc Genet* **7**, 615-624 (2014).

158. Holland, J.M. Serotonin deficiency and prolonged bleeding in beige mice. *Proc Soc Exp Biol Med* **151**, 32-39 (1976).

159. Park, S.G. *et al.* Precursor of pro-apoptotic cytokine modulates aminoacylation activity of tRNA synthetase. *J Biol Chem* **274**, 16673-16676 (1999).

160. Suzuki, A., Sekiya, S., Buscher, D., Izpisua Belmonte, J.C. & Taniguchi, H. Tbx3 controls the fate of hepatic progenitor cells in liver development by suppressing p19ARF expression. *Development* **135**, 1589-1595 (2008).

161. Ludtke, T.H., Christoffels, V.M., Petry, M. & Kispert, A. Tbx3 promotes liver bud expansion during mouse development by suppression of cholangiocyte differentiation. *Hepatology* **49**, 969-978 (2009).

162. Bond, C.E. *et al.* Methylation and expression of the tumour suppressor, PRDM5, in colorectal cancer and polyp subgroups. *BMC Cancer* **15**, 20 (2015).

163. Shu, X.S. *et al.* The epigenetic modifier PRDM5 functions as a tumor suppressor through modulating WNT/beta-catenin signaling and is frequently silenced in multiple tumors. *PLoS One* **6**, e27346 (2011).

164. Waldrip, Z.J. *et al.* A CRISPR-based approach for proteomic analysis of a single genomic locus. *Epigenetics* **9**, 1207-1211 (2014).

165. Nowak, A.K., Chow, P.K. & Findlay, M. Systemic therapy for advanced hepatocellular carcinoma: a review. *Eur J Cancer* **40**, 1474-1484 (2004).

166. El-Khoueiry, A.B. *et al.* S0941: a phase 2 SWOG study of sorafenib and erlotinib in patients with advanced gallbladder carcinoma or cholangiocarcinoma. *Br J Cancer* **110**, 882-887 (2014).

167. Kudo, M. *et al.* Lenvatinib versus sorafenib in first-line treatment of patients with unresectable hepatocellular carcinoma: a randomised phase 3 non-inferiority trial. *Lancet* **391**, 1163-1173 (2018).

168. Zen, C. *et al.* Mixed phenotype hepatocellular carcinoma after transarterial chemoembolization and liver transplantation. *Liver Transpl* **17**, 943-954 (2011).

169. Cotoi, C.G., Khorsandi, S.E., Plesea, I.E. & Quaglia, A. Histological aspects of post-TACE hepatocellular carcinoma. *Rom J Morphol Embryol* **53**, 677-682 (2012).

170. Sun, Z. *et al.* Hepatic and biliary damage after transarterial chemoembolization for malignant hepatic tumors: incidence, diagnosis, treatment, outcome and mechanism. *Crit Rev Oncol Hematol* **79**, 164-174 (2011).

7. Appendix

Apoptosis signature genes				necroptosis signature genes
APAF1	CRADD	BIRC7	NFKBIB	BIRC2
BAD	DAPK1	BIRC8	NFKBIE	CASP8
BAK1	DEDD	BNIP3	NFKBIZ	CFLAR
BAX	DEDD2	BNIP3L	NLRP1	CYLD
BBC3	DIABLO	BOK	NOD1	FADD
BCAP31	FAS	CARD18	NOD2	MLKL
BCL10	FASLG	CARD6	PEA15	RIPK1
BCL2	HIP1	CARD9	PMAIP1	RIPK3
BCL2A1	HRK	CASP1	PYCARD	TRADD
BCL2L1	HTRA2	CASP10	REL	XIAP
BCL2L10	IFT57	CASP14	RELA	
BCL2L11	IKBKB	CASP2	RELB	
BCL2L13	IKBKE	CASP3	RIPK2	
BCL2L14	IKBKG	CASP4	TBK1	
BCL2L2	LTA	CASP5	TNF	
BCL3	LTB	CASP6	TNFRSF10A	
BID	MCL1	CASP7	TNFRSF10B	
BIK	NAIP	CASP8AP2	TNFRSF1A	
BIRC3	NFKB1	CASP9	TNFRSF1B	
BIRC5	NFKB2	CHUK	TNFRSF21	
BIRC6	NFKBIA		TNFSF10	